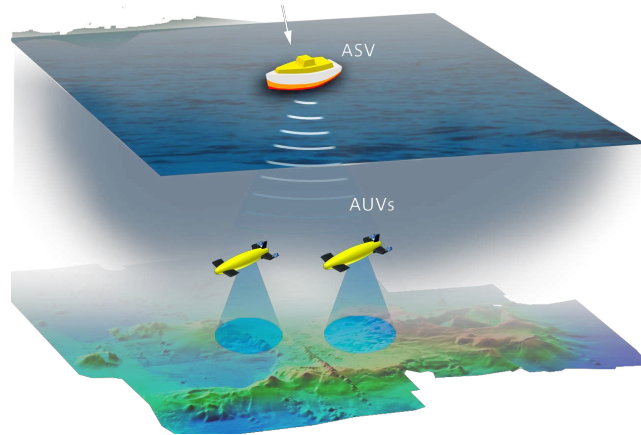




**TÉCNICO**  
LISBOA



# **Cooperative Motion Control of Autonomous Marine Vehicles for Ocean Observation**

**Daniel Oluwatobi Akanji**

Thesis to obtain a Master of Science Degree in  
**Electrical and Computer Engineering**

Supervisors: Prof. Pedro Batista  
Prof. David Cabecinhas

## **Examination Committee**

Chairperson: Prof. José Eduardo Charters Ribeiro da Cunha Sanguino  
Supervisor: Prof. David Cabecinhas  
Member of the committee: Prof. Daniel de Matos Silvestre

**November 2023**



### **Declaration**

I declare that this document is an original work of my own authorship and that it fulfils all the requirements of the Code of Conduct and good practices of the Universidade de Lisboa.



Dedicated to Jesus, the wisdom and power of God...



## Acknowledgements

The hallmark of my two-year master's journey, which commenced at the Université de Toulon, France and is concluding here at the Instituto Superior Técnico, Lisbon, lies in the period of working on my Master's thesis. What rendered this period noteworthy was the opportunity bestowed upon me by my supervisors, Prof. Pedro Batista and Prof. David Cabecinhas, to conduct my research at the Institute for Systems and Robotics (ISR) / Dynamical Systems and Ocean Robotics (DSOR) laboratory. The skills and experiences I acquired while working with the lab's resources were truly remarkable. I extend my gratitude to my supervisors, not only for the opportunity but also for the guidance and advice provided throughout the project.

I express profound gratitude to my beloved parents, Dr and Mrs Samuel Akanji, who unwaveringly provided every form of support a child could ever need. To you, I say thank you and God bless you. The narratives of your unwavering love and support shall always be recounted and cherished. My siblings—Lydia, Success, and Grace—have also been sources of support during my studies. I extend heartfelt thanks to all of you.

My expression of gratitude would be incomplete without acknowledging some of the brightest minds I encountered at the DSOR lab. These remarkable individuals consistently stood ready to offer assistance whenever needed. Many thanks to Francisco Branco, Eduardo Cunha, and Daniel Rosa. I also thank my other lab colleagues, Ricardo and Miguel, for their mutual support.

I mustn't forget my dear colleagues from the Marine and Maritime Intelligent Robotics (MIR) intake 1, as well as my friend Shamba, for their unwavering support throughout this Master's journey. To all of you, I extend my heartfelt thanks. I also wish to extend my appreciation to our MIR coordinator, Prof. Ricard Marxer, Ms Celia Cau, Prof. Vincent Hugel, and all other MIR staff at the Université de Toulon, for their consistent support.

Finally, my gratitude extends to the European Regional Development Fund (FEDER), which funded my research through the Lisbon Regional Operational Program 2020 (LISBOA-01-0145-FEDER-022157), within the scope of the project (1018P.05390.1.01) EMSO-PT-PINFRA/22157/2016\_LISBOA-01-01 alongside the RAMONES project (H2020 EU project RAMONES - Radioactivity Monitoring in Ocean Ecosystems, g.a. 101017808).



# Resumo

A comunidade científica utiliza variadas tecnologias e instrumentos de observação para medir e monitorizar os oceanos a nível mundial. Algumas destas, como os navios de investigação, são de curto prazo e não conseguem captar as alterações a longo prazo. Observações oceânicas a longo prazo são vitais para compreender as alterações climáticas e melhorar as previsões do clima, do tempo e dos riscos ambientais. Este estudo apresenta um sistema que permite a observação a longo prazo através da utilização de veículos marinhos autónomos. A arquitetura robótica proposta consiste em três nós móveis: uma embarcação de superfície autónoma (ASC) e dois veículos submarinos autónomos (AUV). A estratégia de controlo da formação adopta uma abordagem líder/seguidor; a ASC serve de seguidor/rastreador, enquanto os AUVs actuam como líderes/alvos. A ASC, equipada com sensores, recolhe dados no interface ar-mar e na coluna superior do oceano, enquanto segue de perto os AUVs. Por outro lado, os dois AUVs fazem as suas observações à medida que mergulham através da coluna de água com um determinado ângulo, seguindo um caminho predefinido no plano horizontal, enquanto exibem um movimento tipo dente-de-serra no plano vertical. O Seguimento de Caminho (PF) permite que os veículos-líder sigam um caminho predefinido com o perfil de velocidade desejado no plano horizontal, enquanto o controlo do ângulo de picada cria o movimento no plano vertical. Empregando a abordagem de Seguimento de Alvo (TT), o seguidor continua a ajustar a sua velocidade e orientação em relação ao alvo para garantir um seguimento próximo. A camada final envolve o controlo cooperativo de múltiplas formações, permitindo o movimento sincronizado com os alvos. Duas formações cooperativas são implementadas: rastreamento intermitente de alvos na primeira, e rastreamento e acompanhamento de posições intermediárias entre alvos na segunda.

**Palavras-chave:** Veículo marítimo autónomo, Rastreamento de alvos, Controle cooperativo de formação múltipla, Seguimento de caminho, Linha de visão



# Abstract

Scientists employ diverse observing technologies and instruments to measure and monitor the global oceans. However, some, such as research vessels, are short-term and fall short in capturing long-term changes. Long-term ocean observations are vital for comprehending climate change, variability and improving climate, weather, and environmental hazard forecasting. This study presents a system that enables long-term observation through the use of Autonomous Marine Vehicles. The proposed robotic architecture consists of three mobile nodes: an Autonomous Surface Craft (ASC) and two Autonomous Underwater Vehicle (AUV)s. The formation control strategy adopts a leader-follower approach; the ASC serves as a follower/tracker, while the AUVs act as leaders/targets. The ASC, equipped with sensors, gathers data at the air-sea interface and the upper column of the ocean as it follows the AUVs closely. Conversely, the two AUVs make their observations as they dive through the water column at a given angle, following a predefined path in the horizontal plane while exhibiting a sawtooth-like motion in the vertical plane. Path Following allows the target vehicles to follow a predefined path with the desired speed profile in the horizontal plane while controlling the pitch angle creates the motion in the vertical plane. Employing the Target Tracking approach, the tracker keeps adjusting its speed and orientation to the target to ensure close tracking. The final layer involves cooperative multiple-formation control, enabling synchronized movement with targets. Two cooperative formations are implemented: intermittent tracking of targets in the first, and tracking and following mid positions between targets in the second.

**Keywords:** Autonomous marine vehicle, Target Tracking, Cooperative multiple formation control, Path Following, Line of sight



# Table of Content

<b>Resumo</b>	<b>viii</b>
<b>Abstract</b>	<b>x</b>
<b>List of Figures</b>	<b>xiv</b>
<b>List of Tables</b>	<b>xvi</b>
<b>List of Abbreviations</b>	<b>xvii</b>
<b>1 Introduction</b>	<b>1</b>
1.1 Background . . . . .	2
1.2 Motivation of the Study . . . . .	3
1.3 Problem Description and Objectives . . . . .	5
1.4 State of the Art . . . . .	7
1.5 Main Contribution and Thesis Outline . . . . .	10
<b>2 Problem Formulation</b>	<b>11</b>
2.1 Autonomous Marine Vehicle Model . . . . .	11
2.1.1 Notation and Reference Frames . . . . .	11
2.1.2 Kinematics . . . . .	13
2.1.3 Dynamics . . . . .	14
2.1.4 Simplified Equations . . . . .	15
2.2 Path Following . . . . .	18
2.2.1 Path Following Overview . . . . .	18
2.2.2 Path Following Notation . . . . .	19
2.2.3 Path Parameterization and Path Frames . . . . .	20
2.2.4 Path Following Problem Formulation . . . . .	22
2.2.5 Review of Path Following Strategies . . . . .	23
2.3 Vertical Motion Guidance System . . . . .	26

2.4	Target Tracking . . . . .	27
2.4.1	Target Tracking Problem Formulation . . . . .	27
2.4.2	Target Tracking Strategies . . . . .	28
2.5	Cooperative Multiple Vehicle Formation Control . . . . .	31
2.5.1	Cooperative Motion System . . . . .	32
2.5.2	Control Block Representation . . . . .	34
<b>3</b>	<b>Proposed Solution</b>	<b>36</b>
3.1	System Implementation . . . . .	36
3.1.1	Inner-Outer Loop Approach . . . . .	36
3.1.2	DSOR Software Stack Overview . . . . .	39
3.2	Solving Path Following for the Target Vehicles . . . . .	40
3.3	Target Tracking Heading Controller . . . . .	45
3.4	Target Tracking Speed Controller . . . . .	51
<b>4</b>	<b>Simulation Results</b>	<b>54</b>
4.1	Path Following Simulation . . . . .	54
4.2	Target Tracking Simulation . . . . .	59
4.3	Cooperative Multiple Vehicle Formation Control Simulation . . . . .	63
<b>5</b>	<b>Conclusion and Future Works</b>	<b>68</b>
5.1	Conclusion . . . . .	68
5.2	Future Works . . . . .	69
	<b>References</b>	<b>71</b>

# List of Figures

1.1	Cooperative control of two surface ASCs and one AUV [1] . . . . .	2
1.2	Background schematics for the MORPH and WiMUST projects . . . . .	3
1.3	An Image Showing some Mooring, some Drifters and a Buoy in the Open Sea [2],[3],[4] . . . . .	4
1.4	A Simplified Sketch of the Nodes of the RAMONES Project. [5] . . . . .	5
1.5	Formation Control of Multiple AMVs [6] . . . . .	8
2.1	Body-fixed and Inertial Reference frames [7] . . . . .	12
2.2	Geometric illustration of Path Following Problem. . . . .	19
2.3	An illustration of Frenet-Serret $\{\mathcal{F}\}$ in 2D . . . . .	20
2.4	An illustration of Frenet-Serret $\{\mathcal{F}\}$ and Parallel Transport $\{\mathcal{P}\}$ frames in 2D [8] . . . . .	22
2.5	Pure Pursuit Guidance Illustrated, Adapted from [9]. . . . .	29
2.6	Constant Bearing Guidance Illustrated, Adapted from [9]. . . . .	30
2.7	LOS Guidance Illustrated, Adapted from [9]. . . . .	31
2.8	A Directed Graph of the Vehicle Network Topology. . . . .	32
2.9	Scenario I Cooperation Strategy. . . . .	34
2.10	Scenario II Cooperation Strategy. . . . .	35
2.11	Cooperative Control Block Diagram. . . . .	35
3.1	A Sketch of the Inner-loop Outer-loop control structure [10]. . . . .	37
3.2	A Schematics of the NetMarSys Toolchain system. . . . .	39
3.3	Geometric illustration of Path Following Problem. . . . .	40
3.4	Block Diagram for a Single Target Vehicle. . . . .	45
3.5	Illustration of the Target ahead of the Tracker. . . . .	46
3.6	Illustration of the Target behind the Tracker. . . . .	46
3.7	An Illustration of the Straight Line Problem for Target Tracking. . . . .	47
3.8	Straight Line LOS with both Enclosure-based and Lookahead-based steering methods demonstrated . . . . .	49
3.9	A Figure Showing the Impact of Various $K_3$ Values on $u$ [ $u_d = 0.3$ ]. . . . .	53

4.1	Target vehicle following a lawn mower path in the horizontal plane. . . . .	55
4.2	Target vehicle performing a saw-tooth wave maneuver in the vertical plane. . . . .	56
4.3	Error Plots between the Target vehicle and the Reference Path . . . . .	57
4.4	Position Distance Error of Target Vehicle. . . . .	57
4.5	Position Distance Error and Pitch Plot of the Target Vehicle. . . . .	58
4.6	Surge, Pitch, and Yaw of Target Vehicle. . . . .	58
4.7	2D plot of the tracker following the target vehicle . . . . .	60
4.8	3D plot of the tracker following the target vehicle . . . . .	60
4.9	Error Plots between the Target vehicle and the Tracker Vehicle . . . . .	61
4.10	Distance Error plot between the Target vehicle and the Tracker Vehicle . . . . .	62
4.11	Surge, Pitch and Yaw References of the tracker and target vehicles . . . . .	63
4.12	2D plot of the tracker following the target vehicles Intermittently . . . . .	64
4.13	2D plot of the distance between the Tracker and the targets. . . . .	64
4.14	2D plot of the tracker following the target vehicles Intermittently . . . . .	65
4.15	2D plot of the distance between the Tracker and the targets. . . . .	66
4.16	Surge, Pitch and Yaw References of the target vehicles . . . . .	66
4.17	3D Visualization of the tracker following the targets for two scenarios . . . . .	67

# List of Tables

2.1	Notation used for marine vehicles, adapted from Fossen [9] . . . . .	13
3.1	Values for the Parameters used for the Target's PF manoeuvre . . . . .	44
3.2	Values for the parameters used for the Target Vehicle . . . . .	45
3.3	Values for the parameters used for the Tracker Vehicle . . . . .	53

# List of Abbreviations

**AMV** Autonomous Marine Vehicle. x, xiv, 1–5, 7, 8, 10, 26, 36

**ASC** Autonomous Surface Craft. x, xiv, 2–7, 28, 32, 33, 51, 68

**AUG** Autonomous Underwater Glider. 4, 5

**AUV** Autonomous Underwater Vehicle. x, xiv, 2–8, 25, 28, 32–34, 41, 68

**DSOR** Dynamical Systems and Ocean Robotics. vi, 39

**ISR** Institute for Systems and Robotics. vi, 39

**MORPH** Marine Robotic System of Self-Organising, Logically Linked Physical Nodes. 2, 3

**PF** Path Following. x, xiii, 6–8, 10, 18–26, 31, 36, 40, 54, 59, 62, 68, 69

**PI** Proportional and Integral. 36, 38

**PID** Proportional Integral and Derivative. 8, 10, 36–38

**RAMONES** Radioactivity Monitoring in Ocean Ecosystems. xiv, 1, 5

**SNAME** Society of Naval Architects & Marine Engineers. 11, 12, 19, 73

**WiMUST** Widely scalable Mobile Underwater Sonar Technology. 3

# Chapter 1

## Introduction

The increase in atmospheric carbon dioxide (CO<sub>2</sub>) levels resulting from human activities has not only led to climate change but has also caused the ocean to absorb a substantial amount of CO<sub>2</sub>. This absorption has resulted in ocean acidification, whereby seawater pH decreases. Acidification poses a threat to calcifying organisms such as coral reefs, shellfish, and certain plankton species, as it hinders their ability to build and maintain their shells or skeletons. This and many more ocean processes exert a profound influence on the Earth's climate, weather patterns, carbon cycling, biodiversity, and coastal landscapes, amongst others. Therefore, monitoring, understanding, and accurately predicting ocean processes is vital to the survival of life on Earth. Hence, with ocean observation, scientists can collect and analyse data and information about the ocean environment that will be useful in making informed decisions about the planet.

Among the various methods and technologies used in ocean observation is the use of autonomous robotic platforms. The Radioactivity Monitoring in Ocean Ecosystems (RAMONES) project [5] is a compelling example of the application of not just a single Autonomous Marine Vehicle (AMV), but a group of heterogeneous AMVs working in cooperation for radioactivity monitoring. The area of Guidance, Navigation and Control is instrumental in the realization of this system.

Similarly, within the framework of Guidance, Navigation and Control, this thesis presents an approach to the problem of control and cooperation needed to realise a system that will be capable of performing long-term ocean observation. The goal of the system is to have a surface vehicle working in cooperation with two underwater vehicles, thereby allowing data to be collected both at the surface and at depth. Therefore, the proposed method will encompass control algorithms that will ensure that the surface vehicle tracks accurately the underwater vehicles as they follow a predefined path.

## 1.1 Background

In recent times, there has been an increase in the use of AMVs for various marine operations such as seafloor mapping, port protection, mines countermeasure, reconnaissance survey, ocean observation and sampling, and surveillance missions. This system provides substantial advantages in terms of cost, data acquisition, and greater operational efficiency to traditional ocean exploration methods. In ocean sampling and observation, the cost of traditional methods such as ships and their inability to stay out at sea for a long time has created interest in the use of autonomous robotic platforms such as Autonomous Surface Crafts (ASCs) and Autonomous Underwater Vehicles (AUVs). This paradigm shift is made possible due to advances in navigation sensors, low-power electronics, more efficient energy storage and advanced AI and control algorithm, amongst other factors [11].

There is a growing demand for improved observation capabilities, encompassing broader data coverage, longer duration, and refined measurement methods. However, the above-mentioned demands are complex, time-consuming and computationally demanding for a single marine vehicle. In this scenario, failure of any sensor, actuator, or any part of the vehicle will jeopardize such an expedition. Hence, an alternative solution embraced by researchers is the use of multiple marine vehicles that work in cooperation to meet those demands, as depicted in Figure 1.2b.

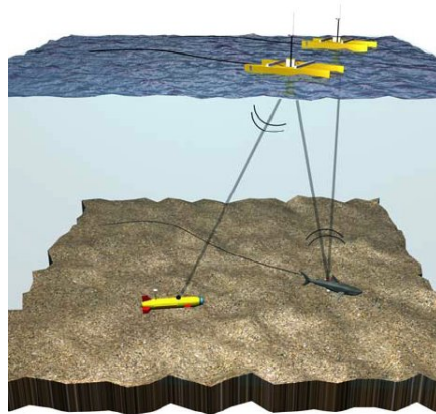


Figure 1.1: Cooperative control of two surface ASCs and one AUV [1]

With the cooperation of multiple marine vehicles, significant mission characteristics, such as completion time, fault tolerance, cognition and perception of the augmented system, can be positively impacted [12]. A particularly important scenario that motivates the cooperation of multiple autonomous vehicles, and in similar manner, poses great challenge to system engineers, both from a theoretical and practical standpoint, is automatic ocean exploration/monitoring for scientific and commercial purposes. In this scenario, using a single vehicle can lead to system failure since the vehicle will be heavily equipped. However, cooperation between a group of vehicles connected via a mobile communications network has the potential to overcome this limitation [13]. The Marine Robotic System of Self-Organising, Logically Linked Physical Nodes (MORPH) [14]

and Widely scalable Mobile Underwater Sonar Technology (WiMUST) [15] projects are typical demonstrations of the capabilities of cooperation of AMVs. In the MORPH project, an ASC and four AUVs were used in the mapping of underwater habitats in unstructured environments. Each vehicle in the formation had a specific task to accomplish. On the other hand, the goal of the WiMUST project was the improvement of seismic data acquisition by replacing the conventional method of data acquisition with a fleet of AMVs. The project made it possible to acquire more seismic data with better resolution. The image in Figure 1.2 shows the formation of the vehicles in the network for both the instances of WiMUST and MORPH respectively.

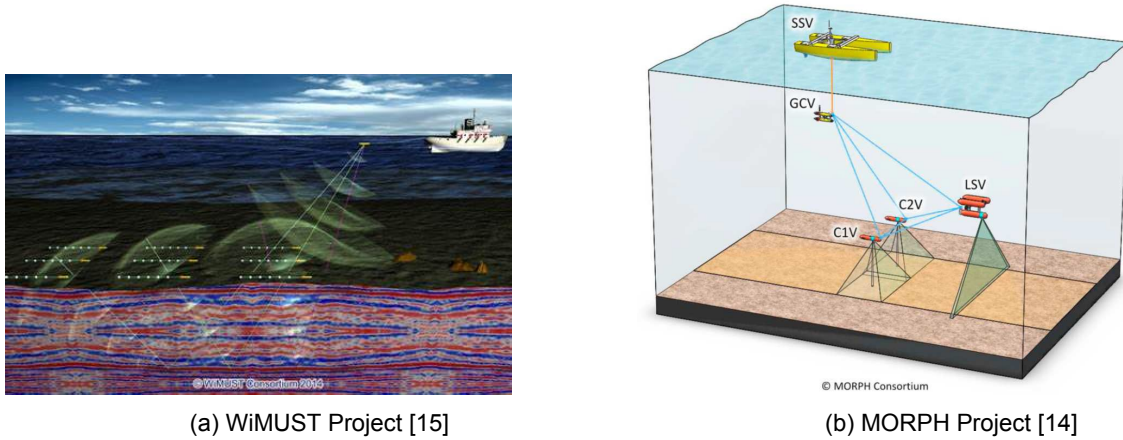


Figure 1.2: Background schematics for the MORPH and WiMUST projects

## 1.2 Motivation of the Study

Data is critical to any scientific discovery. In today's world, most of the inventions and discoveries have been accelerated through the collection, analysis, and interpretation of meaningful data. The vast ocean is not left out of the quest for data. Ocean data gathering enables scientists to know the condition of the ocean and the life in it and hence will influence decisions taken to shape the economic, climate, and geopolitical front of our world.

Many techniques have been employed by ocean explorers, scientists and researchers to gather data in their respective fields. These techniques can either be in-situ measurements or remote measurements. Research ships are examples of in situ measurement techniques. Research vessels deploy instruments such as Conductivity Temperature and Depth (CTD), sediments traps, tide gauges, cameras, etc., for ocean observation. However, such expeditions can only last for a few days or weeks and only provide snapshots. This technique cannot capture changes that occur over months or years, nor can they capture sudden, unpredictable events unless they happen at that instance. To truly comprehend Earth's dynamic behaviour and to monitor how it affects human lives back on shore, ocean and earth scientists must do more than observe small regions for short periods. There is, therefore, a need for sustained long-term observations in order to know how the ocean changes with seasons, years, and decades.[16]

Moorings, drifters, and buoys as seen in Figure 1.3, are excellent long-term in situ measurement tools and can reveal patterns and changes in the sea. However, they can only carry out measurements at the surface of the water column. Satellite observations, on the other hand, are examples of remote measurement. They offer useful broad and long-term observations of the ocean. Their limitation lies in the fact that can only penetrate a few metres of the water column. With the advances in autonomous robotic platforms, some of the above limitations can be mitigated.

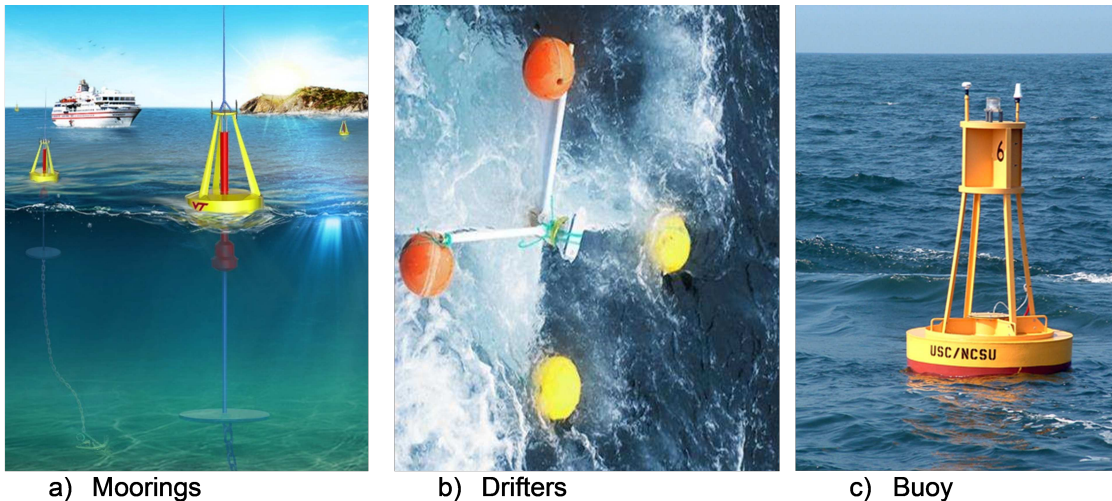


Figure 1.3: An Image Showing some Mooring, some Drifters and a Buoy in the Open Sea [2],[3],[4]

AUVs, ASCs and Autonomous Underwater Gliders (AUGs) are examples of autonomous robotic platforms which are also in-situ measurement techniques. These can be used for the measurement of oceanographic parameters such as chlorophyll, temperature pressure, nitrate, salinity, etc., both at and below the surface of the ocean. Consequently, the characteristic features that come with the use of these AMVs, such as their ability for long-term autonomous operation in open and coastal oceans, their ability to perform ocean observations and sampling at various depths, their ability to travel far distances over long periods complement some of the deficiencies encountered in other ocean observation systems. For instance, Autonomous Surface Crafts traverse the ocean surface gathering data above, below and at its boundary. This makes them suitable for studies that involve understanding the dynamics of the air-sea interface and interactions. The AUVs, on the other hand, are underwater vehicles that are capable of diverse ocean observations and sampling at various depths. This is because they are well-equipped with various sensors. However, they are not well suited for long-term operations at sea, unlike the AUGs. Autonomous Underwater Gliders are a type of AUV that move up and down through the water column collecting data. Their ability to travel far distances over long periods, without servicing, makes them desirable for ocean observation. These available advantages are sufficient enough reasons to motivate a study on the use of marine robots for ocean observation. However, enormous benefits lie in harnessing the potential of various heterogeneous AMVs

in cooperation, which is the crux of this thesis. A vivid example is the ongoing Radioactivity Monitoring in Ocean Ecosystems (RAMONES) project [5], which is one of the inspirations for this thesis.

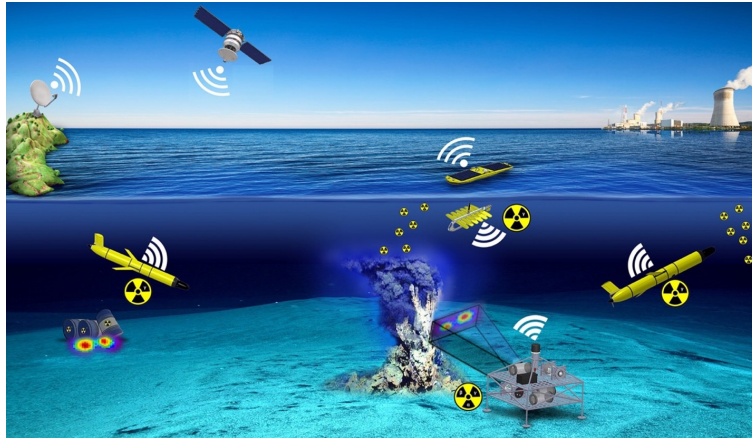


Figure 1.4: A Simplified Sketch of the Nodes of the RAMONES Project. [5]

The goal of the RAMONES project is to offer a systematic novel solution for long-term, continuous in situ monitoring of radioactivity in the oceans. The system consists of three mobile nodes; an ASC, two AUGs, and a fixed node; a static benthic laboratory, all equipped with radiological instruments for radioactivity monitoring [5]. A pictorial representation of this formation can be seen in Figure 1.4. In this project, each node in the network has a specific task to accomplish; thereby allowing each vehicle to perform maximally and contributing to the overall effectiveness of the mission.

Furthermore, one of the reasons that make this technology worth investing in is its wide spectrum of applications in climate studies, ocean ecosystem monitoring, the aquaculture industry, in tracking and detecting oceanic features such as upwelling events, red tides, and coastal eddies and in the tracking of large ocean mammals such as Whales.

### 1.3 Problem Description and Objectives

Guidance, navigation, and control are at the core of any successful cooperative motion system of AMVs. Depending on the application interest, concepts like point stabilization, trajectory tracking, and path following, as described in [9], are considered. Moreover, the control strategy, the cooperative maneuvering method, the communication protocol and other parameters are largely dependent on the area of application. When it comes to the use of AMVs for ocean data gathering, the formation of the vehicles is designed to maximise data collection in the area to which they are deployed. Hence, the end goal of this thesis is to have an ASC tracking two AUVs whose motion in the horizontal plane is following a predefined path and in the vertical plane performing a saw-tooth wave-like maneuver. In other words, for the surface vehicle to track the two AUVs, it can either track the midpoint between the two vehicles or follow each target interchangeably. By choosing any of these formations, the ASC will be able to collect similar data at the surface of the water

column as the AUVs are doing below the water column. On the other end, the AUVs profile the water column as they perform their saw-tooth motion in the vertical plane and at the same time, traverse large distances as they follow a predefined path. With this system, data gathered will yield meaningful information about the changes on a temporal and spatial scale, since they are collected simultaneously below and at the surface of the water column.

### **Research Approach**

Having described the general problem, it is also expedient to become familiar with the technical aspects of the problem. The technical aspect has been divided into sub-problems for simplicity's sake. The first problem to be solved is the Path Following (PF) problem. In PF, the goal is to drive the vehicle to and maintain it on a pre-defined path while tracking a path-dependent speed profile [8]. In PF, the vehicle is not required to be at specific positions at specific instants of time, which is a strong requirement in Trajectory Tracking [8]. This enables PF to yield a smoother vehicle motion than Trajectory Tracking. Hence, the PF method will be adopted by the two AUVs. Therefore, Path Following will characterise the motion of the two vehicles in the horizontal plane.

Secondly, the problem of controlling the motion of the AUVs in that vertical plane will be addressed. To ensure that the AUVs follow and track a saw-tooth wave-like motion in the vertical plane, the pitch angle of the AUVs will be controlled to achieve the desired motion. Since the control strategy that will be employed is the inner-loop outer-loop approach (to be discussed in the Section 1.4), a pitch command will be given to the inner loop of the vehicles to track. With this, the AUVs will be able to perform a saw-tooth wave-like motion in the vertical plane.

The third problem is to achieve cooperation between the two AUVs and the ASC. To solve this problem, the Target Tracking approach will be employed such that the tracker (ASC) will be required to track the targets (AUVs) either at midpoints or track them interchangeably. The Target Tracking controller will ensure that the ASC will always adjust its speed, and heading to be in line with the vehicle(s) it is tracking. The intuition behind this Target Tracking controller as follows: when the tracker is behind the target, it will increase its speed to catch up with the target and move in synchrony with the speed of the target after it catches up, and consequently, when the tracker is ahead it will slow down its speed for the target to meet up with the target it is tracking. This way, cooperation is achieved between the surface and underwater vehicles.

For this study, the criteria for the transmission of information will be the time when each AUVs completes its dive and surfaces. Whereas, since the ASC is always communicating with the satellite, it can transmit its data after 5 minutes. However, since communication protocol is out of the scope of this project, it will not be addressed.

## 1.4 State of the Art

In this section, we would examine the existing theories that support this study. These theories were carefully selected in order to have an efficient control structure for the desired vehicle formation.

To achieve successful cooperative control of multiple vehicles, formation control becomes a tool par excellence to consider. Formation control is an important research topic of cooperative control within the recent fields of multi-vehicle systems [17]. It pertains to the challenge of controlling the relative positions and orientations of autonomous vehicles within a group, enabling the group to move cohesively [6]. The steps involved in achieving formation control may encompass one or more of the following elements: assignment of feasible formation control strategies, moving in formation, maintenance of formation shape, and/or switching between formations. Bikramaditya et al. [6] categorized formation control into two distinct classes: formation regulation control and tracking control. In the former, the primary focus lies in maintaining the formation's shape during cooperation, while the latter emphasizes tracking a designated leader. Formation regulation control finds practical applications in areas such as pipeline surveillance, underwater surveys, and the study of underwater environments. On the other hand, tracking control is commonly employed in tasks like path-tracking maneuvers, guidance, tracking activities, and underwater surveys, among others. While presenting the research, the two broad classes were further divided into subcategories. Considering the specific context of this study, the tracking control category aligns with our research interests. Among the various topologies discussed within tracking formation control, the leader-follower approach is the formation method chosen for this study.

In the leader-follower technique, an AMV is elected as the leader AMV. it executes a PF algorithm at a required forward speed and relays its position to the remaining AMVs in the formation [18] [19]. It is the responsibility of the follower AMVs to maintain the formation based on the information received from the leader [6] as depicted in Figure 1.5. In this specific context, the leader-follower approach involve two AUVs act as the leaders or targets while the ASC is the follower or tracker. The ASC can either follow the leaders interchangeably or follow the leaders at their midpoints. The leaders are in charge of executing the Path Following algorithm. The follower has access to the speed, attitude and position information of the leaders in the formation. With the information received, the follower can track the leaders in the formation. This approach is simple and relatively easy to understand and implement.

Another concept which is one of the backbones of this study is Path Following. The problem of PF involves making a vehicle converge to and follow a spatial path while asymptotically tracking the desired speed profile along the path. Since the problem at hand is not time-constrained, the PF method is the right algorithm to use in comparison to trajectory tracking, which is time-constrained. Its primary objective is a geometric one, which is aimed at steering an AMV to reach a desired geometric path, while the secondary objective is a dynamic one; to force the AMV to move along the path satisfying given dynamic specifications [20] [21]. PF finds application in missions that are not time-constrained such as environmental sampling and monitoring, marine data collection and resource exploration, coastal surveillance, reconnaissance surveys,

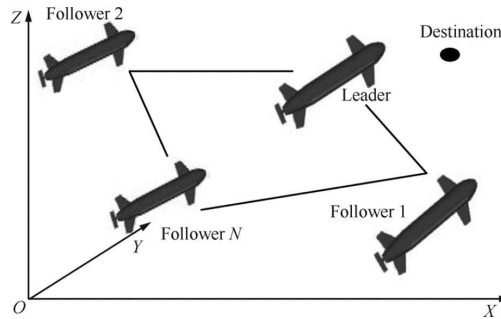


Figure 1.5: Formation Control of Multiple AMVs [6]

and underwater surveys. In such missions, the demands in terms of energy and actuator precision required to drive the vehicle to and along the path will not be demanding. In this thesis, the objective of PF remains the same. The PF technique is responsible for generating the speed and the heading references of the target vehicles in the formation. The references that are being generated are idiosyncratic to each target vehicle. PF is responsible for the motion in the horizontal plane. However, since we desire the targets to profile the water column by performing a saw-tooth maneuver in the vertical plane, there is, therefore, a need to control the pitch reference of the vehicle.

Works of literature such as [22], [23], and [24] have presented various approaches to the control of the pitch angle of AUVs. In [23], an adaptive pitch control system for AUVs was designed using type 2 fuzzy logic controllers. Ravishankar et al. [22] presented the use of a norm-based robust controller to achieve the design requirements for the attitude control of the MAYA AUV in the presence of parametric uncertainty and disturbances. In [24], Linear Quadratic Regulator (LQR) and Fractional Order PID (FOPID) techniques were applied to determine the controller for better pitch control performance in the presence of disturbances. A common theme in these papers is to address depth-keeping and attitude stability control of an AUV. In simpler terms, achieving the desired depth of the vehicle can be accomplished by implementing an efficient pitch control law [22]. To reach this goal in this thesis, pitch control will be implemented using PID controllers. The pitch references will be generated for the target vehicle based on the desired depths (max and min depth) attained by the target vehicle. In simple terms, when the target vehicle reaches the surface, say a depth of 1m, the provided pitch reference will constrain its orientation in the downward direction. Consequently, when it reaches the desired maximum depth, another pitch reference is outputted that constraints its motion in the upward direction. This way, the target vehicles exhibit an up-and-down motion in the vertical plane.

Furthermore, another key theory in this study is Target Tracking. According to [25], autonomous target tracking has been observed to be one of the most researched fields of interest and finds an extensive range of applications, including civilian and military fields, specifically in border patrolling, convoy protection, underwater surveillance, and aerial surveillance. Target Tracking is usually used whenever the information about the target's path is not known and there is no trajectory to track [9]. The only available information is the state (position, velocity, acceleration, etc.) of the target either provided by the target sensors or estimated

by the tracker itself. Condomines [26] in his book classified sensors used for measurement purposes in the application of aerial, underwater tracking or mobile robotics into two categories namely proprioceptive sensors and exteroceptive sensors.

Proprioceptive sensors, such as the gyroscope and accelerometer, are employed to assess the vehicle's spatial movement by interpreting locally obtained data, such as acceleration measurements. This approach yields results that are easy to utilize and unaffected by environmental factors, which are important in autonomous UAV (Unmanned Aerial Vehicle) navigation. Conversely, exteroceptive sensors collect information about the vehicle's surroundings, including pressure, magnetic fields, and more. This dataset provides observations relative to an absolute reference frame linked to the environment, such as satellite position. These sensors offer valuable data that can enhance the localization achieved through proprioceptive sensors, enabling continuous monitoring of the vehicle's motion. Common examples of exteroceptive sensors include Satellite positioning systems, Barometric altimeters, Magnetometers, Cameras and telemeters (SONAR, LiDAR), Inertial Measurement Units (IMU), Inertial Navigation Systems (INS) and Attitude and Heading Reference Systems (AHRS) [25].

When these sensors detect the existence of a target, they typically sample the sensed signals (e.g., light, acoustics, images, or video) to obtain observation information. Subsequently, the target's position is often mathematically computed by relating this information to the target state. To enhance tracking accuracy in the presence of measurement noise, an additional filtering component can be integrated into the process. The tracking process is then finalized by determining the target's position at each step and designing a control law to guide the tracker toward the target position. Common key components in the target tracking process include target detection, position determination, target model construction, state filtering and prediction, and target engagement [25] [27]. However, since the subject of navigation is out of scope for this study, the focus will be on target engagement, under the assumption that the target position and other information are known. The Target Tracking algorithm is implemented by the tracker vehicle. With Target Tracking, the tracker can converge to the target asymptotically in finite time. This approach generates the control law for the heading and the speed of the tracker vehicle. These control laws are dependent on the information of the target in sight. In addition, Target Tracking ensures cooperation between the tracker and the target vehicles such that, the control law makes up for the speed of the tracker whenever it is ahead or behind the target.

In conclusion, the control system architecture stands as another crucial topic to address when examining the current state of the art. The control strategy employed in the system significantly influences system performance. A widely used approach is the inner-loop outer-loop control strategy, as illustrated in Figure 3.1. The inner-loop outer control structure constitutes a two-tiered control system, where the outer-loop control implements a guidance strategy such as Way-point tracking, Trajectory Tracking, Path Following, and Target Tracking. It generates the desired linear and angular speeds or orientations necessary to steer the vehicles in the formation. Conversely, the inner-loop architecture generates suitable forces and torque for the vehicles to track the desired references, thus achieving the mission objectives. These controllers can

be based on PID or linear-quadratic Gaussian (LQG) or  $H_\infty$  control design techniques, or other non-linear controllers. In this study, however, the inner-loop system is based on a set of PID controllers.

Additionally, as the focus is on the outer-loop control design, tuning the inner-loop controllers becomes a priority to achieve a sufficiently fast response of these controllers for tracking the references from the outer loop. The guidance system was designed by considering only the kinematics model of the vehicle.

## 1.5 Main Contribution and Thesis Outline

Throughout this work, concepts presented in the state-of-the-art section such as PF, Target Tracking were explored in-depth. Though these scientific tools are by no means novel to the area of Guidance, Navigation and Control, however, their application to a certain area can bring a new perspective to the versatility of such tools. Hence, having applied some of these tools for the study, the main contributions that this thesis presents are as follows:

- The target tracking speed tracking control law presents a control strategy such that the tracker is able to correct its speed and follow the target in synchrony.
- The saturation command introduced to the target tracking speed control law enabled non-zero, non-negative reference output.
- The two configurations (the tracker following the target intermittently and the tracker following the targets at their mid-position) by which the tracker follows the targets present a new ocean data observation strategy for oceanographers. With the two strategies presented, researchers can choose which formation best suits the mission characteristics.
- The system presents an advantage of studying the variation of oceanographic parameters at the surface and at depths, as data will be gathered at the same time.

The report is organized into seven chapters, following the reasoning presented in Section 1.3. Chapter 2.1 presents the model of AMVs, alongside concepts that help in describing the motion of the vehicles. Chapter ?? addresses the PF problem, with an overview of various algorithms proposed by different authors, and a comprehensive description of the algorithm applied to the problem at hand. In Chapter ??, the Target Tracking problem was addressed with emphasis on the specific method used to solve the target tracking problem of the tracker vehicle. Chapter 2.5 proposes the idea behind the cooperative formation of the vehicles in the network. Chapter 4 discusses the results obtained in all of the modules. Chapter 5 presents the outcome of the study and some recommendations for further studies of this type of system.

# Chapter 2

## Problem Formulation

### 2.1 Autonomous Marine Vehicle Model

This section presents a mathematical model of a generic Six Degrees of Freedom (6 DOF) and Three Degrees of Freedom (3 DOF) autonomous marine vehicle. This section is divided into four subsections. Subsection 2.1.1 presents the notations and reference frames as given by the Society of Naval Architects & Marine Engineers (SNAME) [28] in 1950, and Subsections 2.1.2 and 2.1.3 present the kinematics and dynamics of the vehicles. Subsection 2.1.4 presents a simplified equation of motion of the two models.

#### 2.1.1 Notation and Reference Frames

It is important to explicitly state the notations and define the reference frames used throughout this thesis to obtain the vehicle model. These conventions are in keeping with the SNAME [28] conventions. Generally, in robotics, two orthonormal coordinate frames are commonly used: the Earth-fixed inertial frame  $\{\mathcal{I}\}$ , composed of axes  $x_{\mathcal{I}}, y_{\mathcal{I}}, z_{\mathcal{I}}$ , and the body-fixed frame  $\{B\}$ , composed of the  $x_B, y_B, z_B$  axes, as shown in Figure 2.1.

The Earth's fixed inertial frame is a Cartesian spatial reference system that represents locations on the Earth as X, Y, and Z measurements from its center of mass [29]. To establish an Earth-fixed inertial frame, any point on the Earth's surface can be fixed as the frame of reference; assuming that the accelerations of any point at the surface of the Earth can be neglected [30]. The convention of this frame is similar to the North-East-Down (NED) convention, where  $x_{\mathcal{I}}$  points towards the true North,  $y_{\mathcal{I}}$  points towards the East, while the  $z_{\mathcal{I}}$  points downwards normal to the Earth's surface.

On the other hand, the body-fixed frame is attached to the vehicle, and fixed to its center of mass, which means that the axis  $x_B, y_B,$  and  $z_B$  coincide with the principal axes of inertia and are usually defined as  $x_B$  being the longitudinal axis (directed from the stern of the vehicle to fore),  $y_B$  being the transversal axis

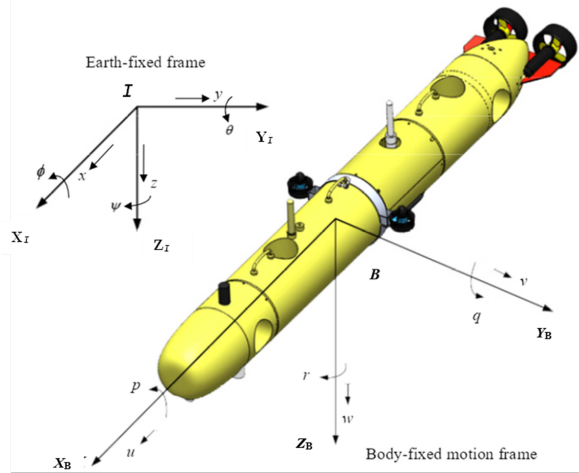


Figure 2.1: Body-fixed and Inertial Reference frames [7]

(directed from port to starboard), and  $z_B$  being the normal axis (directed from top to bottom). Hence, the position and orientation of a said vehicle with  $\{B\}$  are described relative to  $\{I\}$ , while the linear and angular velocities of the vehicle should be expressed in the body-fixed coordinate system.

For a typical marine vehicle with six degrees of freedom, six independent coordinates are needed to describe its position and orientation. The first three define the three-dimensional position  $(x, y, z)$  and are represented as the *surge*, *sway* and *heave* respectively. The last three are the Euler angles, which define its orientation and are given by  $(\psi, \theta, \phi)$  that represent the *roll*, *pitch*, and *yaw* of the vehicle respectively. To further define other notations, which will be called, in the subsequent discussion, the SNAME [28] notation is adopted and is defined as

- $\eta_1 = [x, y, z]^T$ : position of the origin of  $B$  expressed in the  $I$ , North ( $x$ ), East ( $y$ ), Down ( $z$ ),
- $\eta_2 = [\psi, \theta, \phi]^T$ : orientation of  $B$  with respect to  $I$ , Roll ( $\phi$ ), Pitch ( $\theta$ ), Yaw ( $\psi$ ),
- $\nu_1 = [u, v, w]^T$ : linear velocity of the origin of  $B$  relative to  $I$ , expressed in  $B$ ,
- $\nu_2 = [p, q, r]^T$ : angular velocity of  $B$  relative to  $I$ , expressed in  $B$ ,
- $\tau_1 = [X, Y, Z]^T$ : actuating forces expressed in  $B$ ,
- $\tau_2 = [K, M, N]^T$ : actuating moments expressed in  $B$ .

The above list and Table 2.1 are obtained from Fossen [9].

In a more compact form, it yields

$$\boldsymbol{\eta} = [\eta_1^T, \eta_2^T], \quad (2.1)$$

$$\boldsymbol{\nu} = [\nu_1^T, \nu_2^T], \quad (2.2)$$

$$\boldsymbol{\tau}_{RB} = [\tau_1^T, \tau_2^T]. \quad (2.3)$$

Table 2.1: Notation used for marine vehicles, adapted from Fossen [9]

Degree of Freedom	Forces and Moments	Linear and Angular Velocities	Positions and Euler Angles
1. Motions in the x-direction (surge)	$X$	$u$	$x$
2. Motions in the y-direction (sway)	$Y$	$v$	$y$
3. Motions in the z-direction (heave)	$Z$	$w$	$z$
4. Rotation about the x-axis (roll)	$K$	$p$	$\psi$
5. Rotation about the y-axis (pitch)	$M$	$q$	$\theta$
6. Rotation about the z-axis (yaw)	$N$	$r$	$\phi$

## 2.1.2 Kinematics

Kinematics deals with the geometrical aspects of motion and relates the velocities with position. Using the notation defined in Subsection 2.1.1 in Table 2.1, the kinematic equations can be expressed as

$$\dot{\eta} = \mathbf{J}(\eta)\nu, \quad (2.4)$$

where

$$\mathbf{J}(\eta) = \begin{bmatrix} {}^I_B\mathbf{R}(\Theta) & \mathbf{0}_{3 \times 3} \\ \mathbf{0}_{3 \times 3} & \mathbf{T}_\Theta(\Theta) \end{bmatrix}, \quad (2.5)$$

where  ${}^I_B\mathbf{R}(\Theta)$  is the rotation matrix from the  $\{B\}$  to  $\{I\}$  and  $\Theta = [\phi, \theta, \psi]^T$  is the attitude (Euler angles). In guidance, navigation and control applications, it is common to define this rotation by three successive rotations ( $zyx$ -convention) in terms of the Euler angles corresponding to  $\psi$ ,  $\theta$  and  $\phi$ . Mathematically, the rotation sequence is equivalent to

$${}^I_B\mathbf{R}(\Theta) := \mathbf{R}_{z,\psi}\mathbf{R}_{y,\theta}\mathbf{R}_{x,\phi}. \quad (2.6)$$

The principal rotation matrices are defined as

$$\mathbf{R}_{x,\phi} = \begin{bmatrix} 1 & 0 & 0 \\ 0 & c\phi & -s\phi \\ 0 & s\phi & c\phi \end{bmatrix}, \quad \mathbf{R}_{y,\theta} = \begin{bmatrix} c\theta & 0 & s\theta \\ 0 & 1 & 0 \\ -s\theta & 0 & c\theta \end{bmatrix}, \quad \text{and} \quad \mathbf{R}_{z,\psi} = \begin{bmatrix} c\psi & -s\psi & 0 \\ s\psi & c\psi & 0 \\ 0 & 0 & 1 \end{bmatrix}, \quad s \cdot = \sin(\cdot), \quad c \cdot = \cos(\cdot). \quad (2.7)$$

Substituting (2.7) into (2.6) yields the matrix

$${}^I_B\mathbf{R}(\Theta) = \begin{bmatrix} c\psi c\theta & c\psi s\theta s\psi - s\psi c\phi & c\psi s\theta c\phi + s\psi s\phi \\ s\psi c\theta & s\psi s\theta s\phi + c\psi c\phi & s\psi s\theta c\phi - c\psi s\phi \\ -s\theta & c\theta s\phi & c\theta c\phi \end{bmatrix}, \quad s \cdot = \sin(\cdot), \quad c \cdot = \cos(\cdot). \quad (2.8)$$

Furthermore,

$$\mathbf{T}_\Theta(\Theta) = \begin{bmatrix} 1 & s\phi t\theta & c\phi t\theta \\ 0 & c\phi & -s\phi \\ 0 & \frac{s\phi}{c\theta} & \frac{c\phi}{c\theta} \end{bmatrix}, \quad t \cdot = \tan(\cdot), \quad \theta \neq \pm 90^\circ, \quad (2.9)$$

is the Euler attitude transformation matrix that relates the body-fixed angular velocities  $(p, q, r)$  with the roll( $\phi$ ), pitch( $\theta$ ) and yaw( $\psi$ ) rates. However, this matrix is not defined for a pitch angle  $\theta = \pm 90^\circ$ . One solution is to use quaternion representation as described by Fossen [9] or another solution might be to avoid the singular points where the pitch angle  $\theta = \pm 90^\circ$ . The latter solution will be explored in this study.

It is worth noting that the kinematic equation in (2.4) is typical for six degrees of freedom underwater vehicles. However, this representation would not fit a surface craft with three degrees of freedom (surge, sway and yaw). Hence, in order to represent the kinematic equation for a typical 3-DOF surface craft, it is generally assumed that the roll angle ( $\phi$ ) and the pitch angle  $\theta$  are small and can be neglected. This is a good approximation for most conventional ships, surface crafts and rigs. Hence,  ${}^I_B \mathbf{R}(\Theta) = \mathbf{R}_{z,\psi} \mathbf{R}_{y,\theta} \mathbf{R}_{x,\phi} \approx \mathbf{R}_{z,\psi}$  and  $\mathbf{T}_\Theta(\Theta) \approx \mathbf{I}_{3 \times 3}$ . Neglecting the elements corresponding to heave, roll and pitch finally yields

$$\dot{\boldsymbol{\eta}} = \mathbf{R}(\psi) \boldsymbol{\nu}, \quad (2.10)$$

where  $\mathbf{R}(\psi) := \mathbf{R}_{z,\psi}$  with  $\boldsymbol{\nu}_r = [u, v, r]^T$  and  $\boldsymbol{\eta}_r = [x, y, \psi]^T$ .

### 2.1.3 Dynamics

This section presents the equations that deal with the forces and moments that act on the motion of a marine vehicle. In order to derive these equations of motion, Newton's second law of motion can be useful as illustrated by Fossen [9], since the forces and moments are generated by relative motion between the body and the fluid. Hence, it is convenient to formulate Newton's law in the body-fixed frame of the vehicle  $\{B\}$ . The rigid-body equation can be written as

$$\mathbf{M}_{RB} \dot{\boldsymbol{\nu}} + \mathbf{C}_{RB}(\boldsymbol{\nu}) \boldsymbol{\nu} = \boldsymbol{\tau}_{RB}, \quad (2.11)$$

where  $\mathbf{M}_{RB}$  is the rigid-body mass matrix,  $\mathbf{C}_{RB}$  is the rigid-body Coriolis and centripetal matrix due to the rotation of  $\{B\}$  about the inertial frame  $\{I\}$ ,  $\boldsymbol{\nu} = [u, v, w, p, q, r]^T$  is the generalized velocity vector expressed in  $\{B\}$  and  $\boldsymbol{\tau}_{RB}$  is a generalized vector of external forces and moments expressed in  $\{B\}$ .  $\boldsymbol{\tau}_{RB}$  can be further decomposed as

$$\boldsymbol{\tau}_{RB} = \boldsymbol{\tau} + \boldsymbol{\tau}_A + \boldsymbol{\tau}_D + \boldsymbol{\tau}_R + \boldsymbol{\tau}_{dist}. \quad (2.12)$$

- The term  $\boldsymbol{\tau}$  represents a vector of forces and torques related to thrusters/surfaces, usually for propulsion, and can be viewed as the control input.
- The term  $\boldsymbol{\tau}_A$  represents the vector of forces and moments due to the hydrodynamic added mass and

can be described as

$$\tau_A = -M_A \dot{v} - C_A(v)v, \quad (2.13)$$

where  $M_A$  is the added inertia matrix and  $C_A(v)$  is the hydrodynamic added Coriolis and centripetal contribution.

- $\tau_D$  represents the forces and moments generated by the hydrodynamic damping, which is the energy carried away due to lifting, drag, and skin friction, among others, represented in the form

$$\tau_D = -D(v)v, \quad (2.14)$$

where  $D(v)$  denotes the hydrodynamic damping matrix, which must be positive definite.

- $\tau_R$  represents the restoring forces and torques due to gravity and fluid density and can be expressed as

$$\tau_R = -g(\eta), \quad (2.15)$$

where  $g(\eta)$  denotes the restoring term.

- $\tau_{dist}$  represents the external disturbances such as waves, wind, and ocean currents.

Combining (2.13), (2.14), and (2.15) into (2.12) and then substituting the results into (2.11) yields

$$\underbrace{M_{RB}\dot{\nu} + C_{RB}(\nu)\nu}_{\text{Rigid-body terms}} + \underbrace{M_A\dot{\nu} + C_A(\nu)\nu + D(\nu)\nu}_{\text{Hydrodynamic terms}} + \underbrace{g(\eta)}_{\text{restoring term}} = \tau + \tau_{dist}. \quad (2.16)$$

(2.16) can therefore be represented as

$$M\dot{\nu} + C(\nu)\nu + D(\nu)\nu + g(\eta) = \tau + \tau_{dist}, \quad (2.17)$$

where  $M = M_{RB} + M_A$  is the combination of the rigid-body inertia matrix and the added inertia matrix, and  $C(\nu) = C_{RB}(\nu) + C_A(\nu)$  is the combination of the Coriolis and centripetal terms and the hydrodynamic added Coriolis and centripetal contribution matrix,  $D(\nu)$  is the damping matrix,  $g(\eta)$  is the vector of gravitational/buoyancy forces and moments and  $\tau$  is the vector of control inputs.

## 2.1.4 Simplified Equations

In this work, since we are working with vehicles that operate both in the 2D and 3D planes, a set of simplified equations will be presented accordingly.

For the vehicle operating in the 2D plane (surface vehicle), we assume that the roll angle  $\phi = 0$ , pitch angle  $\theta = 0$  and the heave  $z = \text{constant}$ . With this assumption, we end up with only three degrees of freedom

[surge ( $x$ ), sway ( $y$ ) and yaw ( $\psi$ )] to control. Following (2.10), in Section 2.1.2 with the rotation matrix

$$\mathbf{R}_z(\psi) = \begin{bmatrix} \cos(\psi) & -\sin(\psi) & 0 \\ \sin(\psi) & \cos(\psi) & 0 \\ 0 & 0 & 1 \end{bmatrix}, \quad (2.18)$$

a simplified kinematic model can be written as

$$\begin{aligned} \dot{x} &= u \cos(\psi) - v \sin(\psi), \\ \dot{y} &= u \sin(\psi) + v \cos(\psi), \\ \dot{\psi} &= r. \end{aligned} \quad (2.19)$$

The equation above does not account for external environmental disturbances whatsoever. The above assumption can be applied to the vehicle dynamics too, where the roll, pitch, and heave motion of the under-actuated vehicle are not considered. Without considering any disturbance, the dynamic equation can be written as

$$\begin{aligned} m_u \dot{u} - m_v vr + d_u u &= \tau_u, \\ m_v \dot{v} - m_u ur + d_v v &= 0, \\ m_r \dot{r} - m_{uv} uv + d_r r &= \tau_r, \end{aligned} \quad (2.20)$$

where  $\tau_u$  is the external force in the  $x$  direction (common mode), where the two thrusters work together to generate a surge motion. The external torque about the  $Z$ -axis (differential mode) is  $\tau_r$ , where the two thrusters work in opposite directions, creating a rotating motion for the vehicle. From the (2.20) above, it can be seen that the  $\tau_v$  is zero since the sway motion of a typical surface craft is not controllable because there are no control forces available. Explicitly stating the other terms of (2.20),

$$\begin{aligned} m_u &= m - X\dot{u}, & m_v &= m - Y\dot{v}, \\ m_r &= I_z - N\dot{r}, & m_{uv} &= m_u - m_v, \\ d_u &= -X_u - X_{|u|u}|u|, & d_v &= -Y_v - Y_{|v|v}|v|, \\ d_r &= -N_r - N_{|r|r}|r|, \end{aligned} \quad (2.21)$$

where  $m_u$ ,  $m_v$ , and  $m_{uv}$  represent the mass and hydrodynamic added mass with  $X\dot{u}$  being the force in the  $X$ -direction due to an acceleration in the  $x$ -direction,  $Y\dot{v}$  representing a force in the  $Y$ -direction due to an acceleration in the  $y$ -direction,  $N\dot{r}$  is the moment about the  $Z$ -axis expressed in  $\{B\}$  due to angular acceleration in the  $Z$ -axis and  $I_z$  is the moment of inertia about the  $Z$ -axis.  $d_u$ ,  $d_v$ , and  $d_r$  represent the hydrodynamic damping effects with  $X_{|u|u}|u|$  being the surge damping force due to surge motion,  $Y_{|v|v}|v|$  is the sway damping force due to sway motion and  $N_{|r|r}|r|$  is the yaw damping moment due to the yaw.

In the equation presented for the 3-DOF dynamic model, it can be observed that the restoring force and moment vector  $g(\eta)$  was not part of the equations. This is because the vehicle is neutrally buoyant and the center of gravity and the center of buoyancy is located vertically on the z-axis of the body-fixed frame  $B$ .

For the vehicle operating in the 3D plane, the 6-DOF equations of motions will be decomposed into a subsystem simple enough to capture the dynamics of the vehicle capable of solving the problem at hand. We assume that the sway ( $y$ ), the roll angle ( $\phi$ ) and the heave  $z$  can be neglected, thereby reducing the control task to the surge ( $x$ ), pitch ( $\theta$ ), and yaw ( $\psi$ ). Following these assumptions, a simplified kinematic model can be written as

$$\begin{aligned}\dot{x} &= u \cos(\psi) \cos(\theta) - v \sin(\psi), \\ \dot{\theta} &= q, \\ \dot{\psi} &= r.\end{aligned}\tag{2.22}$$

Furthermore, in formulating the dynamics of the vehicle, the same assumptions still hold resulting in the following

$$\begin{aligned}m_u \dot{u} + d_u u &= \tau_u, \\ m_q \dot{q} + d_q q + g &= \tau_q, \\ m_r \dot{r} + d_r r &= \tau_r,\end{aligned}\tag{2.23}$$

where  $\tau_u$  is the external force in the  $x$  direction (common mode), where the two thrusters work together to generate a surge motion, the external torque about the  $Z$ -axis (differential mode) is the  $\tau_r$ , where the two thrusters work against each other, creating a rotating motion for the vehicle and  $\tau_q$  is the external torque about the  $Y$ -axis. Explicitly stating the other terms of (2.23),

$$\begin{aligned}m_u &= m - X\dot{u}, & m_q &= I_y - M\dot{q}, \\ m_r &= I_z - N\dot{r}, \\ d_u &= -X_u - X_{|u|u}|u|, & d_q &= -M_q - M_{|q|q}|q|, \\ d_r &= -N_r - N_{|r|r}|r|, & g_q &= (BG_z W) \sin(\theta)\end{aligned}\tag{2.24}$$

where  $X\dot{u}$  is the force in the  $X$ -direction due to an acceleration in the  $x$ -direction,  $M\dot{q}$  is the pitch added mass coefficient due to pitch acceleration,  $N\dot{r}$  is the moment about the  $Z$ -axis expressed in  $\{B\}$  due to angular acceleration in the  $Z$ -axis and  $I_z$  and  $I_y$  is the moment of inertia about the  $Z$ -axis and  $Y$ -axis respectively.  $M_{|q|q}|q|$  being the damping force due to pitching, and  $N_{|r|r}|r|$  is the yaw damping moment due to the yaw.  $g$  is the restoring force,  $W$  is the weight of the body,  $B$  is the buoyancy force,  $G_z$ , the distance between the center of gravity (CG) and center of buoyancy (CB) along the  $Z$ -axis,  $m_u$ ,  $m_q$ , and  $m_r$  represent the mass

and hydrodynamic added mass and  $d_u$ ,  $d_q$ , and  $d_r$  represent the hydrodynamic damping effects.

## 2.2 Path Following

Path Following (PF) is one of the fundamental building blocks of this cooperative motion system. This guidance system is part of the motion control system implemented by the target/leader vehicles, thereby making it an indispensable subject matter. Therefore, this section outlines the existing theory and the frameworks supporting PF motion control. This will entail formulating the PF problem, reviewing already existing PF algorithms, their strengths and limitations, and choosing the most suitable for the task at hand. Hung et al. [8] did an extensive review on this subject and the topics developed in this chapter will bear some similarities with that research. And because the proposed PF approach only takes care of the motion in the horizontal plane, this chapter will also discuss an additional guidance system for vertical motion.

### 2.2.1 Path Following Overview

The problem of PF entails making a vehicle converge to, and then follow, a spatial path while asymptotically tracking the desired speed profile along the path as a secondary objective, as shown in Figure 2.2. In Path Following, the vehicle is not required to be at specific positions at specific instants of time, this is a stronger requirement and results in trajectory tracking [8]. In other words, in PF, the path is not parameterized by time but by a geometry-related parameter, usually the path length. With this flexibility, PF has been known to yield a smoother convergence to the path and equally has reduced demands on the actuators of the vehicle, as compared to other guidance systems [8]. One of this mission's characteristics is the requirement for the vehicles to perform long-term ocean observations. Therefore, the motion control algorithm to be selected plays a vital role in the rate at which the vehicle's energy is expended. With less demanding actuation signals and consequent reduction of actuator movement, a substantial amount of energy can be conserved, thereby prolonging the overall mission time of the vehicles. Hence, this makes PF the ideal choice for the target vehicles in this system.

PF is not specific to marine vehicles alone but has been widely applied to aerial vehicles, ground vehicles, autonomous cars, quad-rotors, mobile robots, etc. The typical structure of PF separates the dynamics from the kinematics of the vehicle, with the algorithms working on velocity and yaw rate references for the kinematics of the vehicles, which are identical for all 3D rigid bodies, which are then tracked by an inner loop controller taking into account the dynamics. In fact, some of the algorithms that are now been applied to marine vehicles, which will be discussed in the subsequent section, were originally developed in some of the fields previously mentioned. For instance, in PF, it is general knowledge that one can/should either stabilize the position error in the frame attached to a reference point moving along the path or stabilize the error in the frame attached to the vehicle. The former approach, which has been widely used, was first applied to a unicycle and two-wheeled mobile robots by Samson et al. [31]. This was later developed into a more

advanced PF algorithm by Lapierre et al. [32], Shuyou et al. [33], and Hung et al. [34], etc. These are pointers to the versatility of this scientific tool.

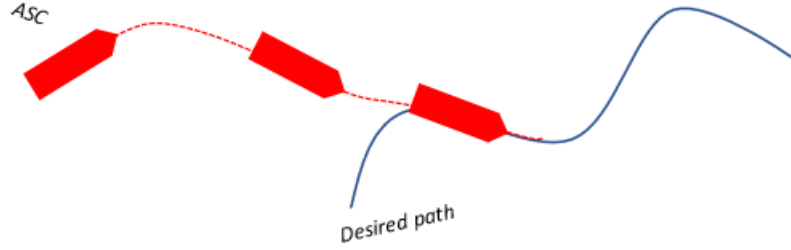


Figure 2.2: Geometric illustration of Path Following Problem.

In solving the PF problem, nonlinear control techniques such as backstepping, feedback linearization, sliding mode control, vector field, linear model predictive control (MPC), and nonlinear MPC (NMPC) are employed. In other PF algorithms, learning-based methods such as learning-based MPC (LB-MPC), and reinforcement learning-based control are also employed. In [32], the controller design builds on Lyapunov theory and backstepping techniques. The resulting nonlinear feedback control law yields convergence of the path following error trajectories to zero. However, the presence of ocean current disturbances was not taken into account in the design of the controller. In contrast, in [34], ocean current disturbance was factored into the design of the controller. In addition to using the Lyapunov design approach similar to the previous one, MPC framework was employed. The proposed MPC approach showed faster convergence to the path compared to the Lyapunov approach. In [33], a general non-linear MPC scheme for the path following problem was employed, where the time evolution of the path parameter and its initial value are all determined online.

In this study, the feedback linearization approach will be employed to solve the PF task. Furthermore, depending on the type of PF algorithm employed, the desired reference output to be tracked varies. The desired references can be the linear speed ( $u$ ), and the vehicle's heading/yaw angle ( $\psi$ ) or heading/yaw rate ( $r$ ) or the assigned speed of the reference point along the path. This and more will be discussed in the sections that follow.

## 2.2.2 Path Following Notation

In Section 2.1.1, some notation and nomenclature were presented after the SNAME [28] convention. Notations particular to the PF problem are presented in this work.

- Let  $Q$  be the center of mass of the vehicle and denote by  $p = [x; y] \in \mathbb{R}^2$  the position of  $Q$  in  $\{\mathcal{I}\}$ .
- Let  $\{B\} = \{x_B, y_B\}$  be a body-fixed frame whose origin is located at  $Q$ .

- In addition, denote by  $\mathbf{v} = [u, v]^T \in \mathbb{R}^2$  the vehicle's velocity vector with respect to the fluid, measured in  $\{B\}$ , where  $u$  and  $v$  are the surge/longitudinal and sway/lateral speeds, respectively.
- Let  $\mathcal{P}(\gamma)$  be the 2D spatial path parametrized by the scalar variable  $\gamma$ .
- Denote by  $p_d$ , the position of a generic point on the path in the inertial frame  $\{I\}$  described by the vector  $\mathbf{p}_d = [x_d(\gamma), y_d(\gamma)]^T \in \mathbb{R}^2$ .
- Let  $\mathbf{e}_p \triangleq [s_1; y_1]^T \in \mathbb{R}^2$  be a vector defining the position error between the vehicle and the reference point  $p_d$ , where  $s_1$  and  $y_1$  are called along-track and cross-track errors, respectively.

### 2.2.3 Path Parameterization and Path Frames

According to the definition given by Skjetne et al. [35], a parametrized path  $\mathcal{P}$  can be defined as a geometric curve  $\mathbf{p}_d(\gamma) \in \mathbb{R}^h$  with  $h \geq 1$  parametrized by a continuous path variable  $\gamma$  (eg. arc-length of the path). Usually,  $\gamma \in \Omega := [a, b]$  where  $a, b \in \mathbb{R}$  are values of  $\gamma$  corresponding to the points at the beginning and end of the path. In designing the PF controller, the desired path will be parametrized.

To formulate the PF problem, additional two frames are usually employed in several works of literature to describe the position error between the vehicle and the path. These are the Frenet-Serret (F-S) and the Parallel Transport (P-T) frames and each has its own advantages and disadvantages, as highlighted in the sequel.

#### Frenet-Serret (F-S) Frame

The Frenet-Serret frame is a mathematical concept used in differential geometry to describe the local behaviour of a curve in three-dimensional space. It provides a coordinate system attached to a curve, consisting of three mutually orthogonal vectors: the tangent vector ( $T$ ), the normal vector ( $N$ ), and the binormal vector ( $B$ ). Figure 2.3 gives a graphic illustration of these vectors.

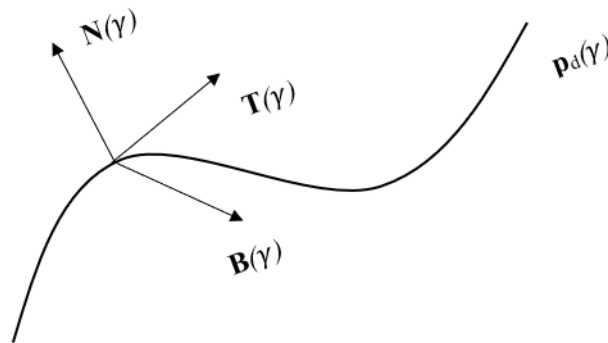


Figure 2.3: An illustration of Frenet-Serret  $\{\mathcal{F}\}$  in 2D

- $T$  is the unit vector tangent to the curve, pointing in the direction of motion.

$$\mathbf{T}(\gamma) = \frac{\dot{\mathbf{p}}_d(\gamma)}{\|\dot{\mathbf{p}}_d(\gamma)\|}. \quad (2.25)$$

- $N$  is the normal unit vector, the derivative of  $T$  with respect to the arc-length parameter  $\gamma$  of the curve, divided by its length. It describes how the curve is bending at a given point and points towards the center of curvature of the curve.

$$\mathbf{N}(\gamma) = \frac{\dot{\mathbf{T}}(\gamma)}{\|\dot{\mathbf{T}}(\gamma)\|} = \frac{\dot{\mathbf{p}}_d(\gamma) \times (\ddot{\mathbf{p}}_d(\gamma) \times \dot{\mathbf{p}}_d(\gamma))}{\|\dot{\mathbf{p}}_d(\gamma)\| \|\ddot{\mathbf{p}}_d(\gamma) \times \dot{\mathbf{p}}_d(\gamma)\|}. \quad (2.26)$$

- $B$  is the binormal unit vector, the cross product of  $T$  and  $N$ . The binormal vector describes the twisting or torsion of the curve.

$$\mathbf{B}(\gamma) = \mathbf{T}(\gamma) \times \mathbf{N}(\gamma) = \frac{\dot{\mathbf{p}}_d(\gamma) \times \ddot{\mathbf{p}}_d(\gamma)}{\|\dot{\mathbf{p}}_d(\gamma)\| \times \|\dot{\mathbf{p}}_d(\gamma)\|}. \quad (2.27)$$

The Frenet–Serret formulas can also be stated more concisely using matrix notation

$$\begin{bmatrix} \dot{\mathbf{T}} \\ \dot{\mathbf{N}} \\ \dot{\mathbf{B}} \end{bmatrix} = \|\dot{\mathbf{p}}_d(\gamma)\| \begin{bmatrix} 0 & \kappa & 0 \\ -\kappa & 0 & \tau \\ 0 & -\tau & 0 \end{bmatrix} \begin{bmatrix} \mathbf{T} \\ \mathbf{N} \\ \mathbf{B} \end{bmatrix}, \quad (2.28)$$

where  $\kappa$  is the curvature and  $\tau$  is the torsion. In simple terms, curvature measures the rate at which the path changes, with higher curvature resulting in sharper turns. The Frenet–Serret formulas apply only to non-degenerate curves, meaning they must have nonzero curvature [36][37], as the F-S frame is not well-defined for paths that have a vanishing second derivative (i.e. zero curvature) such as straight lines or non-convex curves (curvature that extends or bends inward).

However, because we are considering the PF problem in 2D, only the  $T$  unit vector tangent and the normal unit vector  $N$  will be considered.

### Parallel Transport Frame

The Parallel Transport Frame, on the other hand, is composed of a tangent vector  $T$  and two normal vectors ( $N_1, N_2$ ) at each point along the curve. These vectors, when parallel transported along a curve, preserve their orientation without rotation or change in magnitude along the curve. Hence, they maintain a consistent reference frame along the path irrespective of the curvature. This is made possible because, since the tangent vector is always unique, we can always choose any convenient arbitrary normal vector to make it perpendicular to the tangent and vary smoothly throughout the path regardless of the curvature.

In 2D, to define the P-T frame, we specify the tangent basic vector  $T$  as in (2.25). The second basic vector, called normal vector  $N_1$ , is obtained by rotating the tangent vector 90 ° clockwise. This is also equivalent to translating  $\{\mathcal{T}\}$  to the reference point P and then rotating it about the z-axis by the angle

$$\psi_p = \arctan\left(\frac{\dot{y}_d(\gamma)}{\dot{x}_d(\gamma)}\right). \quad (2.29)$$

The difference between the F-S frame and the P-T frame is illustrated in Figure 2.4. With the F-S frame, the normal component always points to the center of curvature thus, its direction switches at inflection points, while the P-T frame has no such discontinuities. From a PF formulation standpoint, with the F-S frame, the path following error is not well-defined at inflection points because the cross-track error (the position error projected on the normal vector) switches sign, which is not the case with the P-T frame [8]. Therefore, owing to the advantage that the P-T frame presents in comparison to the F-S frame, i.e. it avoids the singularity when the path has a vanishing second derivative, e.g. concave paths, the P-T frame will be used in formulating the PF problem in Section 3.2.

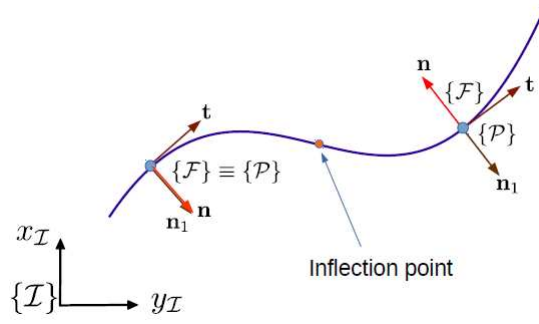


Figure 2.4: An illustration of Frenet-Serret  $\{\mathcal{F}\}$  and Parallel Transport  $\{\mathcal{P}\}$  frames in 2D [8]

## 2.2.4 Path Following Problem Formulation

At the end of the day, we anticipate the target vehicles to demonstrate concurrent motion in the horizontal and vertical planes. To achieve this, there is a need to decouple the horizontal and vertical motions, enabling the development of two distinct guidance laws for each scenario. Consequently, the horizontal guidance law generates the course commands and the vertical guidance law computes the desired pitch angle  $\theta$ . As a result, our PF algorithm will handle the motion in the horizontal plane while the vertical guidance law will be treated in Section 2.3 of this chapter. Hence, our PF problem becomes a 2D task defined as follows.

Given the 2-D spatial path  $\mathcal{P}$  described by  $\mathbf{p}_d = [x_d(\gamma), y_d(\gamma)]^T \in \mathbb{R}^2$ , and a vehicle with the kinematics model described in (2.22), derive a feedback control law for the vehicle's inputs  $(u, r)$  to fulfil the following tasks:

*i.) Geometric task:* To steer the position error  $\mathbf{e}_p \triangleq \mathbf{p} - \mathbf{p}_d$  such that

$$\lim_{t \rightarrow \infty} \mathbf{e}(t) = 0. \quad (2.30)$$

ii.) **Dynamic task:** To ensure that the vehicle's forward speed  $u$ , tracks a positive desired speed profile  $U_d$ , i.e.,

$$\lim_{t \rightarrow \infty} u(t) - U_d(t) = 0. \quad (2.31)$$

Consider  $u_{\mathcal{P}}$  to be the speed of the reference point  $p_d$  on the path with respect to the inertial frame, given by

$$u_{\mathcal{P}} = \|\dot{\mathbf{p}}_d(\gamma)\| \dot{\gamma}, \quad (2.32)$$

where  $\dot{\gamma}$  is the arbitrary rate of evolution  $\gamma$  of the "reference point" along the path. In PF, the reference point  $p_d$  is pivotal in enabling the vehicle to track the path. In some works, the point can be chosen as the nearest point to the vehicle, i.e. the orthogonal projection of the vehicle on the path (in case it is well defined), or can be initialized arbitrarily anywhere on the path with its evolution controlled through  $\dot{\gamma}$ .

Whenever the vehicle achieves a precise Path Following, both the speed of the vehicle and the point  $p_d$  will move with the desired speed profile, such that  $u = u_{\mathcal{P}} = U_d$ . In this case, the equivalent of the dynamic task in (2.31) can also be written as

$$\lim_{t \rightarrow \infty} \dot{\gamma}(t) - v_d(\gamma, t) = 0, \quad (2.33)$$

where  $v_d$  now becomes the desired speed profile for  $\dot{\gamma}$ , and is defined by

$$v_d(\gamma, t) \triangleq \frac{1}{\|\dot{\mathbf{p}}_d(\gamma)\|} U_d(\gamma, t). \quad (2.34)$$

Having spelt out the problem to be solved, the next section will review the main strategies; that have been used to solve it.

## 2.2.5 Review of Path Following Strategies

Various survey papers have presented diverse Path Following methods. However, Hung et al. [8] was able to classify various path-following algorithms into two categories based on the choice of the reference frame in which the path-following error was defined. In the first category, the methods aim to stabilize the position error in the vehicle's body frame, as considered in [38] and [39] whereas, in the second category, the methods stabilize the position error in a frame attached to a reference point moving along the path, such as the Frenet-Serret (F-S) frame or the Parallel Transport (P-T) frame as presented in [40],[33],[34]. The second approach is quite common as the popular Line of sight (LOS) algorithm and its derivatives follow the second convention. Hence, in the section that follows, some of the PF algorithms are presented in line with the second approach. Also, the control strategies used to drive the errors to zero will be discussed, coupled with the strengths and limitations associated with them as researched by Hung et al. [8]. The two approaches will be discussed but with much emphasis placed on the method that stabilizes the PF error in the path frame.

## Stabilizing Path Following Error in the Body Frame

- a. **Method 1:** The work by Aguiar et al. [38] addresses the problem of position trajectory-tracking and path-following control design for underactuated autonomous vehicles in the presence of possibly large modelling parametric uncertainty. A peculiar highlight in this paper is how the solution developed to solve the problem of global boundedness and convergence of the position-tracking error parametric uncertainty was applied to solve the PF problem. The solution developed involved the design of an adaptive switching supervisory controller combined with a nonlinear Lyapunov-based tracking control law. In that literature, attention was paid to modelling parametric uncertainty in the model of the vehicle such as mass and added mass for underwater vehicles which may be subject to large variations according to the payload configuration, and friction coefficients that are usually strongly dependent on the environmental conditions. The idea behind the design of the controller is that instead of employing the classical approach to adaptive control that solely relies on continuous tuning, hybrid adaptive algorithms based on switching and logic were employed. In the supervisory control, a suitable family of candidate controllers were designed, where each controller is designed for an admissible nominal model of the process, and a supervision logic orchestrates the switching among the candidate controllers, deciding, at each instant of time, the candidate feedback controller that is more adequate. In order to guarantee stability and avoid chattering, a form of hysteresis is employed.[38]. The algorithm was applied to a hover vehicle moving in a 2D space and an underwater vehicle moving in a 3D space. Simulations show that the control objectives were accomplished.
- b. **Method 2:** The paper by Alessandretti et al. [39] addresses the design of MPC laws to solve the trajectory-tracking problem and the PF problem for constrained under-actuated vehicles. The proposed MPC controllers are applied to the motion of vehicles moving in 2D and 3D. Allowing an asymptotic tracking error, the terminal set and the terminal law were computed avoiding linearization procedures. This results in MPC strategies where, for a given horizon length, the size of the region of attraction is only limited by the size of the constraints, leading to global solutions for unconstrained systems.

## Stabilizing Path Following Error in the Path Frame

- a. **Method 1:** The work by Micaelli et al. [31] proposes two general controllers for a unicycle-type and two-steering-wheel mobile robots. The first controller employs the feedback linearization strategy to solve the trajectory tracking problem for the robots and the second is the Lyapunov-oriented control design approach to solve the same problem. This method aims to achieve PF by controlling the vehicle's *linear speed* ( $u$ ) and the *angular rate* ( $\omega$  as used in the paper). The robot state is parametrized relative to

the followed path, in terms of distance and orientation. In this method, the "reference point" is chosen as the orthogonal projection of the real vehicle on the path, that is, the point on the path closest to the vehicle (if it is well-defined). With this strategy, the along-track error is always zero, i.e.  $s_1(t) = 0$  for all  $t$ . Thus, only the cross-track  $y_1$  needs to be stabilized to zero to fulfil the geometry task. One of the drawbacks of this algorithm is that an optimization problem has to be solved to find the point on the path closest to the vehicle. This, however, can be computationally demanding onboard computation capabilities.

- b. **Method 2:** Lapierre et al. [32] proposes another method for the design of path-following systems for AUVs. Instead of developing a PF algorithm using the vehicle's kinematic model alone, a PF control system was also designed using the vehicle's dynamic model. Unlike in land vehicles, where kinematics is sufficient for its control, dynamics play a key role in the motion of marine vehicles, thus requiring the development of methodologies for accurate PF systems that explicitly take into account the presence of possibly complex, nonlinear hydro-dynamic terms.

In that work, instead of projecting the vehicle on the path, representing the closest point on the path to the vehicle, the authors adopt another approach in establishing a moving virtual target on the path. The Path Following system is designed by explicitly controlling the rate of progression of the "virtual target" ( $\dot{\gamma}$ ) along the path, thus bypassing the problems that arise when the position of the virtual target is defined by the projection of the actual vehicle onto that path. That is, the Frenet frame is not attached to the point on the path that is closest to the vehicle but is based on the position of this virtual target. This yields an extra controllable degree of freedom corresponding  $\dot{\gamma}$ . Thus, this method aims to achieve PF by controlling the  $u, r$ , and  $\gamma$ . The PF controller design builds on Lyapunov theory and backstepping techniques to achieve the desired result. The first controller is a kinematic controller adopting the yaw rate  $r = (\dot{\psi})$  as a "virtual" control input and assuming that the actual surge speed equals the desired speed  $U_d(t)$ . The second controller addresses the vehicle dynamics, builds on the kinematic controller derived, and uses backstepping techniques to obtain control laws for the input variables force  $F$ , and torque  $\Gamma$ . The resulting nonlinear feedback control law yields convergence of the path following error trajectories to zero. One drawback of this method, is that because there are three tuning parameters ( $k_1, k_2, k_3$ ) for the controller, tuning the controller to give the desired result will require a good understanding of how each parameter affects the dynamics of the controller.

- c. **Method 3:** In the work by Fossen et al. [41], a nonlinear controller for path following of 3-DOF marine craft was derived using only two controls namely; surge and yaw control. The control laws in surge and yaw are derived using the vectorial backstepping approach. In addition, the controller utilizes the popular line-of-sight algorithm to minimize cross-track error. The Line of sight (LOS) method is one of if not the most, notable PF algorithm in guidance and control systems. The LOS compute the desired steering angle of the vehicle, based on a certain measure of distance to a target or position in sight

[42]. In other words, the LOS algorithm targets a point on the path using a desired measurement method. Since the LOS minimizes the cross-track error, the along track-error  $s_1(t)$  is zero for all  $t$ . This method is similar to the first method earlier described where a point on the path closest to the vehicle is required. However, in this method, the LOS selects a point on the path which might not necessarily be the closest point on the path to the vehicle. Hence, it removes the burden of solving an optimization problem and relaxes the problem to get a point on the path specified by the lookahead distance  $\Delta > 0$ . The authors used a fixed lookahead distance while presenting the LOS algorithm. However, Lekkas et al. [43] introduced a time-varying lookahead distance to improve the convergence to the path.

- d. **Method 4:** Shuyou et al. [33] presents a general nonlinear model predictive control (NMPC) scheme was developed to solve the path-following problem for a car-like mobile robot. In this paper, the time evolution of the path parameter and its initial value are all determined online through an optimization technique. The NMPC uses a prediction input function to solve the optimization problem in order to output a new path parameter. Some nonlinear constraints that minimize the value of the input over the cost functional  $J(x(t))$  are used. The control input in this case is the linear speed and the angular speed. Proof of feasibility and convergence of the introduced NMPC scheme is presented in the paper. However, solving online optimization problems can be computationally intensive for the AMVs.

## 2.3 Vertical Motion Guidance System

As part of the desired characteristic motion of the target vehicle, the target vehicle should be able to perform a saw-tooth wave-like maneuver in the vertical plane. While discussing the intricacies of Path Following as it concerns this study in the sections above, it was noted that PF was applied only to the horizontal motion of the target vehicle. In order to control the vertical motion of the vehicle, we will be controlling the pitch angle of the vehicle which will yield the desired motion in the vertical plane.

Considering the kinematic model of the vehicle presented in (2.22), we assume that all other parameters except the pitch angle will be controlled. The glider vehicle performs optimally if moving in a yo-yo pattern. Hence, the control law for the pitch angle  $\theta$  is defined as

$$\begin{cases} z(t) \leq 1, & \theta(z) = -50^\circ, \\ z(t) \geq n, & \theta(z) = 50^\circ, \end{cases} \quad (2.35)$$

where  $z$  is the depth of the vehicle at time  $t$  and  $n > 1$  is the maximum depth the vehicle will reach during the yo-yo maneuver. From the previous expression, it can be noted that the control law for the pitch is a function of the depth. For the vehicle to perform the required vertical maneuver as it follows its given path in the horizontal plane, the depth information of the vehicle is required for the pitch reference controller.

## 2.4 Target Tracking

Target tracking can be traced back to the development of early radar systems during World War II. Radar technology allows for the detection and tracking of aircraft, ships, and other objects. During those times, target tracking was used in missile systems to engage enemy aircraft. These missile systems carried their own radar to track a target until it was intercepted. Furthermore, in naval warfare, target tracking is also used to detect and track enemy ships and submarines, among other applications. This shows that the prime application of this technology started with military and defence operations. However, over the years, its application has expanded to critical areas of research and development, such as aerospace, robotics, surveillance, autonomous vehicles, and more.

With that being said, it's worth noting that target tracking is native to the animal world as target tracking plays a crucial role in various aspects of their survival, reproduction, and hunting strategies. For instance, the Cheetah is known for its exceptional speed and agility, which it uses to track and predict the future motion of fast-moving prey. Also, dolphins and orcas are skilled at coordinating group hunting efforts to encircle and herd schools of fish, effectively tracking and capturing their targets. In fact, the intuition behind some of the algorithms discussed in this chapter originates from observing the way some of these animals survive in the wild.

In the context of guidance, navigation and control, target tracking refers to the process by which the information received from sensor measurements is used to estimate the state of the target object, such as the target's position, velocity, and orientation. This information is then used to guide and control the tracker vehicle towards the target [25]. In target tracking, information about the path or trajectory and the future motion of the target is unknown. Hence, with only information about the present state of the target, guidance laws can be designed for the tracker/interceptor to track/intercept the target. Therefore, in this section, the theory that supports target tracking will be discussed and guidance laws for the tracker vehicle will be developed as well.

### 2.4.1 Target Tracking Problem Formulation

Consider the 2D position of the target denoted by  $\mathbf{p}_d = [x_d, y_d]^T$  and let the position of the tracker vehicle be denoted by  $\mathbf{p} = [x, y]^T \in \mathbb{R}^2$ , the control objective of a target-tracking scenario can be stated as

$$\lim_{t \rightarrow \infty} [\mathbf{p}(t) - \mathbf{p}_d(t)] = 0, \quad (2.36)$$

where  $\mathbf{p}_d(t)$  is moving by a (non-zero and bounded) velocity  $\mathbf{v}_d(t) \triangleq \dot{\mathbf{p}}_d(t) \in \mathbb{R}^2$ .

To achieve this control objective, control laws for the tracker's speed and orientation are designed to guide the tracker to the target. Unlike in the missile guidance community, where the goal is to intercept and neutralise the target, our goal is for the tracker to catch up with the target and follow the target *pari passu*. In view of the above objective, the following subsections will present the design of these controllers.

## 2.4.2 Target Tracking Strategies

In the missile guidance community, an object that is supposed to destroy another object is referred to as a missile, an interceptor or a pursuer. Conversely, the threatened object is typically called a target or an evader [9]. However, since the area of application is in the field of robotics, the designations tracker and target will be used for the ASC and target AUV, respectively. As used in the missile guidance community, an interceptor typically undergoes three phases during its operation:

1. Launch phase
2. Midcourse phase
3. Terminal phase

The greatest accuracy demand is associated with the terminal phase, where the interceptor guidance system must compensate for the accumulated errors from the previous phases to achieve the smallest possible final miss distance to the target [9]. Our area of focus is the terminal phase of the operation. Breivik et al. [44], presented three terminal guidance strategies, line-of-sight, pure pursuit and constant bearing, which will be discussed in the subsection that follows.

### Pure Pursuit Guidance

Pure pursuit is a tracking algorithm that calculates the bearing that will move an interceptor from its current position to a goal position [45]. The algorithm starts with the choice of a goal position that is some distance ahead of the interceptor, along the line of sight vector between the interceptor and the target, as illustrated in Figure 2.5. The interceptors velocity vector is always directed towards the target, and the rate of turn of the interceptor is always equal to the rate of turn of the line-of-sight [46]. We can think of the interceptor as pursuing a moving point along the LOS vector, at a fixed distance from the interceptor. The interceptor then chooses the desired velocity  $\mathbf{v}_d$  with which it aims to intersect the target. This strategy is inspired by a predator chasing a prey in the animal world, and very often results in a tail chase situation [9]. The desired velocity can be expressed as

$$\mathbf{v}_d = -\kappa \frac{\tilde{\mathbf{p}}}{\|\tilde{\mathbf{p}}\|} \quad (2.37)$$

where  $\kappa > 0$ , and  $\tilde{\mathbf{p}} := \mathbf{p} - \mathbf{p}_d$  is the LOS vector between the interceptor and the target. Pure Pursuit can track both stationary and moving targets. It continuously updates the target point on the desired path based on the vehicle's position.

### Constant Bearing Guidance

Constant Bearing Guidance calculates the steering angle based on the target's current position and maintains a constant angle between the vehicle's heading and the target as illustrated in Figure 2.6. In simple terms,

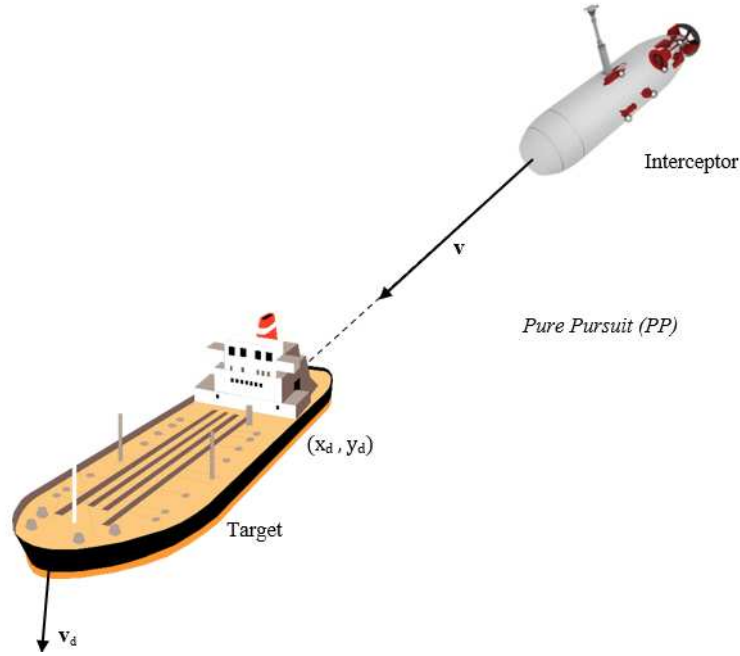


Figure 2.5: Pure Pursuit Guidance Illustrated, Adapted from [9].

the interceptor continuously adjusts its heading or course to maintain a fixed angle relative to the target. This angle is typically measured in relation to the interceptors' current position and is kept constant throughout the guidance process. By doing so, the interceptor will follow a curved path that converges towards the target, assuming there are no external factors affecting its trajectory.

The constant bearing angle is usually set based on the desired position relative to the target. For instance, the constant bearing rule has been used for centuries by mariners to avoid collisions at sea, by steering away from a situation where another craft approaches at a constant bearing. Thus, this guidance principle can be applied to avoid collisions and also to make one happen [9]. The CB guidance desired velocity is given by

$$\mathbf{v} = \mathbf{v}_d + \mathbf{v}_a, \quad (2.38)$$

$$\mathbf{v}_a = -\kappa \frac{\tilde{\mathbf{p}}}{\|\tilde{\mathbf{p}}\|} \quad (2.39)$$

where where  $\mathbf{v}_d$  is the target velocity vector,  $\mathbf{v}_a$  is the approach velocity vector and

$$\kappa = U_a^{max} \frac{\|\tilde{\mathbf{p}}\|}{\sqrt{(\tilde{\mathbf{p}})^T \tilde{\mathbf{p}} + \Delta_p^2}} \quad (2.40)$$

where  $U_a^{max}$  specifies the maximum approach speed toward the target and  $\Delta > 0$  affects the transient interceptor–target rendezvous behaviour.

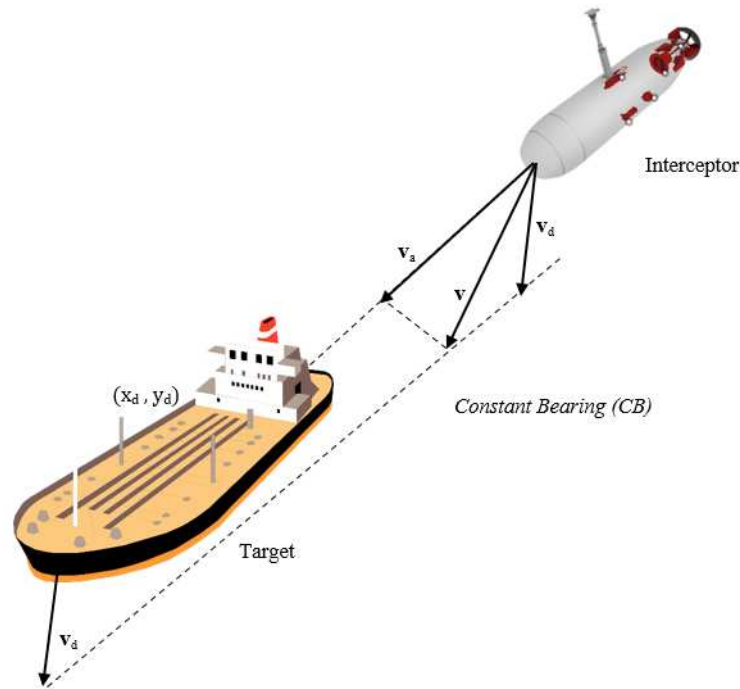


Figure 2.6: Constant Bearing Guidance Illustrated, Adapted from [9].

### Line of Sight Guidance

Line-of-sight (LOS) guidance can be categorized as a three-point guidance system that forms a triangular configuration. This configuration involves a stationary reference point along with the interceptor and the target. As per the definition provided in reference [47], LOS refers to the line originating from a reference point, which can be the aircraft, missile, or vessel and extending through the guidance objective, which is the target. In context of target tracking application, the LOS vector starts at the interceptor and passes through a point  $p_{los}(x_{los}, y_{los})$  which is located on the target's longitudinal axis at a lookahead distance  $\Delta > 0$  ahead of the direct projection of the target's position  $p(x, y)$  on to target's longitudinal axis[48]. Figure 2.7 provides a visual representation of the LOS guidance principle, wherein the velocity vector of the interceptor is pointed to LOS vector to achieve the intended velocity vector  $\mathbf{v}$ .

One strength of Pure Pursuit is its ability to adjust its speed as it approaches the target. However, there are times when the tracker will be slightly ahead of the target and will have to turn back to pursue it again. This is a limitation of Pure Pursuit since it only considers the target's position and nothing else. This is not suitable for our study. Even though the tracker should follow the target in real-time, we do not want the tracker to constantly turn back every time it gets ahead of the target.

On the other hand, Constant Bearing brings a unique approach to how the tracker chases the target. It incorporates the speed information of the target into its own calculations to pursue the target. However, a drawback is that it keeps the target at a constant angle. This may not be energy-efficient, as we require

a system for long-term observation. It will consistently make extra turns that might not be necessary since it always adjusts its angle to remain constant in relation to the target. Therefore, it is not suitable for this study. However, we will consider adapting the way it incorporates the speed information of the target as a feedforward term.

The desired heading algorithm is somewhat similar to one individual closely following another individual, like stalking, but in close proximity. The Line-of-Sight (LOS) strategy is a three-point guidance approach, which considers not only the position of the target and the tracker but also an additional point. Therefore, the LOS guidance strategy will be suitable to achieving the intended vehicle formation. Details of the velocity and orientation computation will be discussed in Section 3.3 and 3.4 respectively.

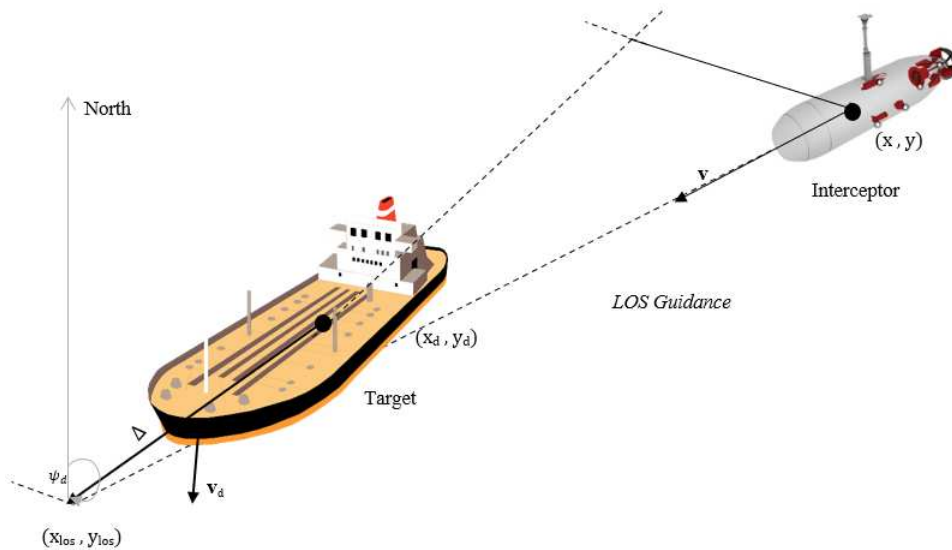


Figure 2.7: LOS Guidance Illustrated, Adapted from [9].

## 2.5 Cooperative Multiple Vehicle Formation Control

In the previous sections of this chapter, the theory behind the concepts that are relevant to the development of underwater vehicle motion control systems has been laid line upon line. However, the goal of this project is not purely Path Following nor is it purely Target Tracking, but cooperation between multiple heterogeneous vehicles. To bring into full view the intended system, cooperation between the vehicles becomes a subject matter for discussion. In this section, the method that will ensure the cooperation of the vehicles in the formation will be discussed.

## 2.5.1 Cooperative Motion System

In general terms, cooperation between autonomous vehicles, be it marine, ground or aerial involves a system where the motion of one or more vehicle(s) in the formation depends on the other or in some cases their motion depends on each other in such formation. To implement such a system, each vehicle control will have to rely on information provided during communication with neighbouring vehicle(s) of interest. Hence, graph theory becomes the tool *par excellence* to model the constraints imposed by the communication topology among the vehicles. Vehicles will broadcast their position, orientation and velocities, and this study is under the assumption that communication is continuous. However, this thesis will not discuss how they are obtained seeing that our interest is in the use of the information obtained in the network and not necessarily how the information is obtained. Therefore, the problem of navigation will not be addressed in this study. Nonetheless, these references [49], [50] and [51] provide depth of insights into the subject of communication amongst marine vehicles.

Following the concepts from algebraic graph theory as described in [52], let  $\mathcal{G}(\mathcal{V}, \mathcal{E})$  be the directed graph used to represent the inter-vehicle communication network, with  $\mathcal{V}$  denoting the set of  $n$  nodes (each corresponding to a vehicle) and  $\mathcal{E}$  the set of edges (each standing for a data link). Nodes  $i$  and  $j$  are said to be adjacent if there is an edge between them. To represent the connections between vehicles, an adjacency matrix  $\mathbf{A}$  is defined, where a link between vehicles is represented in the matrix as  $a_{ij} = 1$  and the lack of a communication channel  $a_{ij} = 0$ , with  $i$  and  $j$  being the line and columns, respectively. The degree matrix  $\mathbf{D}$  of the graph  $\mathcal{G}$  is the diagonal of the matrix that represents the out-degrees of each node in the graph which is the network of vehicles. Figure 2.8 is a representation of the vehicle topology network for this study where each node 1 and node 2 corresponds to the two AUVs and node 0 corresponds to the ASC.

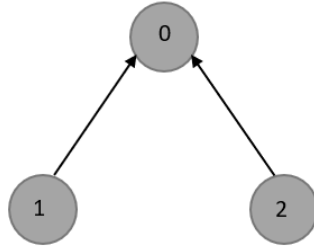


Figure 2.8: A Directed Graph of the Vehicle Network Topology.

The respective matrices that characterise the network are

$$\mathbf{A} = \begin{bmatrix} 0 & 0 & 0 \\ 1 & 0 & 0 \\ 1 & 0 & 0 \end{bmatrix}, \mathbf{D} = \begin{bmatrix} 0 & 0 & 0 \\ 0 & 1 & 0 \\ 0 & 0 & 1 \end{bmatrix}. \quad (2.41)$$

From the above communication topology, the only vehicle that uses the information from the network is the

surface craft while the motion of the two AUVs are independent, i.e., their movement does not depend on what the ASC is doing. The question now becomes how can the ASC use the information to follow the vehicles in the network. To answer this question, we present two approaches in which the surface craft can move in cooperation with the two underwater vehicles.

### Scenario I

In this approach, the ASC is expected to follow the two AUVs intermittently such that it follows one at a time and later switches to the other. To achieve this a time function will be introduced such that the switching of which vehicle it follows will be dependent on the time function. Let the Target Tracking task be Tgt, such that the tracker vehicle tracks one vehicle ( $vh_n$ ) at the time ( $t$ ) where  $n$  is the vehicle's ID. These can be written as

$$\text{Tgt}(t(vh_n)) = \begin{cases} t \in [0, t_{duration}], & \text{track AUV}_1, \\ t \in [t_{duration}, t_{duration} * 2], & \text{track AUV}_2, \\ t \in [t_{duration} * 2, t_{duration} * 3], & \text{track AUV}_1, \\ t \in [t_{duration} * 3, t_{duration} * 4], & \text{track AUV}_2, \\ (\dots) & \end{cases} \quad (2.42)$$

where the duration for tracking each vehicle is  $t_{duration}$  in seconds. In 2.42, the tracker begins to follow the first AUV<sub>1</sub> for the given duration. After following the first vehicle, for the given duration, it switches to track the other vehicle, and this cycle continues. A description of this scenario can be seen in Figure 2.9 below.

In Ocean Observation, there is not much complexity associated with data acquisition other than sampling the parameters that the deployed sensors are equipped to handle. In simple terms, it involves measuring the general chemical and physical properties of the ocean without any specific focus. Hence, there might be no need to use specialized functions, reinforcement learning, or optimization algorithms to implement the switching strategy. Conversely, if a specific phenomenon is under study, such as algae bloom in the ocean, radioactivity monitoring, CO<sub>2</sub> variation in the ocean, or pollutant monitoring, the system will have to rely on feedback measurements from the underwater vehicles to decide which vehicle to follow and for how long. Therefore, a more advanced algorithm will be needed to determine which vehicle path is most important to explore.

### Scenario II

Unlike the first, this approach does not need to switch between the vehicles. This scenario is the most common type of cooperation, in which the vehicle will have to move in synchrony as one single unit. This is the intuition behind this approach. For this formation, the tracker vehicle will have to estimate the midpoint between the two AUVs and then track these points as some sort of virtual target. With this formation, the data



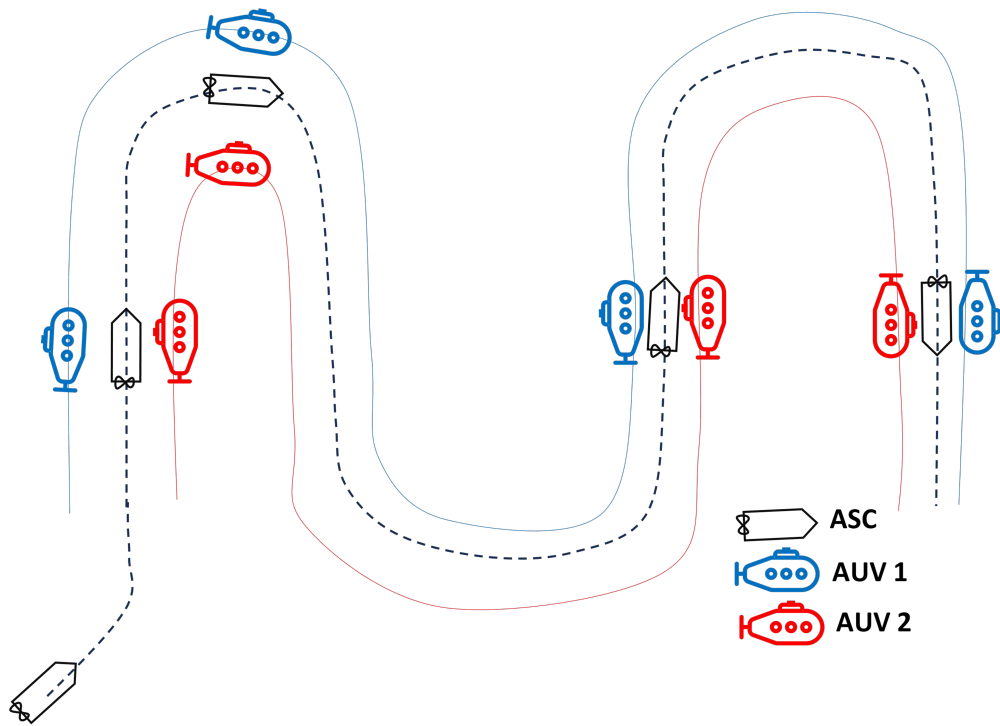


Figure 2.10: Scenario II Cooperation Strategy.

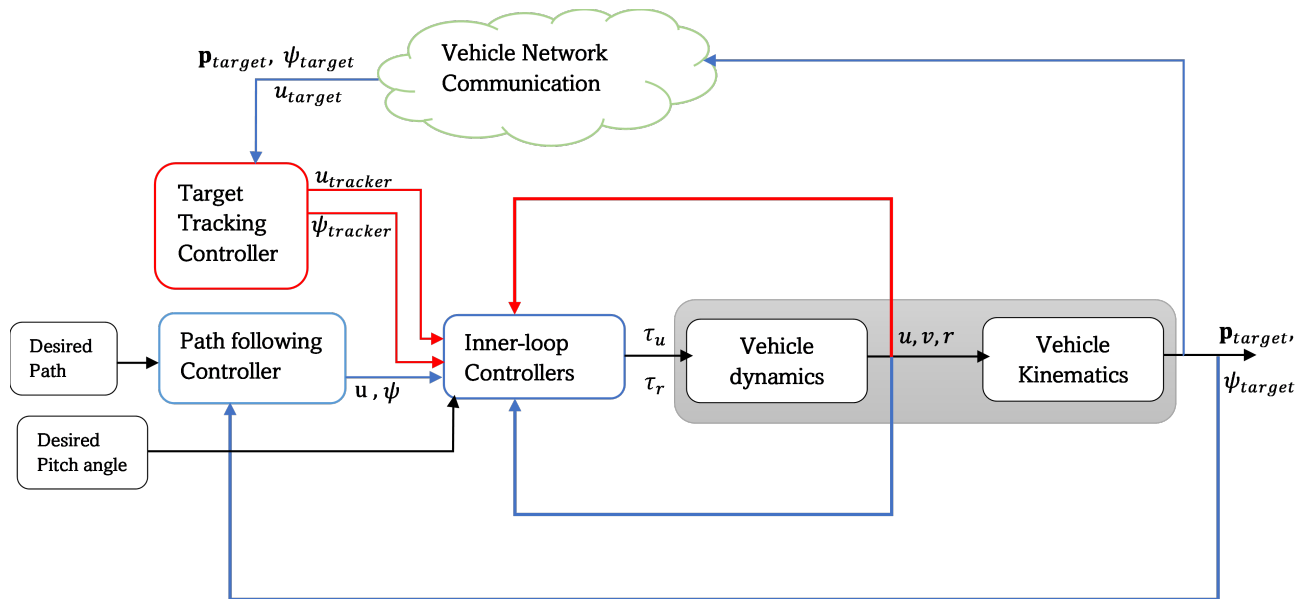


Figure 2.11: Cooperative Control Block Diagram.

# Chapter 3

## Proposed Solution

### 3.1 System Implementation

This section presents an overview of how the system was implemented in simulations.

#### 3.1.1 Inner-Outer Loop Approach

In the design of guidance control systems for AMVs, several techniques such as backstepping, feedback linearization, sliding mode control, and linear model predictive control (MPC) can be employed. Some of these techniques can decide to fuse the kinematic and dynamic models of the vehicle into one single controller. This approach can guarantee stability for a completed PF system but can be too complicated to tune certain parameters during real-life missions. An alternative approach can be to create a separate controller for the kinematic and dynamic models of the vehicle, in what is known as the inner-loop outer-loop control system, as depicted in Figure 3.1. This strategy enables the simplification of the system, such that it becomes easy to tune various parameters of the system. In this kind of system, we assume that the response of the inner loop must be sufficiently fast enough to effect the desired change received from the outer loop. Therefore, the influence of the inner loop on the entire system can be neglected.

The inner loop is responsible for generating the required force and torques required for the vehicle to follow the given reference supplied by the outer loop controller. Depending on the type of reference (surge, yaw, yaw-rate, pitch etc.) given, the tracking controllers are mostly Proportional Integral and Derivative (PID) controllers but can be a Proportional and Integral (PI) in the case of the surge reference. On the other hand, the outer loop system is responsible for calculating the reference values depending on the required task. However, since the inner-loop controllers are not the emphasis of this thesis, the design of the ones used by the outer loop will be briefly discussed in the subsequent sections.

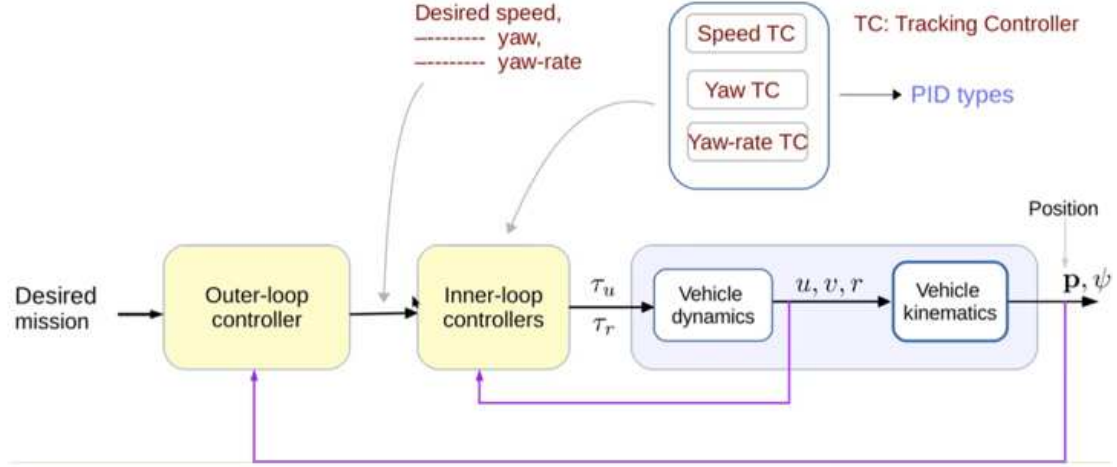


Figure 3.1: A Sketch of the Inner-loop Outer-loop control structure [10].

### Yaw Tracking Controller

The goal of this controller is to drive the tracker vehicle to the desired heading given by the outer-loop target tracking controllers. Define the heading error as

$$e = \psi - \psi_{ref}, \quad (3.1)$$

where the  $\psi_{ref}$  is the heading reference to track and the  $\psi$  is the actual yaw angle of the vehicle. Taking the time derivatives of both sides yields

$$\dot{e} = \dot{\psi} - \dot{\psi}_{ref}. \quad (3.2)$$

Hence, using a simple Proportional Integral and Derivative (PID) control theory to calculate the differential mode  $\tau_r$  between the thrusters, we have

$$\tau_r = k_p e - k_d \dot{e} - k_i \int_0^t e(\tau) d\tau, \quad (3.3)$$

where  $k_p$ ,  $k_d$  and  $k_i$  are positive gains of the proportional, derivative and integral parts of the controller respectively.

### Yaw-rate Tracking Controller

The yaw-rate controller is responsible for driving the yaw-rate reference of the target vehicle to zero. Defining the error, we obtain

$$e = r - r_{ref}, \quad (3.4)$$

where  $r$  is the yaw-rate of the vehicle and  $r_{ref}$  is the reference yaw-rate to track. The Yaw-rate tracking controller is a PI controller responsible for computing the differential mode for the longitudinal thrusters and can be written as

$$\tau_r = -k_p e - k_i \int_0^t e(\tau) d\tau, \quad (3.5)$$

where  $k_p$  and  $k_i$  are the positive gains of the proportional and the integral part of the controller respectively.

### Surge Tracking Controller

The surge tracking controller is responsible for computing the common mode command for the longitudinal thrusters. This controller is used by the target and tracker vehicles. Defining the error, we obtain

$$e = u - u_{ref}, \quad (3.6)$$

where  $u$  is the surge speed of the vehicle and  $u_{ref}$  is the reference surge speed to track. The surge controller is a simple PI controller and can be written as

$$\tau_u = -k_p e - k_i \int_0^t e(\tau) d\tau, \quad (3.7)$$

where  $k_p$  and  $k_i$  are the positive gains of the proportional and the integral part of the controller respectively.

### Pitch Tracking Controller

The pitch tracking controller is similar to the yaw tracking controller. It is responsible for driving the target vehicles to the desired pitch angle. It computes the differential mode for the vertical thrusters. The pitch error can be defined as

$$e = \theta - \theta_{ref}, \quad (3.8)$$

where  $\theta$  is the pitch angle of the target vehicle and  $\theta_{ref}$  is the reference pitch angle to be tracked. Taking the time derivative gives

$$\dot{e} = \dot{\theta} - \dot{\theta}_{ref}. \quad (3.9)$$

With a simple PID controller, the pitch controller can be written as

$$\tau_q = k_p e - k_d \dot{e} - k_i \int_0^t e(\tau) d\tau, \quad (3.10)$$

where  $k_p$ ,  $k_d$ , and  $k_i$  are positive gains of the proportional, derivative, and integral parts of the controller, respectively.

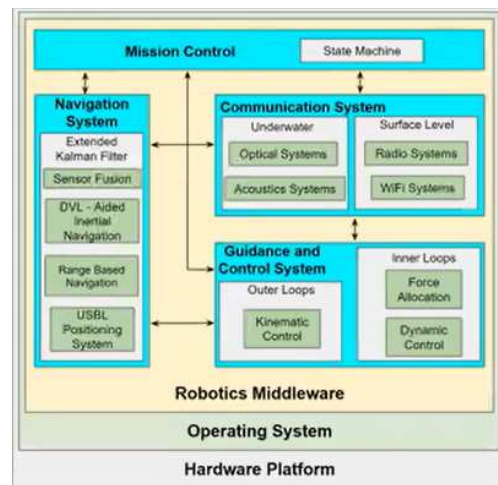
### 3.1.2 DSOR Software Stack Overview

The Dynamical Systems and Ocean Robotics (DSOR) of the Institute for Systems and Robotics (ISR) Lisboa, has over the years developed a set of Robotic Operating System (ROS) packages in Python and C++ capable of various kinds of marine robots simulations. The software stack also uses some packages commonly used in the robotic community by researchers, such as the 3D Gazebo simulator. The stack is quite robust and allows interaction between the simulator with various algorithms, vehicle models and a wide range of sensor models within the stack. Hence, the implementation of this project was simulated using this great scientific tool.

The stack, also referred to as the NetMarSys Toolchain system, is a combination of three stacks, which are the 3D simulation stack, code stack, and the operation interface, as shown in Figure 3.2.



(a) Gazebo Interface



(b) Stack Chart Overview



(c) Ponte Interface

Figure 3.2: A Schematics of the NetMarSys Toolchain system.

- The Gazebo is the 3D simulation stack, which contains the 3D world view of an object, the 3D model of the vehicle that is being simulated, and the sensors of the simulator. Figure 3.2a is a graphic view of the Gazebo simulation platform.
- The second part is the code stack which consists of the Guidance and Control primitives, Navigation and Communication stacks. An overall description of the system can be seen in Figure 3.2b. The code stack is an open-source repository on GitHub where all the controllers are available and a pre-built simulation with the Medusa class of vehicles.
- The third stack of the system is the operations interface. This is the Ponte graphical user interface, which allows for a 2D visualization of any mission. This console, as seen in Figure 3.2c, enables the user to send missions and view missions such as path following, waypoints, trajectory tracking etc.

### 3.2 Solving Path Following for the Target Vehicles

The PF problem can be broken down into two basic steps, which are as follows:

1. Deriving the dynamics of the path following error between the vehicle and the path in a path frame (e.g. F-S or P-T frame).
2. Driving these errors to zero using a nonlinear control technique to achieve path following.

We derive the dynamics of the PF errors between the vehicle and the path to achieve PF. The illustration in Figure 3.3 shows the reference point that the vehicle must track to achieve PF.

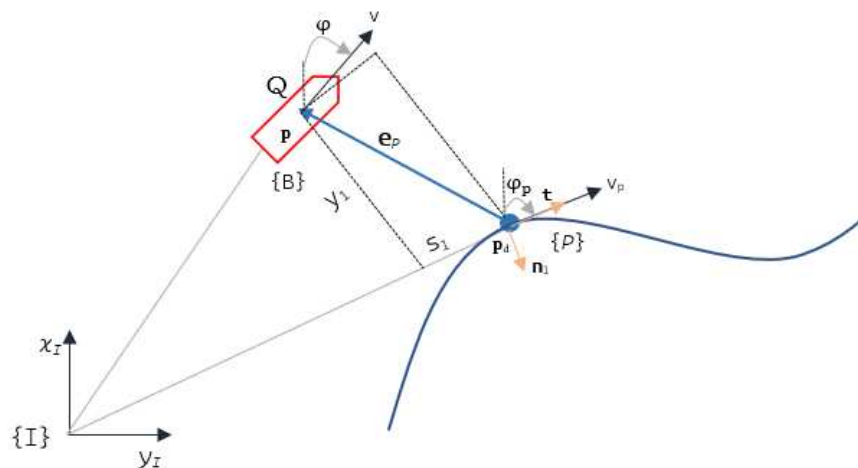


Figure 3.3: Geometric illustration of Path Following Problem.

Considering the kinematic equation of the target vehicle (AUV) as given in (2.22),

$$\begin{aligned}\dot{x} &= u \cos(\psi), \\ \dot{\psi} &= r.\end{aligned}\tag{3.11}$$

Under the assumption that the pitch angle is not controlled in the horizontal motion, and there are no external disturbances such as ocean currents, the derivative of its position becomes

$$\dot{\boldsymbol{\eta}} = \mathbf{R}(\psi) \begin{bmatrix} u \\ 0 \end{bmatrix},\tag{3.12}$$

where  $r$  is the yaw rate and  $\psi$  is the heading angle. The control input variables that will be tracked by the controller are the  $u$ , and  $r$ .

Let  $\{\mathcal{P}\}$  be the P-T frame attached to this point defined by rotating the inertial frame by angle  $\psi_{\mathcal{P}}$ , where  $\psi_{\mathcal{P}}$  is the angle that the tangent vector at  $\mathbf{p}_d$  makes with  $x_{\mathcal{I}}$  as seen in Figure 3.3. With the position vector  $\mathbf{e}_{\mathcal{P}}$  of the vehicle expressed in  $\{\mathcal{P}\}$ , it can be expressed mathematically as

$$\mathbf{e}_{\mathcal{P}} = \mathbf{R}_{\mathcal{I}}^{\mathcal{P}}(\psi_{\mathcal{P}})(\mathbf{p} - \mathbf{p}_d),\tag{3.13}$$

where  $\mathbf{R}_{\mathcal{I}}^{\mathcal{P}} \in SO(2)$  is the rotation matrix from  $\mathcal{I}$  to  $\mathcal{P}$  defined as

$$\mathbf{R}_{\mathcal{I}}^{\mathcal{P}}(\psi_{\mathcal{P}}) = \begin{bmatrix} \cos(\psi_{\mathcal{P}}) & \sin(\psi_{\mathcal{P}}) \\ -\sin(\psi_{\mathcal{P}}) & \cos(\psi_{\mathcal{P}}) \end{bmatrix},\tag{3.14}$$

and

$$\begin{bmatrix} s_1 \\ y_1 \end{bmatrix} = \mathbf{R}_{\mathcal{I}}^{\mathcal{P}}(\psi_{\mathcal{P}}) \begin{bmatrix} x - x_p \\ y - y_p \end{bmatrix}.\tag{3.15}$$

Note that  $\mathbf{R}_{\mathcal{I}}^{\mathcal{P}}(\psi_{\mathcal{P}}) = [\mathbf{R}_{\mathcal{P}}^{\mathcal{I}}(\psi_{\mathcal{P}})]^T$ . Taking the time derivative of (3.13) to obtain a solution, we have

$$\dot{\mathbf{e}}_{\mathcal{P}} = [\dot{\mathbf{R}}_{\mathcal{P}}^{\mathcal{I}}(\psi_{\mathcal{P}})]^T (\mathbf{p} - \mathbf{p}_d) + \mathbf{R}_{\mathcal{I}}^{\mathcal{P}}(\psi_{\mathcal{P}})(\dot{\mathbf{p}} - \dot{\mathbf{p}}_d).\tag{3.16}$$

Following the proof in [9] (Rotation matrix differential equation, Theorem 2.2), let  $\mathbf{R}_A^B \in SO(2)$  be the rotation matrix from  $\{A\}$  to frame  $\{B\}$ . Then,

$$\dot{\mathbf{R}}_A^B = \mathbf{R}_A^B \mathbf{S}(\omega_{A/B}^A),\tag{3.17}$$

where  $\mathbf{S}(\omega_{A/B}^A)$  is the skew-symmetric matrix and  $\omega_{A/B}^A \in \mathbb{R}^n$  is the angular velocity of  $\{A\}$  with respect to  $\{B\}$  expressed in  $\{A\}$ . Applying that to (3.16), it becomes

$$\dot{\mathbf{e}}_{\mathcal{P}} = -\mathbf{S}(\boldsymbol{\omega}_{\mathcal{P}})\mathbf{e}_{\mathcal{P}} + \mathbf{R}_{\mathcal{I}}^{\mathcal{P}}(\psi_{\mathcal{P}})\dot{\mathbf{p}} - \mathbf{R}_{\mathcal{I}}^{\mathcal{P}}(\psi_{\mathcal{P}})\dot{\mathbf{p}}_d, \quad (3.18)$$

where  $\mathbf{S}(\boldsymbol{\omega}_{\mathcal{P}}) \in \mathbb{R}^{2 \times 2}$  is a skew symmetric matrix parameterized by  $\boldsymbol{\omega}_{\mathcal{P}} = r_{\mathcal{P}}$ , which is the angular velocity of  $\{\mathcal{P}\}$  with respect to  $\{\mathcal{I}\}$ , expressed in  $\{\mathcal{P}\}$ . Note that  $r_{\mathcal{P}}$  satisfies the relation

$$r_{\mathcal{P}} = k(\gamma)u_{\mathcal{P}}, \quad (3.19)$$

where  $u_{\mathcal{P}}$  is the total speed of point  $\mathbf{p}_d$  as shown in (2.32) and  $k(\gamma)$  is the signed curvature of the path at  $\mathbf{p}_d$ , given by

$$k(\gamma) = \frac{\dot{x}_d(\gamma)\ddot{y}_d(\gamma) - \ddot{x}_d(\gamma)\dot{y}_d(\gamma)}{\|\dot{\mathbf{p}}_d(\gamma)\|^3}. \quad (3.20)$$

The proof of this can be found at the article on curvature [53] at Wolfram MathWorld. Note also that if  $\gamma$  is the arc length of the path, then  $\|\dot{\mathbf{p}}_d(\gamma)\| = 1$ . In this case,  $u_{\mathcal{P}} = \dot{\gamma}$ , i.e. the speed of the “reference point” equals the rate of change of the path length.

Define the orientation error,  $\psi_e$ , between the vehicle’s heading and the tangent of the path,

$$\psi_e \triangleq \psi - \psi_{\mathcal{P}}. \quad (3.21)$$

By expanding the second and the third part of (3.18), the following sets of equations are obtained

$$\mathbf{R}_{\mathcal{I}}^{\mathcal{P}}(\psi_{\mathcal{P}})\dot{\mathbf{p}} = \begin{bmatrix} u \cos(\psi_e) \\ u \sin(\psi_e) \end{bmatrix}, \quad (3.22)$$

$$\mathbf{R}_{\mathcal{I}}^{\mathcal{P}}(\psi_{\mathcal{P}})\dot{\mathbf{p}}_d = \mathbf{v}_{\mathcal{P}}, \quad (3.23)$$

where  $\mathbf{v}_{\mathcal{P}} \triangleq [u_{\mathcal{P}}, 0]^T \in \mathbb{R}^2$  is the velocity of  $\mathcal{P}$  with respect to  $\{\mathcal{I}\}$  expressed in  $\{\mathcal{P}\}$ . Substituting the expression in (3.22), (3.23) into (3.18), we obtain the dynamics of the position error as

$$\dot{\mathbf{e}} = -\mathbf{S}(\boldsymbol{\omega}_{\mathcal{P}})\mathbf{e}_{\mathcal{P}} + \begin{bmatrix} u \cos(\psi_e) \\ u \sin(\psi_e) \end{bmatrix} - \begin{bmatrix} u_{\mathcal{P}} \\ 0 \end{bmatrix}, \quad (3.24)$$

and the dynamics of the orientation error is given by

$$\dot{\psi}_e = r - k(\gamma)u_{\mathcal{P}}. \quad (3.25)$$

### Nonlinear Controller Design

Having derived the error dynamics, it is expedient to design the control laws that will drive the position and orientation error to zero. The derivation presented in this section follows the proof of theorem presented

in[8]. Writing (3.24) and (3.25) in a more compact form, we have

$$\begin{cases} \dot{s}_1 = r_{\mathcal{P}} y_1 + u \cos(\psi_e) - u_{\mathcal{P}}, \\ \dot{y}_1 = -r_{\mathcal{P}} s_1 + u \sin(\psi_e), \\ \dot{\psi} = r - k(\gamma) u_{\mathcal{P}}. \end{cases} \quad (3.26)$$

A Lyapunov candidate function ( $V_1$ ) will be employed in deriving the required control laws. Candidate Lyapunov Functions are like an energy function that can be used to characterize the stability of a system. In many important applications, it is very beneficial to have a continuously differentiable Lyapunov function whose derivative along the trajectories of the system can be made negative definite by an appropriate choice of feedback [54]. Following the basic theorem of the Lyapunov function, we will:

- i. Find a positive definite function  $V(\cdot)$  on  $\mathbb{R}^n$ , such that  $V(x) > 0 \forall x \neq 0$ ,  $V(0) = 0$  and radially unbounded provided  $\lim_{|x| \rightarrow +\infty} V(x) = +\infty$ .
- ii. Take the derivative  $\dot{V}(x)$  of  $V(x)$ .
- iii. choose a suitable control feedback law that satisfies the function  $\dot{V}(x) \leq 0$ .
- iv. Conclude that, if  $\dot{V}(x) \leq 0$  is negative semi-definite and is uniformly continuous, it is stable in the sense of Lyapunov.

The function is given as

$$V_1 = \frac{1}{2} \mathbf{e}_{\mathcal{P}}^2 + \frac{1}{2k_2} (\tilde{\psi})^2, \quad (3.27)$$

where  $\mathbf{e}_{\mathcal{P}}^2 = (s_1^2 + y_1^2)$ , and

$$\tilde{\psi} = \psi_e - \delta(y_1, u). \quad (3.28)$$

Note that  $(s_1^2 + y_1^2)$  represents the distance between the vehicle and the path, which must converge to zero and  $\delta(y_1, u)$  is a time-differentiable design function that can be used to shape the manner in which the vehicle approaches the path. The design of  $\delta(y_1, u)$  must satisfy the following condition:

**Condition 3.2.1. :**

- i.)  $\delta(y_1, u) = 0, \forall u,$
- ii.)  $y_1 \cdot u \cdot \sin(\delta(y_1, u)) \leq 0 \forall u, \forall y.$

Taking its time derivative yields

$$\dot{V}_1 = \mathbf{e}_{\mathcal{P}}^T \dot{\mathbf{e}}_{\mathcal{P}} - \frac{1}{k_2} \tilde{\psi} \dot{\tilde{\psi}} \quad (3.29)$$

where  $\tilde{\psi} = r - k(\gamma)u_{\mathcal{P}} - \dot{\delta}$ . Expanding and simplifying the equation yields

$$\begin{aligned}\dot{V}_1 &= s_1 \cdot \dot{s}_1 + y_1 \cdot \dot{y}_1 + \frac{1}{k_2}(\psi_e - \delta)(\dot{\psi}_e - \dot{\delta}) \\ &= s_1(r_{\mathcal{P}}y_1 + u \cdot \cos(\psi_e) - u_{\mathcal{P}}) + y_1(-r_{\mathcal{P}}s_1 + u \sin(\psi_e)) + \frac{1}{k_2}(\psi_e - \delta)(\dot{\psi}_e - \dot{\delta}) \\ &= s_1(u \cos(\psi) - u_{\mathcal{P}}) + y_1 u \sin(\delta) + \frac{1}{k_2}(\psi_e - \delta) \left( \dot{\psi}_e - \dot{\delta} + k_2 \cdot y_1 \cdot u \cdot \frac{\sin(\psi_e) - \sin(\delta)}{\psi_e - \delta} \right).\end{aligned}\quad (3.30)$$

We can now define the control laws

$$\begin{cases} u_{\mathcal{P}} = u \cos(\psi) + k_3 s_1, \\ \dot{\psi}_e = \dot{\delta} - k_2 \cdot y_1 \cdot u \cdot \frac{\sin(\psi_e) - \sin(\delta)}{\psi_e - \delta} - k_1(\psi_e - \delta), \end{cases}\quad (3.31)$$

where  $k_1$ ,  $k_2$  and  $k_3$  are positive gains. Substituting (3.31) into (3.30), cancelling the undesirable terms, the derivative of the Lyapunov function becomes

$$\dot{V}_1 = -k_3 s_1^2 + y_1 u \sin(\delta) - \frac{k_1}{k_2}(\tilde{\psi})^2.\quad (3.32)$$

Note that from the second condition in 3.2.1, we conclude that  $\dot{V}_1 \leq 0$  for all  $t$ . Furthermore, the above equation shows that  $\dot{V}_1$  is uniformly continuous; thus, invoking Barbalat's lemma, we can state that  $\dot{V}_1(t)$  converge to 0 as  $t \rightarrow \infty$ .

Therefore, the control law for  $u$  and  $r$  can be written as

$$u = U_d,\quad (3.33)$$

where  $U_d$  is the positive desired speed profile for the vehicle to track and

$$r = \kappa(\gamma)u_{\mathcal{P}} + \dot{\delta} - k_1(\tilde{\psi}) - k_2 y_1 u \frac{\sin(\psi_e) - \sin(\delta)}{\tilde{\psi}},\quad (3.34)$$

where  $k_1, k_2 > 0$  are tuning parameters, where  $k_1 \kappa(\gamma)$  is defined in 3.20,  $\psi_e$  and  $\tilde{\psi}$  is given by (3.21 and 3.28) respectively, and  $u_{\mathcal{P}}$  is given 3.31. Then,  $\mathbf{e}_{\mathcal{P}}(t), \psi_e(t) \rightarrow 0$  as  $t \rightarrow \infty$ .

The control law for  $u_{\mathcal{P}}$  in (3.31) implies that if the vehicle is behind/ahead of the "reference point" ( $s_1 < 0 = s_1 > 0$ ) then the "reference point" decreases/increases its speed. Intuitively, it aims to adjust the speed of the "reference point" to coordinate with the vehicle along the tangent axis of the P-T frame so as to reduce the along-track error to zero. This method prevents the vehicle from having to solve an optimization problem in order to find the closest point on the path to itself.

Table 3.1: Values for the Parameters used for the Target's PF manoeuvre

$k_1$	$k_2$	$k_3$	$\theta$	$k_{\delta}$	$u$
1.3	0.16	0.2	1.5	0.8	0.3 m/s

Table 3.2: Values for the parameters used for the Target Vehicle

<i>Parameters</i>	$k_p$	$k_i$	$k_d$
Surge	27	-	3
Yaw	0.06	0.009	0.04
Pitch	0.015	0.01	0.02

### Target Vehicle Motion Control System Block

The proposed control system block for the horizontal and vertical motion system for a single target vehicle is described by the block diagram in Figure 3.4.

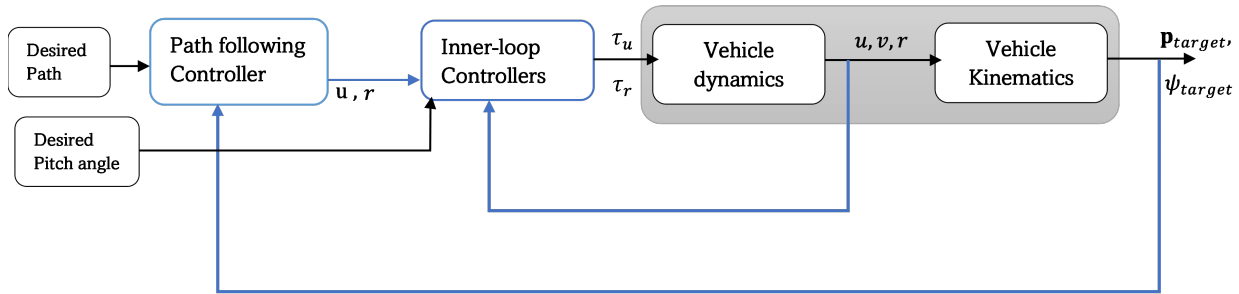


Figure 3.4: Block Diagram for a Single Target Vehicle.

### 3.3 Target Tracking Heading Controller

As stated in Section 2.4.2, the LOS algorithm will be applied in designing a controller for the heading. The underlying intuition behind the LOS algorithm is that, for the tracker vehicle to catch up with and move in synchrony with the target vehicle, the tracker vehicle will always have to direct its velocity at a look-ahead distance of the target vehicle at all times. With this strategy, even if by circumstance the tracker vehicle is ahead of the target vehicle as illustrated in Fig 3.6, it will not have to turn around to meet the target vehicle but rather, will project the position of the target vehicle along the vehicle's longitudinal axis. On the other hand, if it is behind the target vehicle as shown in Fig 3.5, it will still direct its velocity at a look-ahead distance of the target vehicle. The heading of the tracker will always be directed towards a look-ahead distance of the target vehicle in question. With this assumption, it becomes easy to solve the LOS as a straight-line problem.

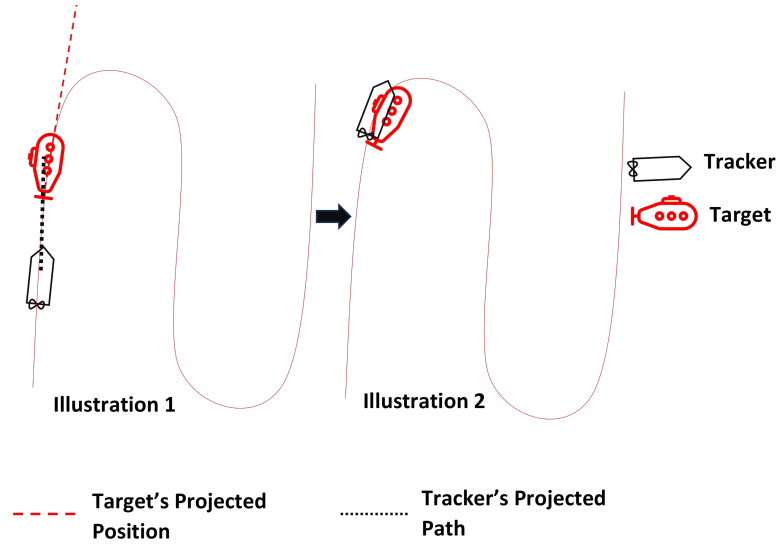


Figure 3.5: Illustration of the Target ahead of the Tracker.

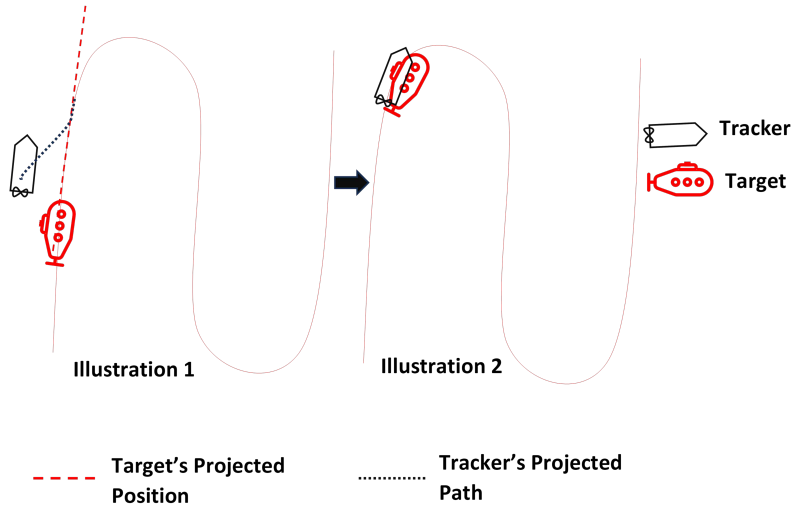


Figure 3.6: Illustration of the Target behind the Tracker.

### Steering Laws for Straight Lines

Consider an imaginary straight-line path implicitly defined by two waypoints;  $\mathbf{p}_d \triangleq [x_d, y_d]^T \in \mathbb{R}^2$  and  $\mathbf{p}_{d+\delta} \triangleq [x_{d+\delta}, y_{d+\delta}]^T \in \mathbb{R}^2$  respectively.  $\mathbf{p}_d$  represents the position of the target along a predefined path and  $\mathbf{p}_{d+\delta}$  is the projection of the target position  $\mathbf{p}_d$  by an arbitrary distance  $\delta$  along the targets longitudinal axis. Also, consider a body-fixed frame with origin at  $\mathbf{p}_d$ , whose x-axis has been rotated a positive angle  $\psi_d \triangleq \text{atan2}(y_{d+\delta} - y_d, x_{d+\delta} - x_d) \in \mathbb{S}$  relative to the x-axis of the stationary reference frame  $\{\mathcal{I}\}$  as illustrated in Figure 3.7.

Hence, the coordinates of the kinematic vehicle in the body-fixed frame of the target can be computed by

$$\boldsymbol{\varepsilon}(t) = \mathbf{R}_{\mathcal{I}}^{\beta}(\psi_d)^T (\mathbf{p}(t) - \mathbf{p}_d(t)), \quad (3.35)$$



respectively. The overall control objective remains the same as presented in (2.36). However, since the task is viewed as a straight-line problem, only the cross-track error becomes relevant such that  $e(t) = 0$  means that the tracker has converged to the straight line along the longitudinal axis of the target. The along-track error between the tracker and the target is also important and therefore, the target tracking speed controller that will be discussed in the next section will cater for that.

The control objective associated with this straight-line problem becomes

$$\lim_{t \rightarrow \infty} e(t) = 0. \quad (3.40)$$

In the forthcoming subsections, we will introduce two steering laws that guarantee the convergence of  $e(t)$  to the origin. The first method, known as enclosure-based steering, is commonly employed in ship motion control systems [9]. The second method, referred to as lookahead-based steering, draws inspiration from classical guidance principles found in missile literature. While both steering methods operate on a similar principle, it becomes evident that the lookahead-based approach offers several advantages over the enclosure-based approach. The control law formulated from the latter approach will serve as the control law for our heading controller.

### Enclosure-Based Steering

In Enclosure-based steering, a circle with a sufficiently large radius  $R$  is chosen such that the circle will intersect the straight line at two points. Assuming that the direction the target is travelling is known, the intersection point that the tracker will direct its velocity towards, can be chosen accordingly. From Figure 3.8 below, the course angle  $\chi(t)$  can be determined, since

$$\tan(\chi(t)) = \frac{\Delta y(t)}{\Delta x(t)} = \frac{y_{los} - y(t)}{x_{los} - x(t)}, \quad (3.41)$$

where  $\mathbf{p}_{los}(t) \triangleq [x_{los}, y_{los}]^T \in \mathbb{R}^2$  represents the intersection point of interest. The desired course angle can then be computed as

$$\chi(t) = \text{atan2}(y_{los} - y(t), x_{los} - x(t)). \quad (3.42)$$

In order to calculate  $\mathbf{p}_{los}(t)$  (two unknowns), the following two equations must be solved

$$[x_{los} - x(t)]^2 + [y_{los} - y(t)]^2 = R^2, \quad (3.43)$$

$$\tan(\psi) = \frac{y_{d+\delta} - y_d}{x_{d+\delta} - x_d} = \frac{y_{los} - y_d}{x_{los} - x_d} = \text{constant}. \quad (3.44)$$

When it comes to the implementation of this project,  $\psi$  is equivalent to the heading angle of the target vehicle. (3.43) and (3.44) can be solved analytically assuming first that  $|\Delta x| > 0$  and second, for the case  $\Delta x = 0$ .

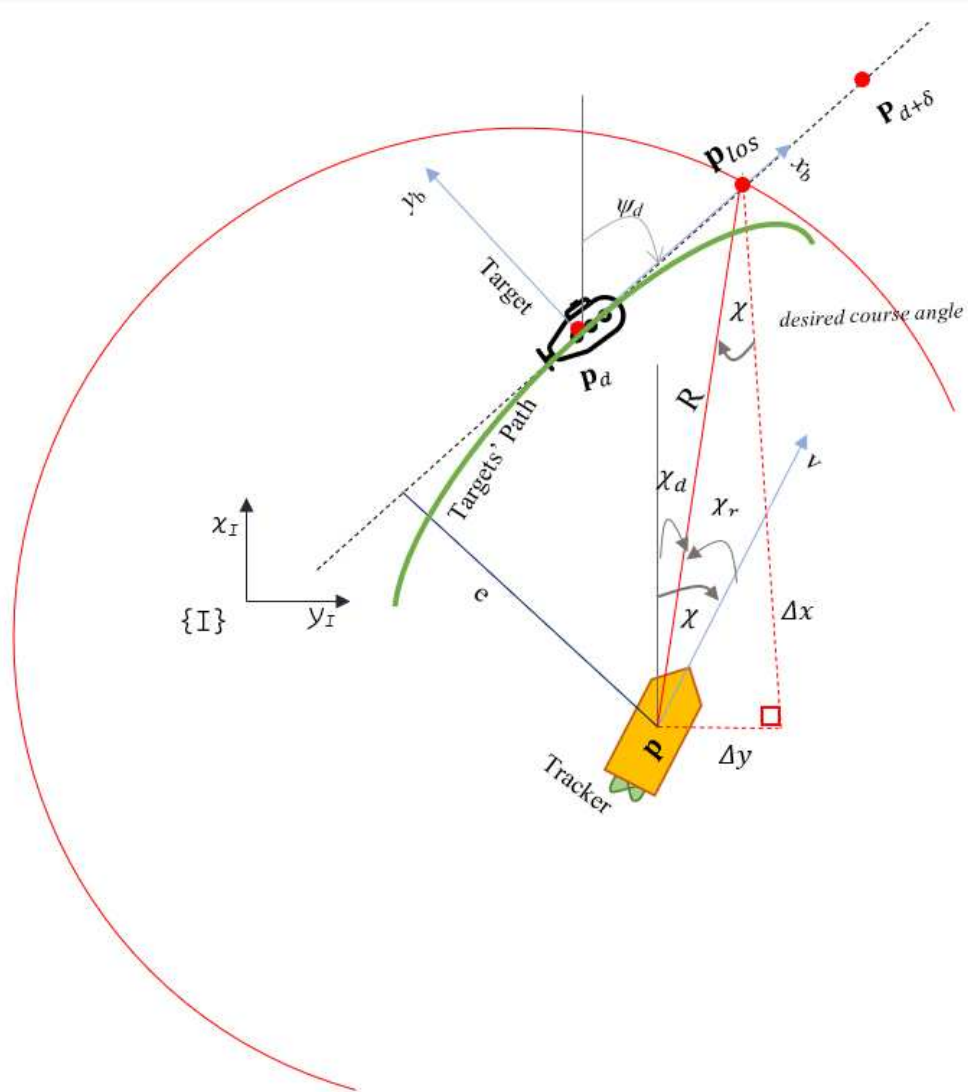


Figure 3.8: Straight Line LOS with both Enclosure-based and Lookahead-based steering methods demonstrated

In the first case,

$$x_{los} = \frac{-b \pm \sqrt{b^2 - 4ac}}{2a}, \quad (3.45)$$

$$y_{los} = d(x_{los} - x_d) + y_d,$$

and for the second case

$$x_{los} = x_d = x_{d+\delta},$$

$$y_{los} = \begin{cases} y + \sqrt{R^2 - (x_{los} - x)^2}, & \text{if } \Delta y > 0, \\ y - \sqrt{R^2 - (x_{los} - x)^2}, & \text{if } \Delta y < 0, \end{cases} \quad (3.46)$$

where

$$\begin{aligned} d &:= \left(\frac{\Delta y}{\Delta x}\right), & w &:= x_d, & f &:= y_d, & g &:= f - d \cdot w = y_d - \left(\frac{\Delta y}{\Delta x}\right) \cdot x_d \\ a &:= 1 + d^2, & b &:= 2(d \cdot g - d \cdot y - x), & c &:= x^2 + y^2 + g^2 - 2g \cdot y - R^2. \end{aligned}$$

The case for which  $\Delta x = 0$  and  $\Delta y = 0$  is not an option, since it would mean the vehicle was on top of the LOS generated point, which is impossible considering the condition set for this point.

### Lookahead-Based Steering

This approach involves determining the desired course angle  $\chi_d$  using an auxiliary lookahead distance that defines the  $\mathbf{p}_{los}$ , the intersection point of the LOS on the path. Since we know the position of the target  $\mathbf{p}_d$ , the lookahead distance is employed to locate  $\mathbf{p}_{los}$  further along the imaginary straight-line path from the target. For the Lookahead-based steering, the desired course angle  $\chi$  is assigned by two components

$$\chi(e) = \chi_d + \chi_r(e), \quad (3.47)$$

where  $\chi_d = \psi_d$  is the same angle that was discussed in the Enclosure-based steering method, while

$$\chi_r(e) = \arctan\left(\frac{-e}{\Delta}\right) = \arctan(-K_p e), \quad (3.48)$$

is a velocity-path relative angle, which ensures that the velocity is directed toward a point on the path that is located at a lookahead distance  $\Delta(t) > 0$ . This feature can be quite useful since the angle is always restricted between  $\chi_r(e) \in [-\pi/2, \pi/2]$ . In what follows,  $K_p = 1/\Delta > 0$  and works like proportional gain. (3.47) can be written as

$$\chi(e) = \psi_d + \arctan\left(\frac{-e}{\Delta}\right). \quad (3.49)$$

Notice that the lookahead-based steering scheme is less computationally intensive than the enclosure-based approach. It is also valid for all cross-track errors, whereas the enclosure-based strategy requires  $R \geq |e(t)|$ . The LOS guidance laws presented in this section are expressed as course commands. However, marine craft frequently rely on compass measurements to determine the heading angle. The control objective is satisfied by transforming the course angle command  $\chi$  to a heading angle command  $\psi$  by using

$$\psi = \chi - \beta, \quad (3.50)$$

where  $\beta = \arcsin\left(\frac{v}{V}\right)$  is the side slip angle, or otherwise known as the crab angle. For the maneuvers and vehicles involved,  $\beta$  will be small ( $\beta \approx 0$ ) but should be verified in the experiments. With this, the  $\chi = \psi$ .

### 3.4 Target Tracking Speed Controller

Having presented the heading control law, discussing the velocity control law is expedient. Since we are dealing with an ASC whose sway motion is not controllable, the speed control law that will be presented in this section will be for the surge motion. Following the intuition presented in Section 3.3 such that the tracker vehicle should move side by side with the target vehicle, the speed control law will be responsible for regulating its speed to meet up when it is behind the target or to slow down for the target vehicle if it is ahead at any time. With this strategy, whenever the tracker catches up with the target, it will move at the same speed as the target.

The velocity laws presented in the pure pursuit strategy will only ensure that the tracker intercepts the target, and upon interception, the velocity of the tracker becomes zero. This approach is not suitable for this study as the tracker vehicle will always have to pick up its speed every time it intercepts the target. On the other hand, in the constant bearing approach, the speed measurements of the target are used as a feed-forward term ensuring that, at interception, the velocity of the tracker equals that of the target. This approach is quite useful for this problem, as it ensures that their velocities are equal upon interception. The only difference is that our goal is not to neutralize but to follow the target. The speed control law in this section will use the same intuition of a feed-forward term as that of the constant bearing approach. Hence, the speed control law implements the synchronization approach for the tracker and the target vehicles.

Consider the Lyapunov function candidate

$$V_2 = \frac{1}{2}(s^2 + e^2), \quad s \neq 0, e \neq 0. \quad (3.51)$$

The desired approach angle  $\psi_d$  is the function of the cross-track error  $e$  as given in (3.49). The error coordinates for control design purposes for  $s$ ,  $e$  and  $\tilde{\psi}_e = \psi_d - \psi$  between the target and tracker should be driven to zero.  $\tilde{\psi}_e = \chi_r = \arctan(-e/\Delta)$  as given in (3.49).

The time derivative of  $V_2$  under the assumption that  $\tilde{\psi}_e = \chi_r$  is

$$\begin{aligned} \dot{V}_2 &= s \cdot \dot{s} + e \cdot \dot{e} \\ &= s \left( r_B e + u - u_d \cos(\tilde{\psi}_e) \right) + e \left( -r_B s + u_d \sin(\tilde{\psi}_e) \right) \\ &= s \left( u - u_d \cos(\tilde{\psi}_e) \right) + e u \sin(\tilde{\psi}_e), \end{aligned} \quad (3.52)$$

where  $r_B$  is the angular velocity of the  $\{B\}$  of the target with respect to  $\{I\}$  expressed in its  $\{B\}$  obtained from the skew symmetric matrix given in (3.17),  $u$  is the speed of the tracker with respect to  $\{I\}$  and  $u_d$  is the speed of the target. We can now define the control law

$$\begin{cases} u = u_d \cos(\tilde{\psi}_e) - k_3 s. \end{cases} \quad (3.53)$$

where  $k_3 > 0$  is a positive gain. Substituting (3.53) into (3.52), cancelling the undesirable terms, the derivative of the Lyapunov function becomes

$$\dot{V}_2 = -k_3 s^2 + e u_d \sin(\tilde{\psi}_e). \quad (3.54)$$

Exploiting the fact that  $\chi_r$  given by (3.48) satisfies

$$\sin(\tilde{\psi}_e) = \frac{-e}{\sqrt{e^2 + \Delta^2}}, \quad (3.55)$$

then the derivative of the Lyapunov  $V_2$  can be written as

$$\dot{V}_2 = -k_3 s^2 - \frac{u_d}{\sqrt{e^2 + \Delta^2}} e^2 < 0, \quad s \neq 0, e \neq 0, \quad (3.56)$$

for  $u_d > 0$  and  $\Delta > 0$ . We can conclude that  $\dot{V}_2 \leq 0$  for all  $t$ . Since the Lyapunov function is positive definite and radially unbounded, while its derivative with respect to time is negative, standard Lyapunov arguments for the system prove that the equilibrium point  $(s, e, \tilde{\psi}_e) = (0, 0, 0)$  is uniform global asymptotical stable (UGAS). These control laws ensure that the position and orientation of the tracker converge to that of the target in a finite time.

From the control law in (3.53), it can be observed that the  $u_d$  variable is a sort of feed-forward term that ensures that whenever the cross-track and along-track error are zero, the speed of the tracker equals the speed of the target. A proof that the speed control law in (3.53) converges to the speed of the tracker when the position error between the vehicle is zero can be seen in the illustration below.

$$s = 0, \tilde{\psi}_e = 0, k_3 > 0 \quad u = u_d \cos(0) - k_3(0), \quad u \approx u_d. \quad (3.57)$$

In Figure 3.9 below, we can observe that whenever the orientation error and the along-track error are zero, the speed of the tracker vehicle becomes the same as that of the target vehicle, which is 0.3m/s in this case. Furthermore, it is also important to examine the influence of the tuning parameter  $k_3$  on the speed output. Hence, the plot in Figure 3.9 shows the relationship between the speed and the along-track error  $s$  base on various  $k_3$  values.

From Figure 3.9, we can observe that for a positive along-track error i.e., the tracker is ahead of the vehicle, it outputs negative speed (with respect to the target); and for a negative along-track error (where the tracker is behind the target), it outputs positive speed (with respect to the target). However, since we do not want the tracker vehicle to move backwards during the mission (i.e., with the negative relative speed), and at the same time, we do not want the reference speed that this controller will generate to be above the maximum speed limit of the tracker vehicle, we would introduce a saturation command to the control law. This saturation command will ensure that the control law output does not yield negative speed and that the maximum reference speed will not exceed the maximum speed limit of the tracker vehicle. Hence, the

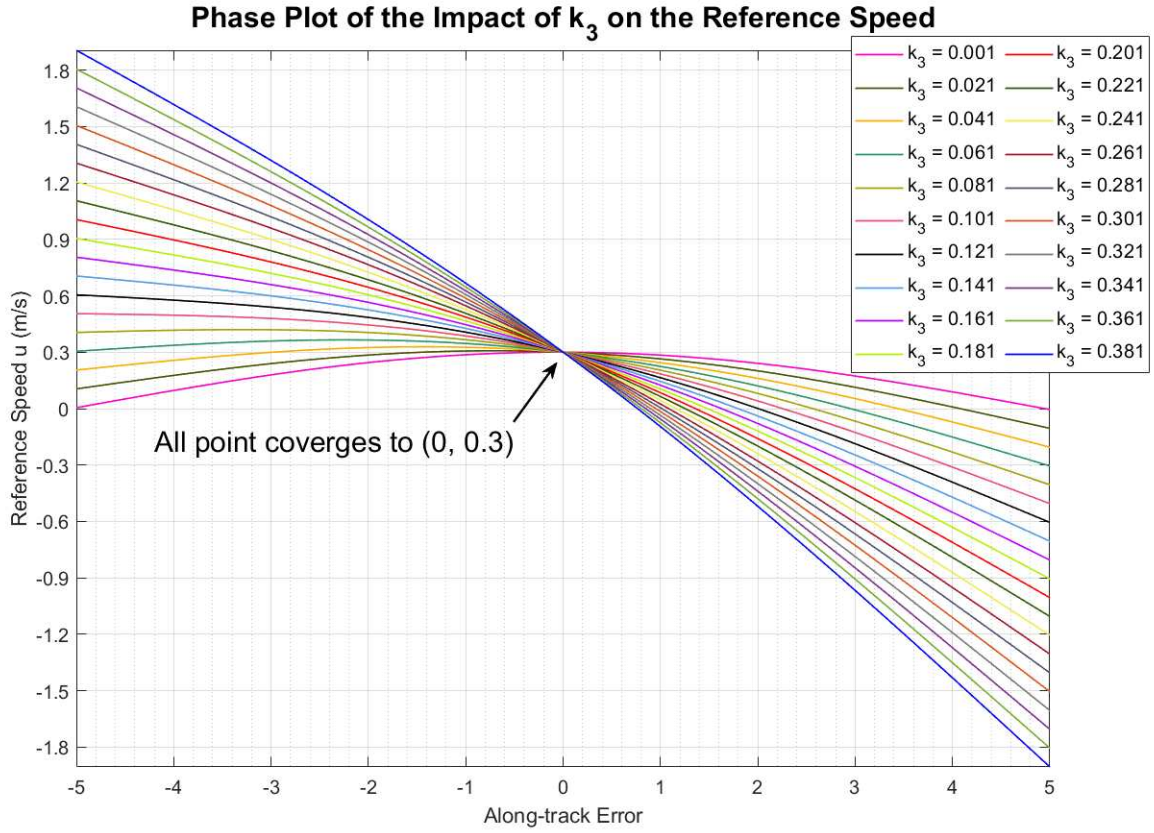


Figure 3.9: A Figure Showing the Impact of Various  $K_3$  Values on  $u$  [ $u_d = 0.3$ ].

saturation command can be written as

$$u_{sat} = Sat(u) := \begin{cases} u_{sat} = 0.05, & u \leq 0, \\ u_{sat} = 1.5, & u > 1.5, \\ u_{sat} = u_d \cos(\psi_e) + k_3 s, & \text{otherwise.} \end{cases} \quad (3.58)$$

Table 3.3: Values for the parameters used for the Tracker Vehicle

parameter	$k_p$	$k_i$	$k_d$
Surge	10	-	5
Yaw	0.08	0.0005	0.12

## Chapter 4

# Simulation Results

This chapter presents the simulations of concepts described in the earlier chapters. Also, the simulations are carefully discussed in attempting to explain the results and their implications. In the first section of this chapter, only a single-vehicle simulation will be presented, while the second section presents a simulation of two heterogeneous vehicles and in the last section, simulations involving three vehicles will be presented.

### 4.1 Path Following Simulation

The simulations in this section present a single vehicle performing Path Following in the horizontal plane and a saw-tooth wave-like manoeuvre in the vertical plane, much like an underwater glider vehicle. In order to further explain the implication of the plots, error plots will also be presented. Each of them is divided into various subheadings for better presentation and understanding.

#### 1. Path Following

Figure 4.1 shows the vehicle converges to the path and follows the path smoothly with a steady state error of  $\pm 1.2m$ . It is worth noting here that the vehicle was also performing the saw-tooth wave-like manoeuvre in the vertical plane when it was following a Lawn-mower path.

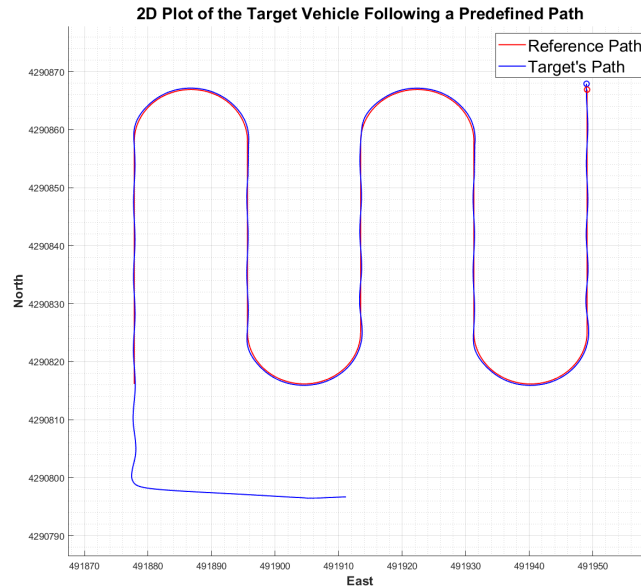


Figure 4.1: Target vehicle following a lawn mower path in the horizontal plane.

## 2. Saw-tooth Wave-like Maneuver

Figure 4.2 shows the vehicle moving up and down through the water column. It can be observed that the maximum depth of penetration as given in the simulation is 23m before it begins to resurface. It begins to dive back again as it reaches the surface at 1m. It maintains this cycle as it traverses its path in the horizontal plane. Controlling the vehicle's pitch has resulted in the simulation in Figure 4.2. It can be observed from the plot that it travels faster way down than it does way up. This is because the dynamics of the vehicle is not naturally buoyant. Without the vehicle stabilizer control, which consists of the roll, depth, and pitch controllers, the vehicle will sink. In order to control the vehicle for this task, the vehicle stabilizer has to be turned off.

## 3. Error Plots

One of the tools that can be employed to analyze the efficacy of a control algorithm is the error plot between the reference signal and the actual signal obtained. Figure 4.3 shows the along-track and cross-track error as discussed in Chapter ?? of this document. The along-track error plot on the left shows the error around the neighborhood of zero except for perturbations when the path alternates between a straight line and an arc-circle, and vice-versa. These perturbations result from the curves associated with the lawn-mower path. As shown in Figure 4.1, there are four major curves along the path corresponding to the four perturbations, as depicted in Fig 4.3a on the left side of the figure. This can be explained by the constant adjustment of the yaw reference to accommodate the curves, which leads to slight deviations as observed in the error plot. Despite these minor deviations, the controllers effectively counteract and rapidly recover from the experienced perturbations. The cross-track error on the other hand oscillates around  $\pm 1$ . For future development of this

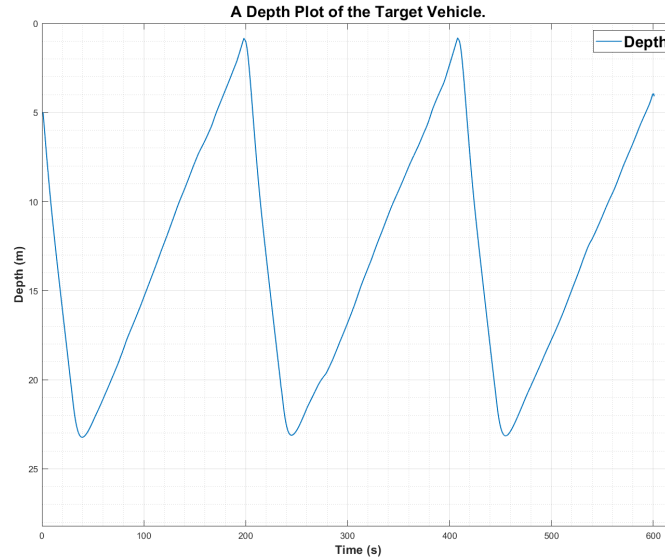
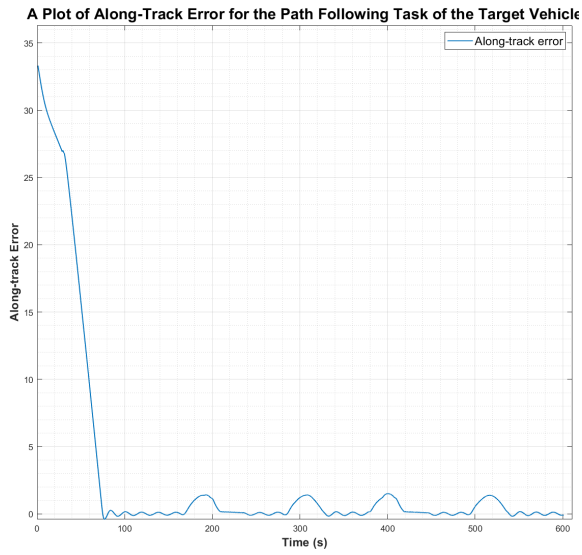


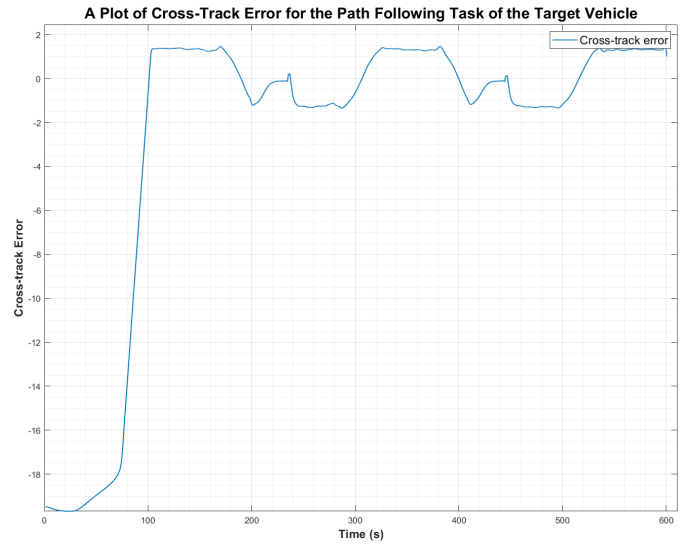
Figure 4.2: Target vehicle performing a saw-tooth wave maneuver in the vertical plane.

work, a more robust inner-loop controller can be adapted to reject some of these external disturbances.

Overall, to better depict the error, euclidean distance measurement was employed to visualize the position error between the vehicle and the predefined path. The plot can be seen in Figure 4.4 below. The plot shows how the target vehicles converge with a distance of  $< 1\text{m}$  between itself and the path. This plot reveals another interesting aspect: the error converges to 0 at around 230s and 430s and then returns to a steady-state error of 1m. The times when the vehicle reaches 0 error coincide with the moments when the vehicle initiates a dive, corresponding to a change in pitch reference for the descent mode. Besides the vehicle descending faster than it ascends, as shown in the yo-yo maneuver plot in Fig 4.2, it does so smoothly without encountering any resistance, descending under its own weight. To provide a clearer understanding of this behavior, the pitch reference and the position distance plot are displayed side by side in Figure 4.5. The area delineated by a red dotted line with an arrow in the plot (Fig 4.5) corresponds to the times on the position error plot that aligns with those on the pitch plot.



(a) Along-track error plot



(b) Cross-track error plot

Figure 4.3: Error Plots between the Target vehicle and the Reference Path

Position Distance Plot for Path Following of the Target Vehicle

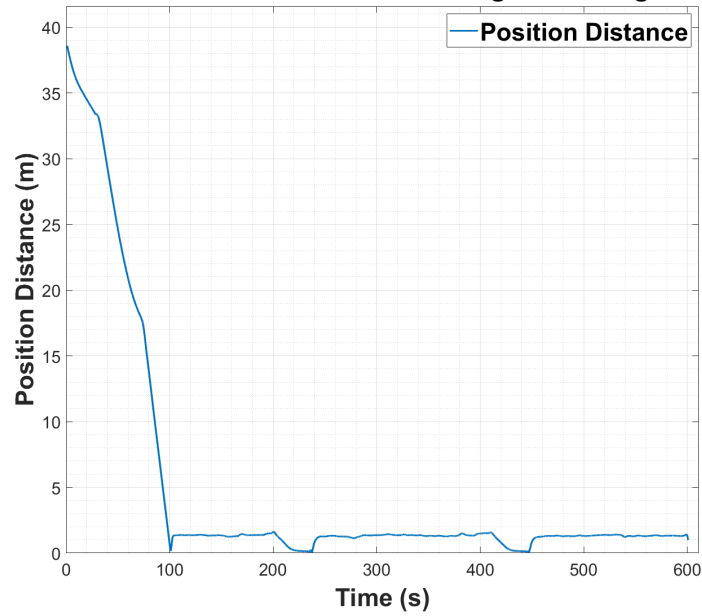


Figure 4.4: Position Distance Error of Target Vehicle.

**A Plot of Position Distance between the Target and the Tracker Vehicles.**

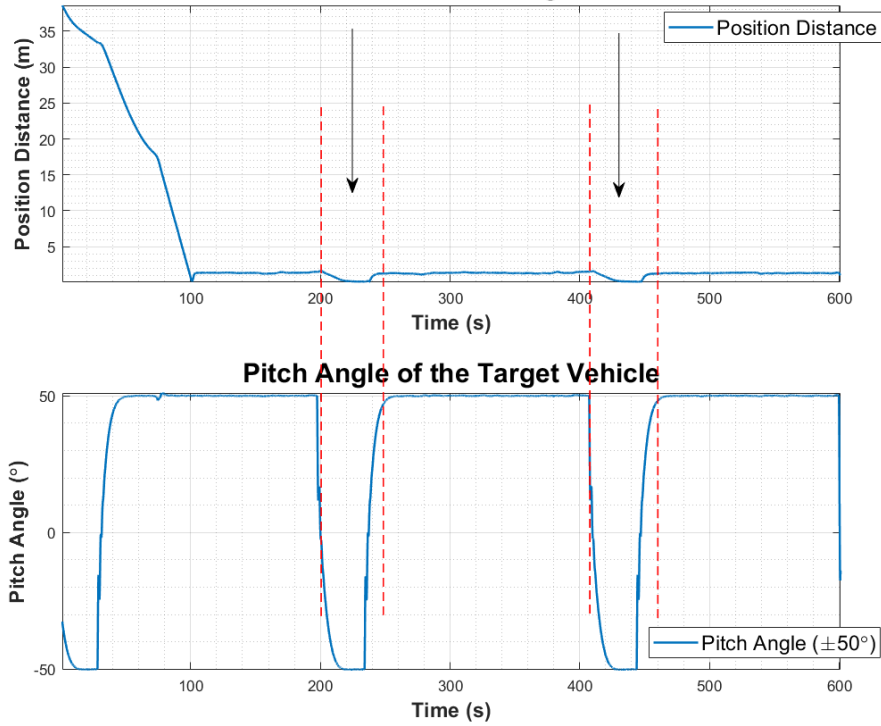


Figure 4.5: Position Distance Error and Pitch Plot of the Target Vehicle.

#### 4. Inner-loop References of the Target Vehicle

The three inner-loop references were responsible for driving the vehicle along the desired path. The surge

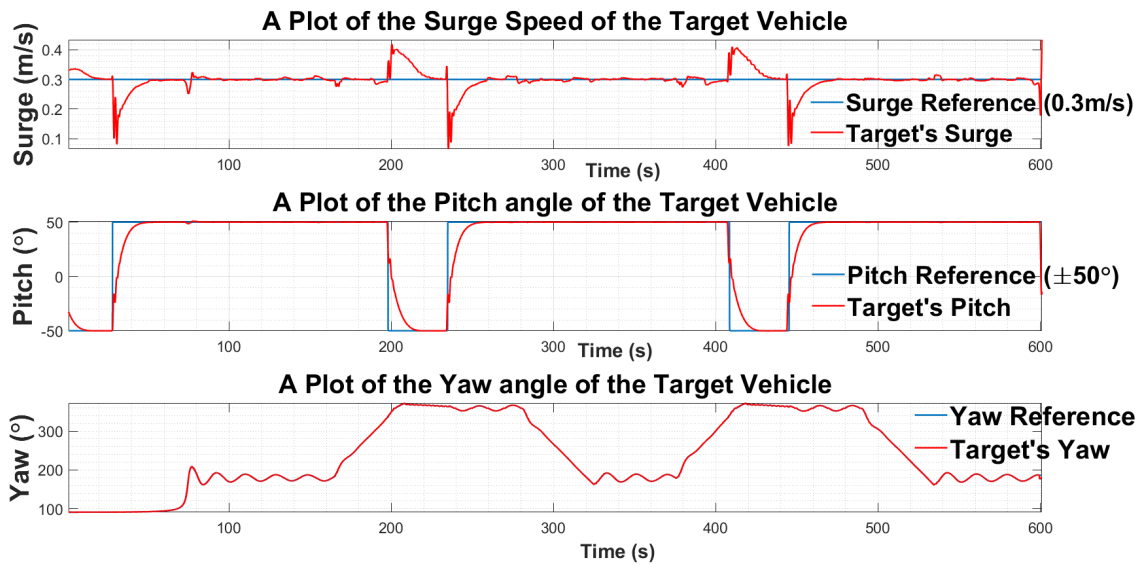


Figure 4.6: Surge, Pitch, and Yaw of Target Vehicle.

plot with a constant reference speed of 0.3m/s shows how the vehicle was able to converge to the reference signal despite the perturbations. The perturbations that are seen on the surge plot can be attributed to the time when the pitch reference signal changes. On the pitch plot, the vehicle seamlessly tracked its reference signal of  $\pm 50^\circ$ . For a reference of  $-50^\circ$ , the vehicle descends and for a reference of  $+50^\circ$ , it begins to ascend.

Though the pitch reference is similar in magnitude but different in direction, its performance differs between the two directions. It exhibits a faster response in the descending mode compared to ascending. This discrepancy can be attributed to the vehicle used in the simulation, which is not naturally buoyant. Consequently, it relies on vehicle stabilizer control to remain at the surface during deployment. The vehicle stabilizer control encompasses roll, pitch, and depth control, each with its references set to 0. Consequently, this clarifies why the vehicle descends more rapidly than it ascends.

The yaw plot also showed how the vehicle tracked the reference heading supplied by the PF controller. It can be observed that the yaw reference, which was indicated by the blue line is not visible in the plot. The reference signal has been overlain by the vehicle's yaw signal indicative of the fact that the yaw controller was able to track the yaw signal effectively. The parameter table for the inner-loop controller references for the target vehicle is presented in Table 3.2.

## 4.2 Target Tracking Simulation

In this section, simulations of a single target and tracker vehicles will be presented. At this stage of the simulation, the target vehicle is able to perform all the simulations presented in the previous section above. Hence, another layer of the tracker's capabilities will be added to the system in this section. The tracker vehicle only begins to track the target whenever the target begins to follow a predefined path.

### 1. Tracker Following the Target Vehicle

The strategy by which the tracker is able to track and follow the target was presented in Chapter ???. Hence, Figure 4.7 presents the result, which shows how well the tracker vehicle was able to stay on the target vehicle. It can be seen that the tracker's path followed the target intimately with a steady state error of  $\approx 1m$ .

### 2. 3D Plot of the Target and Tracker Vehicles

To visualize the system in a 3D context, a 3D plot of the tracker following the target vehicle.

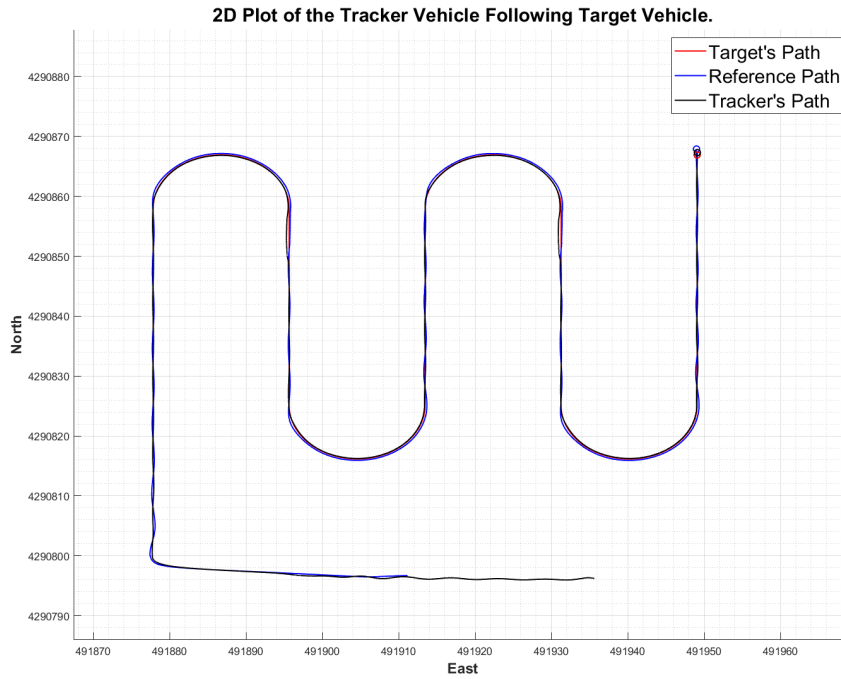


Figure 4.7: 2D plot of the tracker following the target vehicle

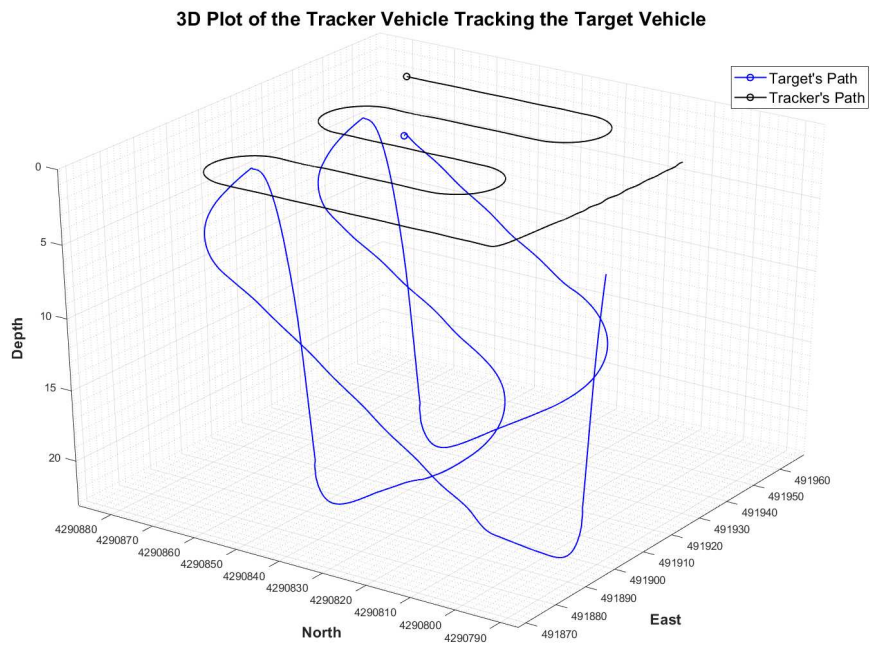
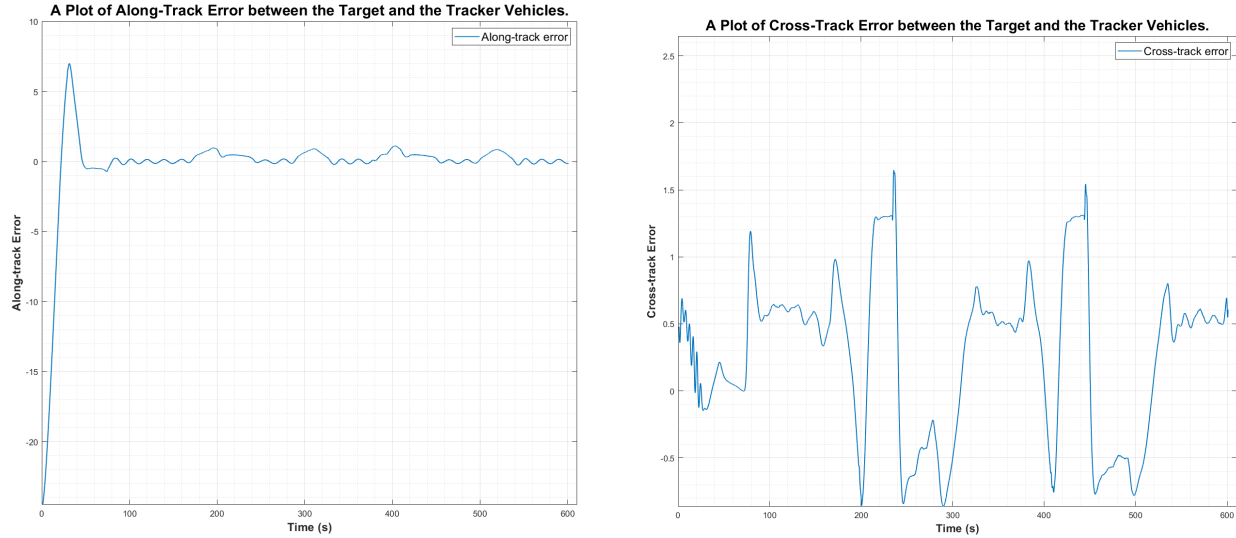


Figure 4.8: 3D plot of the tracker following the target vehicle

### 3. Error Plots

In order to ascertain how well the tracker was able to follow the target, the along-track, cross-track error and the position error between the target and the tracker expressed in the target frame are presented below. The



(a) Along-track error plot

(b) Cross-track error plot

Figure 4.9: Error Plots between the Target vehicle and the Tracker Vehicle

along-track error shows that the tracker followed the target seamlessly. As the tracker began to converge to the target's position, there was an overshoot as seen in the along-track error plot on the left, however, it can be seen that the tracker had to slow down for the target vehicle to catch up resulting in the sharp-peaked point on the plot. On the other hand, the cross-track error looks quite small (+1.5 to -0.8) and this makes the oscillation visible. The cross-track error is an error between the vehicle's longitudinal axis (x-axis). The plot shows that the tracker was able to converge to the x-axis of the target. This is because the tracker's starting position and the target are almost aligned along the target's x-axis as seen in Figure 4.7. Hence, we have a small error throughout the simulation unlike in the along-track error where it took some time for the tracker to converge to the target's y-axis. The oscillations in the plot can be attributed to the curves in the predefined path of the target and the moments when the pitch direction is changed. Since the conditions in the simulation change with time, repetitions in oscillations can be observed. For instance, oscillations at 100s and 300s are similar, and the same goes with the oscillations around 200s and 400s. To visualize the error terms of the distance error (Euclidean distance), Figure 4.10 shows the distance error between the target and the tracker.

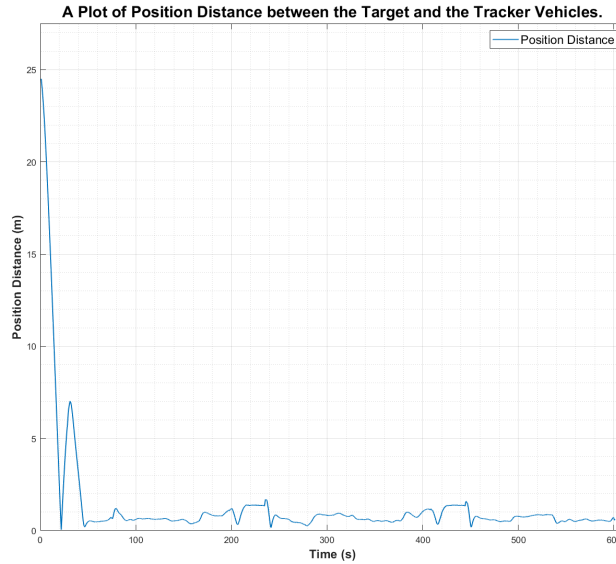


Figure 4.10: Distance Error plot between the Target vehicle and the Tracker Vehicle

#### 4.Inner-Loop References of the Target and Tracker Vehicles

Figure 4.16 shows the surge and yaw plots of the target and tracker vehicles. As discussed in Chapter ??, the tracker vehicle is supposed to follow the target vehicle *pari passu* such that when the tracker converges to the target's position, the speed of the tracker should be approximately equal to that of the targets'. From the error plots shown in Figure 4.10 and 4.9a, the tracker was able to follow the target closely and this was evidenced in the similarity of the surge speed of the tracker (green line) to that of the target speed (red line).

However, the tracker's speed appears to be slightly higher than the target's speed. This can be attributed to the fact that the underwater vehicle performs a more complex maneuver compared to the surface vehicle, resulting in reduced thruster performance for the underwater vehicle. Specifically, the underwater vehicle executes a yo-yo maneuver involving movement in both the horizontal and vertical planes, while the surface vehicle only maneuvers in the horizontal plane. The differences were quite evident in the surge output of the tracker vehicle, however, the surge controller of the tracker was able to keep the tracker vehicle in line with the target vehicle .

The yaw plot, on the other hand, shows the heading of the tracker aligning itself to that of the targets. Since the heading reference is always supplied by the outer-loop PF controller, the heading will definitely be subject to change.

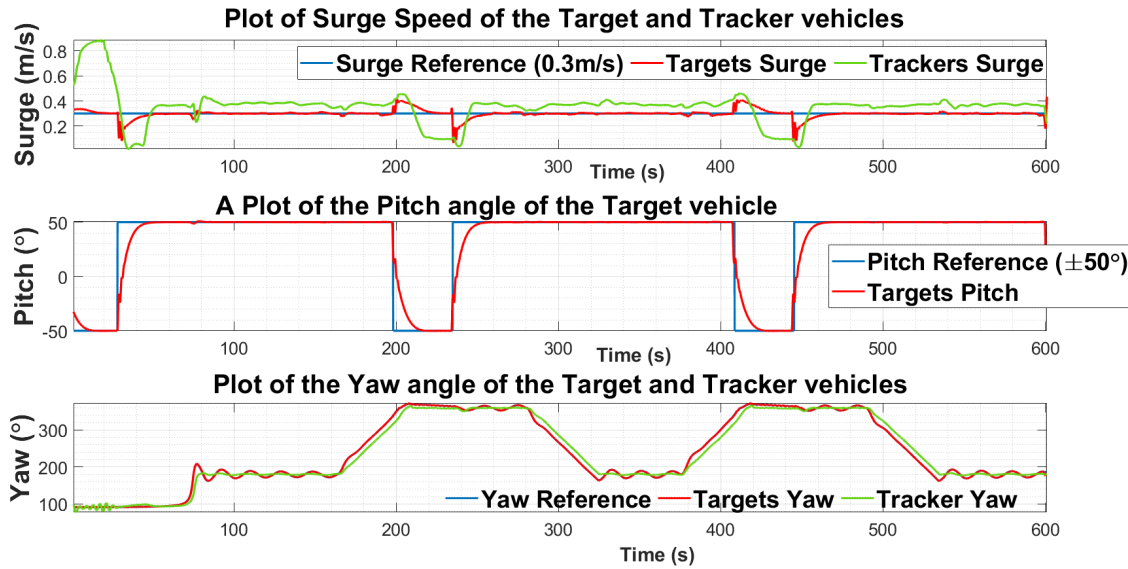


Figure 4.11: Surge, Pitch and Yaw References of the tracker and target vehicles

### 4.3 Cooperative Multiple Vehicle Formation Control Simulation

Having presented the simulation involving a single target and tracker vehicle, the next layer to complete the system is to present a simulation involving two target vehicles and a single tracker vehicle. While discussing the intricacies of cooperation as it concerns ocean observation in Chapter 2.5, two scenarios for cooperation were presented. In the same manner, will the simulation also be presented.

#### 1. Scenario I

Figure 4.12 shows the tracker vehicle with the black coloured path intermittently following the targets with the blue and green paths. Each of the targets is independently following a lawn mower path. The condition for tracking each target is after every 240 sec. Furthermore, it can be seen from the plot how the tracker vehicle smoothly transitions from one target to another and vice versa. In order to have a better visualisation of the switching between the tracker and the two target vehicles, a plot of the distance between each vehicle in 2D was created. The representation of the colour used in the previous plot (Figure 4.12) remains unchanged in the current distance plot as presented in Figure 4.13. In Fig 4.13, it can be observed that each of the line plots goes close to the reference baseline (black colour) at regular intervals. This baseline is the position of the tracker vehicle initialised to 0. The points where it goes close to the reference baseline indicate moments where the tracker tracks and follows the given target while it unfollows the other and vice versa. The two lines exhibit a counter motion, opposite of the other, where one peak cancels out the crest of the other just like a destructive wave signal.

#### 2. Scenario II

In this second configuration, the tracker vehicle tracks the mid position between the two targets as seen in Figure 4.14. Just as we presented a plot of the distance of the tracker to the target in scenario I, the same is

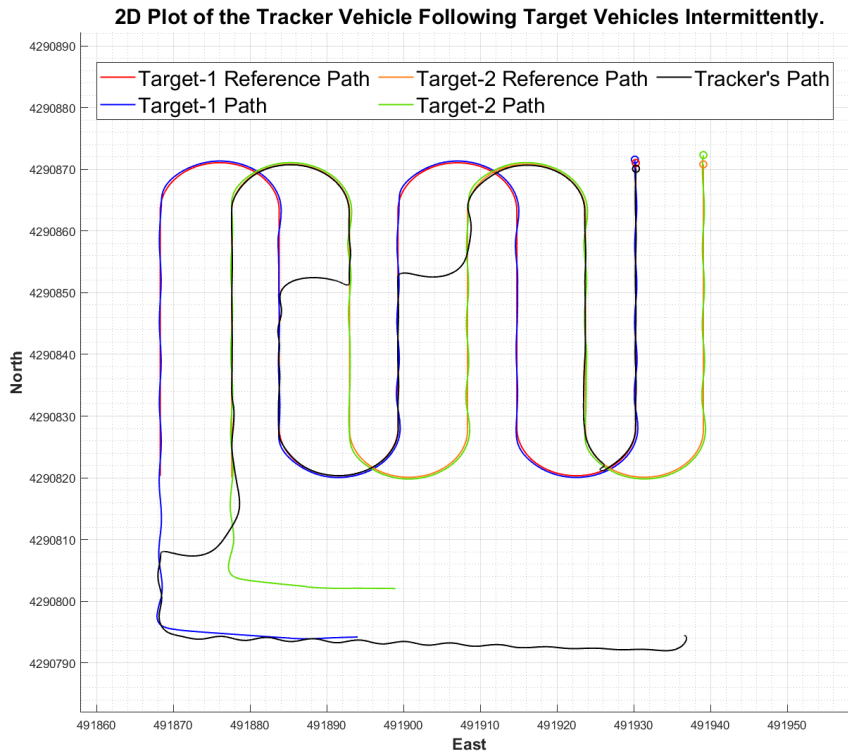


Figure 4.12: 2D plot of the tracker following the target vehicles Intermittently

**Plot of distance of the Tracker to the Target vehicles. (Scenario I)**

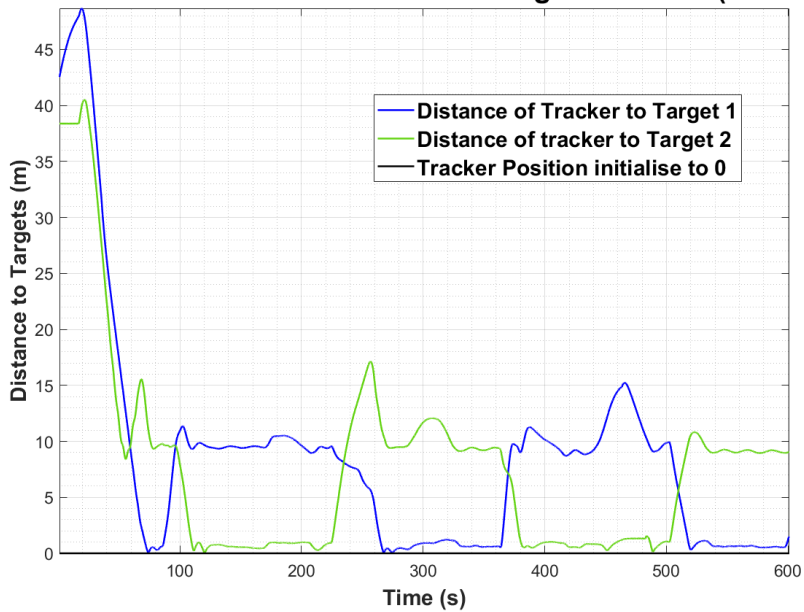


Figure 4.13: 2D plot of the distance between the Tracker and the targets.

done for this also. Fig 4.15 represents the distance from the tracker to each target. In fact, this plot provides a better insight into visualising how well the tracker was able to maintain a mid position in the horizontal plane between the two targets. It can be observed that the tracker was able to maintain approximately similar distance between the targets with a standard deviation of  $\pm 0.72m$ .

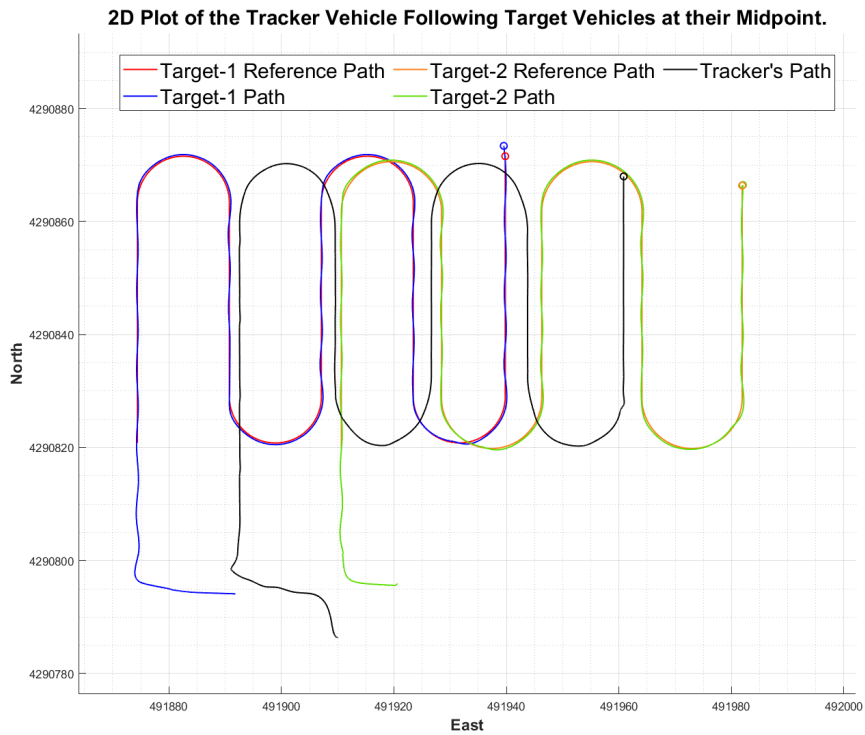


Figure 4.14: 2D plot of the tracker following the target vehicles Intermittently

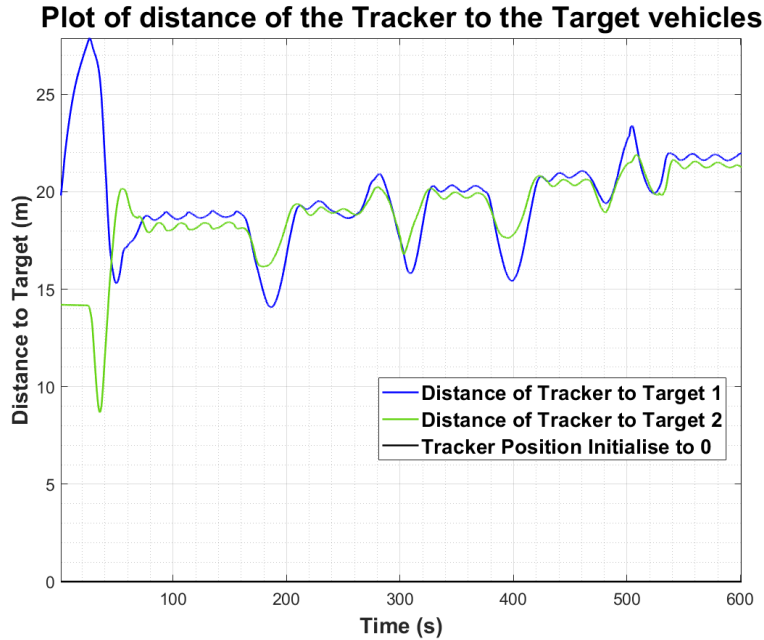


Figure 4.15: 2D plot of the distance between the Tracker and the targets.

### 3. Inner-Loop References of the Target Vehicles

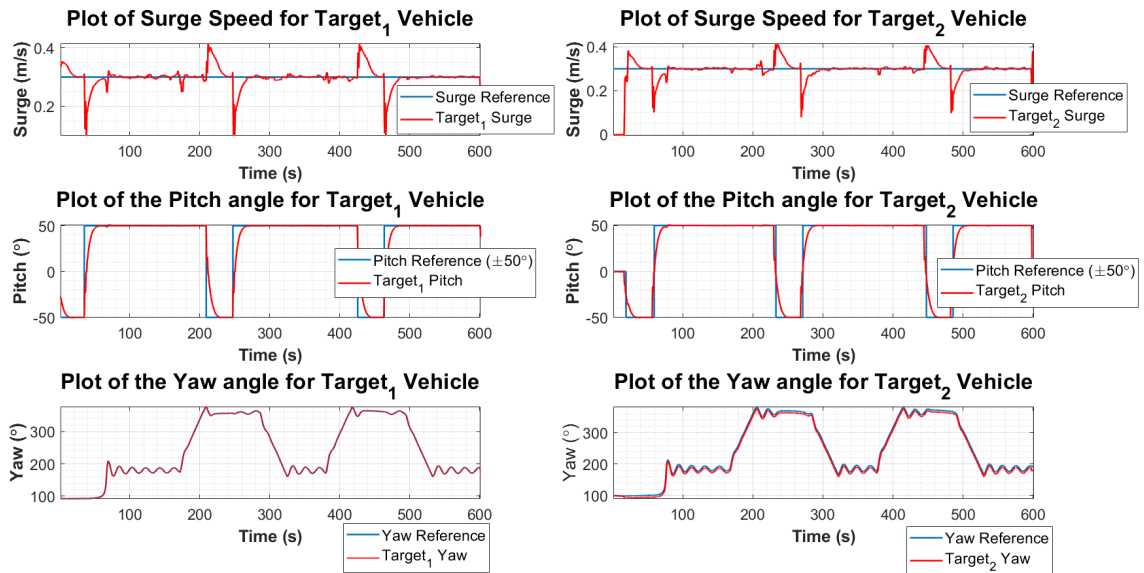
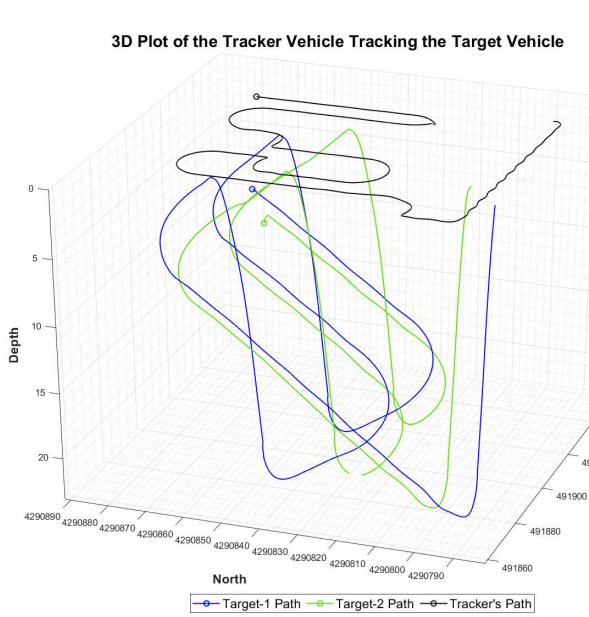


Figure 4.16: Surge, Pitch and Yaw References of the target vehicles

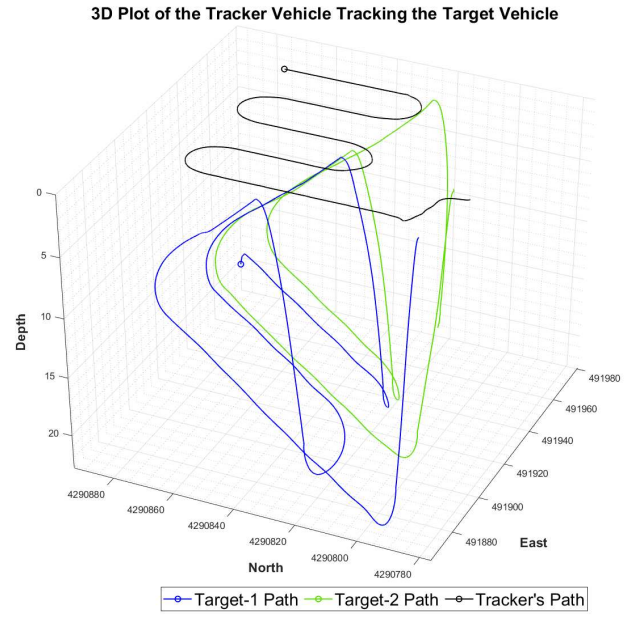
The references of each of the vehicles follow the same convention as that of the single target vehicle presented in section 4.1 of this chapter. However, in the references of the second target vehicle, it can be observed that the values start from zero. This is because the second vehicle was launched after the first

vehicle.

#### 4. 3D Plot of the Two Scenarios



(a) 3D Plot for Scenario I



(b) 3D Plot for Scenario II

Figure 4.17: 3D Visualization of the tracker following the targets for two scenarios

# Chapter 5

## Conclusion and Future Works

### 5.1 Conclusion

In conclusion, this study addressed the problem of cooperative control between heterogeneous vehicles for the purpose of Ocean observation. In providing a solution for this problem, existing theory and concepts in the area of guidance navigation and control such as Path Following, Target Tracking, graph theory, etc., were presented and applied. The system implemented in this study involved two AUVs and a single ASC, where the ASC moves in synchrony alongside the two underwater vehicles. Meanwhile, as the ASC is tracking the two AUVs, the AUVs are performing a saw-tooth maneuver in the vertical plane as they follow a predefined path in the horizontal plane.

Path Following is one of the crucial building blocks in this study as it is one of the motion systems implemented by the target vehicle. Hence, selecting the right algorithm is important to have a system capable of staying longer at sea. Lapierre et al. [32] algorithm was suitable for this task as it presents a virtual target that will determine the progression of the vehicle along a certain path, thereby giving rise to smooth convergence to the path. Having established the horizontal motion of the target vehicle, controlling the motion of the vehicle in the vertical plane was also addressed. This was achieved by controlling the pitch reference of the vehicle to generate a saw-tooth motion in the vertical plane. Having addressed the motion of the target vehicles, addressing the motion of the tracker vehicle was the next task.

Target Tracking was another tool par excellence applied to address the motion system of the tracker vehicle. The popular line of sight (LOS) was applied in the design of the speed and yaw reference controllers. The yaw controller is responsible for pointing the vehicle towards the target while the speed controller is responsible for regulating the speed as the tracker follows the target. In designing these control laws, Lyapunov techniques for stability analysis and the design of nonlinear controllers were employed. Having established the motion of the two kinds of vehicles in the formation, coupling the vehicles in cooperation was the next problem addressed.

In cooperative multiple-vehicle formation control, two cooperation strategy was introduced to ensure that the tracker follows the target in synchrony. In the first formation, the tracker follows the targets intermittently such that it tracks one vehicle at a time after which it switches to follow another target. In the second formation, the tracker estimates the midpoint of the positions of the target and follows this estimated point. These formations aim to maximise the data obtained. However, when we compared the performance of the formations in the light of ocean observation, the second formation might be more desirable to yield data that can represent the state of the area covered.

In the overall view, the system described in Section 1.3 was achieved, with simulations using the kinematic model of the vehicles throughout this thesis. The simulations presented allow for a better understanding of each concept and theory discussed and provided a compelling demonstration of the theoretical principles. Furthermore, the choice of the algorithm selected will go a long way to determining the durability of the vehicles on a mission. Since the goal of the entire system is to ensure long-term Ocean observation, the algorithms applied were carefully selected. The Target Tracking speed control law implemented ensured smooth reference output such that the performance of the actuator will not be rough. The same can also be said for the choice of Path Following as the motion system for the target. With these strategies in place, it became possible to have an autonomous system capable of Ocean Observation.

## 5.2 Future Works

The problem addressed in this work covers the area of guidance and control. However, there are still possible avenues for future development.

- **Cooperative Navigation:** Solving the problem of navigation, especially for underwater vehicles is important for such a study as this. A possible estimation filter can be used to improve the estimation of the position of the vehicles.
- **Environmental Disturbance Inclusion:** While developing this model, the effect of winds, and currents were neglected. To be able to develop a more robust system that can mimic the real ocean environment, there is, therefore, a need to factor some of these disturbances into the model.
- **Dynamic Model:** All the work developed and simulated in this study takes into consideration only the kinematic model of the vehicles. Although the dynamic model of the vehicles was outside of the scope of this study, however, the dynamic model can be a bridge between the kinematic system and the real-world vehicle.
- **Multiple Vehicles:** The system was developed for three vehicles in the network. To upgrade such a system on a commercial many-nodes scale, more vehicles can be introduced and as such there will be a need to solve the complexity that more vehicles will introduce into the formation, regarding

motion control (to avoid collisions) but also communications (underwater communications. are very low bandwidth).

- **Formation Control:** In this work, two types of formations were introduced, and the conditions for switching formations were also presented. However, various decision-based AI tools, optimization tools, etc., can be applied to determine how the tracker follows the target, thereby harnessing more data.

# References

- [1] A. Pedro Aguiar, João Almeida, Behzad Bayat, Bruno Cardeira, Rita Cunha, Andreas Häusler, Pramod Maurya, A. Oliveira, Antonio Pascoal, Arvind Pereira, Manuel Rufino, Luis Sebastiao, Carlos Silvestre, and F. Vanni. Cooperative autonomous marine vehicle motion control in the scope of the eu grex project: Theory and practice. In *OCEANS 2009-EUROPE*, pages 1 – 10, 06 2009.
- [2] Majid Manteghi Kexiong Zeng Alireza Shahanaghi Xiaofan Li Eric Dupuis Ali Fahraji Pedram Loghmannia Yaling Yang, Lei Zuo. Long-range ocean communication links powered by energy harvesting. <https://www.faculty.ece.vt.edu/yyang8/ocean-wave.html>. (Accessed: 15-June-2023).
- [3] Jackie Mackenzie. Drifters will help reveal secrets of the seas. <https://www.ross-shirejournal.co.uk/news/drifters-will-help-reveal-secrets-of-the-seas-157675/>. (Accessed: 15-June-2023).
- [4] Mooring Systems Inc. Surface buoy systems. <https://www.mooringsystems.com/surface.htm>. (Accessed: 15-June-2023).
- [5] T. J. Mertzimekis, P. Nomikou, E. Petra, P. Batista, D. Cabecinhas, A. Pascoal, L. Sebastião, J. Escartín, K. Kebkal, K. Karantzalos, A. Mallios, K. Nikolopoulos, and L. Maigne. The eu project ramones – continuous, long-term autonomous monitoring of underwater radioactivity. In *Atas das 7.as Jornadas de Engenharia Hidrográfica / 2. as Jornadas Luso-Espanholas de Hidrografia*, page 351–354. Instituto Hidrográfico, 2022, June 2022.
- [6] Bikramaditya Das, Bidyadhar Subudhi, and Bibhuti Bhusan Pati. Cooperative formation control of autonomous underwater vehicles: An overview. *International Journal of Automation and Computing*, 13(3):199–225, June 2016. 10.1007/s11633-016-1004-4.
- [7] Guofang Chen, Yihui Liu, Ziyang Zhang, and Yufei Xu. Adaptive disturbance-observer-based continuous sliding mode control for small autonomous underwater vehicles in the trans-atlantic geotraverse hydrothermal field with trajectory modeling based on the path. *Journal of Marine Science and Engineering*, 10:721, 05 2022.
- [8] Nguyen Hung, Francisco Rego, Joao Quintas, Joao Cruz, Marcelo Jacinto, David Souto, Andre Potes, Luis Sebastiao, and Antonio Pascoal. A review of path following control strategies for autonomous

robotic vehicles: Theory, simulations, and experiments. *Journal of Field Robotics*, 40(3):747–779, 2023.

- [9] Thor I. Fossen. *Handbook of Marine Craft Hydrodynamics and Motion Control: Guidance Systems*, chapter 10, pages 241–284. John Wiley Sons, Ltd, 2011.
- [10] Nguyen Hung. Presentation on path following, lafai presentation, dsor lab, institute for systems and robotics (isr), lisboa. [https://www.dropbox.com/scl/fi/8hb6wzx4wok2y3tenlt7a/zoom\\_0-1.mp4?rlkey=1sohv4gpzggc5y6mchf22v73&d1=0](https://www.dropbox.com/scl/fi/8hb6wzx4wok2y3tenlt7a/zoom_0-1.mp4?rlkey=1sohv4gpzggc5y6mchf22v73&d1=0), December, 2020. (Accessed: 10-December-2022).
- [11] Nuno Cruz. *Adaptive Ocean Sampling with Modular Robotic Platforms*. PhD thesis, 04 2016.
- [12] Charalampos P. Bechlioulis, Fotis Giagkas, George C. Karras, and Kostas J. Kyriakopoulos. Robust formation control for multiple underwater vehicles. *Frontiers in Robotics and AI*, 6, 2019.
- [13] A. Pedro Aguiar, J. Almeida, M. Bayat, B. Carneira, R. Cunha, A. Häusler, P. Maurya, A. Oliveira, A. Pascoal, A. Pereira, M. Rufino, L. Sebastiao, C. Silvestre, and F. Vanni. Cooperative control of multiple marine vehicles theoretical challenges and practical issues. *IFAC Proceedings Volumes*, 42(18):412–417, 2009. 8th IFAC Conference on Manoeuvring and Control of Marine Craft.
- [14] J. Kalwa, A. Pascoal, P. Ridao, A. Birk, T. Glotzbach, L. Brignone, M. Bibuli, J. Alves, and M.C. Silva. Eu project morph: Current status after 3 years of cooperation under and above water. *IFAC-PapersOnLine*, 48(2):119–124, 2015. 4th IFAC Workshop on Navigation, Guidance and Control of Underwater Vehicles NGCUV 2015.
- [15] Giovanni Indiveri, Gianluca Antonelli, Filippo Arrichiello, Andrea Caffaz, Andrea Caiti, Giuseppe Casalino, Nicola Catenacci Volpi, Ivan Bielic de Jong, Daniela De Palma, Henrique Duarte, Joao Pedro Gomes, Jonathan Grimsdale, Sergio Jesus, Konstantin Kebkal, Elbert Kelholt, Antonio Pascoal, Daniel Polani, Lorenzo Pollini, Enrico Simetti, and Alessio Turetta. Overview and first year progress of the widely scalable mobile underwater sonar technology h2020 project\*\*this work has received funding from the european union’s horizon 2020 research and innovation programme under grant agreement no. 645141 (wimust project, <http://www.wimust.eu>). *IFAC-PapersOnLine*, 49(23):430–433, 2016. 10th IFAC Conference on Control Applications in Marine Systems CAMS 2016.
- [16] The Woods Hole Oceanographic Institution. Need for ocean observatories. <https://www.whoi.edu/what-we-do/explore/ocean-observatories/about-ocean-observatories/need-for-ocean-observatories/>. (Accessed: 30-Dec-2022).
- [17] Yang Quan Chen and Zhongmin Wang. Formation control: a review and a new consideration. In *2005 IEEE/RSJ International Conference on Intelligent Robots and Systems*, pages 3181–3186, 2005. 10.1109/IROS.2005.1545539.

- [18] H.G. Tanner, G.J. Pappas, and V. Kumar. Leader-to-formation stability. *IEEE Transactions on Robotics and Automation*, 20(3):443–455, 2004. 10.1109/TRA.2004.825275.
- [19] Yintao Wang, Weisheng Yan, and Wei Yan. A leader-follower formation control strategy for auvs based on line-of-sight guidance. In *2009 International Conference on Mechatronics and Automation*, pages 4863 – 4867, 09 2009. 10.1109/ICMA.2009.5246389.
- [20] Nan Gu, Dan Wang, Zhouhua Peng, Jun Wang, and Qing-Long Han. Advances in line-of-sight guidance for path following of autonomous marine vehicles: An overview. *IEEE Transactions on Systems, Man, and Cybernetics: Systems*, 53(1):12–28, 2023. 10.1109/TSMC.2022.3162862.
- [21] Dragan B. Dacic, Maksim V. Subbotin, and Petar V. Kokotovic. Control effort reduction in tracking feedback laws. *IEEE Transactions on Automatic Control*, 51:1831–1837, 2006.
- [22] Ravishankar P. Desai and Narayan S. Manjarekar. Norm-based robust pitch channel control of an autonomous underwater vehicle. *IFAC-PapersOnLine*, 54(16):258–265, 2021. 13th IFAC Conference on Control Applications in Marine Systems, Robotics, and Vehicles CAMS 2021.
- [23] Devjani Bhattacharya and Puttamadappa C. An effective pitch control technique for unmanned underwater vehicles based on type 2 fuzzy logic controller. In *2021 International Conference on Computational Performance Evaluation (ComPE)*, pages 180–187, 2021. 10.1109/ComPE53109.2021.9752186.
- [24] L. Priyadarshini, S. Kundu, and Bibhu Ganthia. Controller design for the pitch control of an autonomous underwater vehicle. *Engineering, Technology Applied Science Research*, 12:8967–8971, 08 2022. 10.48084/etasr.5050.
- [25] Manav Kumar and Sharifuddin Mondal. Recent developments on target tracking problems: A review. *Ocean Engineering*, 236:109558, 2021. <https://www.sciencedirect.com/science/article/pii/S0029801821009471>.
- [26] Jean-Philippe Condomines. *Nonlinear Kalman Filter for Multi-Sensor Navigation of Unmanned Aerial Vehicles: Application to Guidance and Navigation of Unmanned Aerial Vehicles Flying in a Complex Environment*. 11 2018.
- [27] Junhai Luo, Ying Han, and Liying Fan. Underwater acoustic target tracking: A review. *Sensors (Basel, Switzerland)*, 18(1):112:37, January 2018. 10.3390/s18010112.
- [28] The Society of Naval Architects Marine Engineers (SNAME). <http://www.sname.org/>.
- [29] Alfred Leick. *GPS Satellite Surveying*. John Wiley Sons, Inc, 02 march 2015.
- [30] David Almeida Souto. Autonomous acquisition and optical transmission of underwater images for online marine habitat mapping. Master's thesis, June 2022.

- [31] Alain Micaelli and Claude Samson. Trajectory tracking for unicycle-type and two-steering-wheels mobile robots. <https://inria.hal.science/inria-00074575>, 1993. [Research Report] RR-2097, INRIA.
- [32] Lionel Lapierre, Didik Soetanto, and António Manuel Santos Pascoal. Nonlinear path following with applications to the control of autonomous underwater vehicles. *42nd IEEE International Conference on Decision and Control (IEEE Cat. No.03CH37475)*, 2:1256–1261 Vol.2, 2003.
- [33] Shuyou Yu, Xiang Li, Hong Chen, and Frank Allgöwer. Nonlinear model predictive control for path following problems. *IFAC Proceedings Volumes*, 45(17):145–150, 2012. 4th IFAC Conference on Nonlinear Model Predictive Control.
- [34] Nguyen T. Hung, F. Rego, N. Crasta, and A.M. Pascoal. Input-constrained path following for autonomous marine vehicles with a global region of attraction. *IFAC-PapersOnLine*, 51(29):348–353, 2018. 11th IFAC Conference on Control Applications in Marine Systems, Robotics, and Vehicles CAMS 2018.
- [35] Roger Skjetne, Thor Inge Fossen, and Petar V. Kokotovic. Robust output maneuvering for a class of nonlinear systems. *Autom.*, 40:373–383, 2004.
- [36] J.-A. Serret. Sur quelques formules relatives à la théorie des courbes à double courbure. *Journal de Mathématiques Pures et Appliquées*, 1e série, 16, 1851. [http://www.numdam.org/item/JMPA\\_1851\\_1\\_16\\_\\_193\\_0/](http://www.numdam.org/item/JMPA_1851_1_16__193_0/).
- [37] F. Frenet. Sur les courbes à double courbure. *Journal de Mathématiques Pures et Appliquées*, 1e série, 17, 1852. [http://www.numdam.org/item/JMPA\\_1852\\_1\\_17\\_\\_437\\_0/](http://www.numdam.org/item/JMPA_1852_1_17__437_0/).
- [38] Antonio Pedro Aguiar and João Pedro Hespanha. Trajectory-tracking and path-following of underactuated autonomous vehicles with parametric modeling uncertainty. *IEEE Transactions on Automatic Control*, 52:1362–1379, 2007.
- [39] Andrea Alessandretti, A. Pedro Aguiar, and Colin Jones. Trajectory-tracking and path-following controllers for constrained underactuated vehicles using model predictive control. *2013 European Control Conference, ECC 2013*, pages 1371–1376, 07 2013. 10.23919/ECC.2013.6669717.
- [40] Fotis A. Papoulias. Bifurcation analysis of line of sight vehicle guidance using sliding modes. *International Journal of Bifurcation and Chaos*, 01:849–865, 1991.
- [41] Thor Inge Fossen, Morten Breivik, and Roger Skjetne. Line-of-sight path following of underactuated marine craft. *IFAC Proceedings Volumes*, 36:211–216, 2003.
- [42] Francisco dos Reis Centeio dos Santos Branco. Cooperative marine vehicle navigation and control with applications to geotechnical surveying. Master's thesis, May 2022.

- [43] Anastasios M. Lekkas and Thor I. Fossen. A time-varying lookahead distance guidance law for path following. *IFAC Proceedings Volumes*, 45(27):398–403, 2012. 9th IFAC Conference on Manoeuvring and Control of Marine Craft.
- [44] Morten Breivik and Thor Fossen. *Guidance Laws for Autonomous Underwater Vehicles*. 01 2009. 10.5772/6696.
- [45] R. Craig Coulter. Implementation of the pure pursuit path tracking algorithm. The Robotics Institute Carnegie Mellon University Pittsburgh, Pennsylvania 15213, January 1992. <https://api.semanticscholar.org/CorpusID:62550799>.
- [46] Yilmaz Erkan and Nevsan Sengil. Comparison between the pursuit guidance and the proportional navigation guidance laws regarding a predetermined scenario. page 4, Burgas, Bulgaria, June 2018. trans MOTAUTOAt, Research gate.
- [47] R. Yanushevsky. *Guidance of Unmanned Aerial Vehicles (1st ed.)*. CRC Press, 2011.
- [48] Anastasios Lekkas and Thor Fossen. *Line-of-Sight Guidance for Path Following of Marine Vehicles*, chapter 5. Lambert Academic, June 2013.
- [49] Yuxin Zheng, Lei Zhang, Bing Huang, Cheng Zhu, and Yumin Su. Dynamic event-triggered formation maneuver in cooperative marine surface vehicles control over directed communication networks. *Ocean Engineering*, 281:114622, 2023. <https://doi.org/10.1016/j.oceaneng.2023.114622>.
- [50] Artur Piotr Zolich, David Palma, Kimmo Kansanen, Kay Endre FjØrtoft, João Borges de Sousa, Karl Henrik Johansson, Yuming Jiang, Hefeng Dong, and Tor Arne Johansen. Survey on communication and networks for autonomous marine systems. *Journal of Intelligent & Robotic Systems*, pages 1–25, 2019. <https://doi.org/10.1007/s10846-018-0833-5>.
- [51] Reza Ghabcheloo Kristin Y. Pettersen Antonio Pascoal Carlos Silvestre Even Børhaug, Alexey Pavlov. Formation control of underactuated marine vehicles with communication constraints. *IST*, page 6, 2006. [https://www.academia.edu/13374178/Formation\\_control\\_of\\_underactuated\\_marine\\_vehicles\\_with\\_communication\\_constraints](https://www.academia.edu/13374178/Formation_control_of_underactuated_marine_vehicles_with_communication_constraints).
- [52] Reza Ghabcheloo, Antonio Pedro Aguiar, António Manuel Santos Pascoal, Carlos Silvestre, Isaac I. Kaminer, and João Pedro Hespanha. Coordinated path-following in the presence of communication losses and time delays. *SIAM J. Control. Optim.*, 48:234–265, 2009.
- [53] Weisstein Eric W. Curvature and normal vectors of a curve. <https://mathworld.wolfram.com/Curvature.html>, 2023.
- [54] F. Mazenc and M. Malisoff. Control-lyapunov functions for systems satisfying the conditions of the jurdjevic-quinn theorem. In *Proceedings of the 44th IEEE Conference on Decision and Control*, pages 4724–4729, 2005. 10.1109/CDC.2005.1582908.